



UIT

THE ARCTIC  
UNIVERSITY  
OF NORWAY

Faculty of Science and Technology

Department of Geoscience

# Late Cenozoic erosion in the SW Barents Sea, and its influence on salt movement

**Birgitta Saue Martinsen**

*GEO-3900 Master thesis in Geology*

*May 2019*





# Abstract

The late Cenozoic evolution of the southwestern Barents Sea shelf includes periods of uplift, erosion and glaciations. This part of the stratigraphy has been studied using 2D and 3D seismic data, with emphasis on the interplay between uplift, erosion and glaciations and salt movement. The study area comprises the Svalis, Samson and Norvarg domes and the Nordkapp Basin, where halokinesis has been a major influence on the tectonostratigraphic evolution.

The study includes systemization and categorization of the timing of salt activity relative to the erosion of the shelf, in the Nordkapp Basin, and on the Svalis, Samson and Norvarg domes. Very late to almost recent salt movement has occurred within some of the diapirs in the Nordkapp Basin and the Svalis Dome, evidenced by uplift of the Upper Regional Unconformity (URU) surface and the seafloor above the salt. Furthermore, the study reveals significant local variations in salt movement of the diapirs in the Nordkapp Basin, with a trend of more late salt movement towards the northeast. This is possibly attributed to a larger original salt thickness in this part of the basin compared to in the southwest. A mini-basin filled with glacial sediments is found adjacent to the Svalis Dome, and this is assumed to be a result of a combination of deeper glacial erosion of less resistant strata on the Loppa High, and less exposure to erosion due to the continuous salt rise and elevation of the adjacent dome. The Norvarg and Samson domes are not found to be influenced by late Cenozoic salt movement, which is attributed to factors such as original salt thickness, overburden strength and early Cenozoic erosion. Spatial variations in lithology due to salt-related doming and faulting is assumed to have influenced both the pre-glacial and later glacial erosion of the Norvarg Dome during the Cenozoic.

Overall, the relationship between salt diapirism, erosion and glacial influence is found to be complex. The structural elements within the study area have experienced different pre-Cenozoic evolutions and have been exposed to varying degrees of erosion and also phases of grounded glaciers. The halokinetic history of the structural elements is also different, causing the salt structures within the study area to have different responses to the late Cenozoic uplift, erosion and glaciation of the shelf.



# Preface

This master thesis is submitted as part of the completion of the master program in marine geology and geophysics at the University of Tromsø. Supervisors for the thesis has been Stig-Morten Knutsen and Sondre Krogh Johansen with the Norwegian Petroleum Directorate, and associate professor Tom Arne Rydningen at the university. Data used in the study was released by Equinor Energy AS.

Disclaimer: The views expressed in this paper are the views of the author and do not necessarily reflect the views of Equinor Energy AS.

## Acknowledgements

Fem innholdsrike år på geologi-studiet er over, og for en avslutning det har vært. Det siste året med masterskriving har vært både utfordrende og lærerikt, og jeg vil se tilbake på det og huske både glede og fortvilelse, mye stress og mye latter.

Oppgaven hadde ikke gått i havn uten hjelp fra dyktige veiledere. En stor takk går ut til min hovedveileder Stig-Morten for gode kommentarer, diskusjoner og masse god hjelp. Tusen takk til Sondre for retting av tekst og hjelp med litteratur-leting, og til Tom Arne for gode råd og diskusjoner. Takk til Equinor Energy AS for frigivelse av data.

De siste fem årene har jeg vært omringet av mange flotte folk som virkelig har gjort studietiden til en herlig opplevelse. Takk til alle sammen på brakka for et flott miljø, godt samhold og god deltagelse på lunsj-quizen. Ekstra takk til jentene på brakka for støtte og alle pauser med masse latter og moro. Tusen takk til Kristine for alle diskusjoner og støtte, og til Egil for morgenkaffen som gjorde tidlig oppmøte langt enklere. Og hjertelig takk til Sofie, den beste kontorkameraten jeg kunne bedt om!

Tusen takk til min fine familie for støtte under tøffe tak, og spesielt til mamma som alltid tar telefonen og som har stilt med peptalk før hver eneste eksamen gjennom studiene.

Birgitta Saue Martinsen

The Arctic University of Norway

# Table of Contents

1 Introduction .....	1
1.1 Objectives .....	2
1.2 Study area .....	2
1.3 Salt .....	5
1.3.1 Deposition .....	5
1.3.2 Salt migration .....	5
1.3.3 Seismic imaging .....	7
2 Geological background.....	9
2.1 Tectonic development .....	9
2.1.1 Paleozoic .....	9
2.1.2 Mesozoic .....	9
2.1.3 Cenozoic .....	10
2.2. Stratigraphy and depositional environment.....	10
2.2.1 Paleozoic .....	10
2.2.2 Mesozoic .....	11
2.3 Cenozoic uplift and erosion.....	15
2.3.1 Pre-glacial erosion .....	15
2.3.2 Glacial history .....	18
2.3.3 Late Cenozoic seismic stratigraphy .....	23
2.4 Structural setting.....	24
2.4.1 Nordkapp Basin.....	24
2.4.2 Bjarmeland Platform .....	25
2.4.3 Samson Dome.....	25
2.4.4 Norvarg Dome .....	25
2.4.5 Svalis Dome .....	26
3 Data and methodology.....	27
3.1 Data .....	27
3.2 Seismic reflection theory .....	30
3.2.1 Seismic resolution .....	30
3.2.2 Phase and polarity.....	35
3.2.3 Artefacts and noise .....	36
3.3 Interpretation methodology .....	37

3.3.1 Seismic Interpretation.....	37
3.3.2 Seismic stratigraphy .....	38
3.3.3 Seismic attributes .....	40
4 Results .....	41
4.1 Regional overview.....	41
4.1.1 Upper Regional Unconformity (URU).....	41
4.1.2 Seafloor .....	44
4.1.3 Quaternary sediments .....	49
4.2 Svalis Dome .....	53
4.2.1 Horizons .....	53
4.2.2 Quaternary sediments .....	53
4.3 Samson Dome.....	58
4.4 Norvarg Dome.....	60
4.5 Nordkapp Basin.....	61
4.5.1 Horizons and sediments.....	61
4.5.2 Salt diapirs in the Nordkapp Basin.....	65
5 Discussion .....	91
5.1 Salt movement.....	91
5.1.1 Svalis Dome .....	91
5.1.2 Samson Dome.....	94
5.1.3 Norvarg Dome .....	96
5.1.4 Nordkapp Basin.....	98
5.2 Pre-Cenozoic factors influencing salt movement and erosion .....	105
5.2.1 Original salt thickness .....	105
5.2.2 Overburden weight and strength .....	105
5.2.3 Early Cenozoic erosion.....	106
5.3 Interplay between salt movement and late Cenozoic erosion.....	106
5.3.1 Ice sheet dynamics above the salt structures .....	106
5.3.2 Response of salt structures to erosion.....	107
5.3.3 Influence of salt movement on erosion and sediment dispersal .....	108
6 Conclusions .....	109
7 Further work.....	111
8 References .....	113







# 1 Introduction

Uplift and extensive erosion resulted in the removal of large amounts of sediments from the Barents Sea shelf during the Cenozoic (Vorren et al., 1991; Knies et al., 2009; Smelror et al., 2009; Laberg et al., 2010; Henriksen et al., 2011b). The erosion of the shelf has been under discussion for over a hundred years, since Nansen (1904) published a pioneering study on the topic, and has been a major influence on the present stratigraphy and morphology of the shelf. The region has experienced early Cenozoic erosion related to uplift and the opening of the Norwegian-Greenland Sea (Vorren et al., 1991; Lasabuda et al., 2018a) and late Cenozoic glaciofluvial and glacial erosion (Laberg et al., 2012). Ice sheets covered the shelf periodically, giving high rates of erosion on the shelf and high rates of deposition along the slope (Laberg et al., 2010).

Another major influence on the geological evolution of the shelf is salt tectonics. The movement of salt in the subsurface may result in doming, fracturing and subsequent erosion of strata in some areas, and subsidence and sedimentation in others (Alsop et al., 2012). Salt tectonics have been an important factor in the tectonostratigraphic development of several of the structural elements of the shelf, including the Nordkapp Basin and the Norvarg-, Samson- and Svalis domes (Gabrielsen et al., 1990; Rowan and Lindsø, 2017). The timing and extent of salt tectonics is influenced by erosion. During the late Cenozoic glaciations 2000 meters of strata are estimated to have been removed above the Nordkapp Basin (Worsley, 2008; Henriksen et al., 2011b) and according to Koyi et al. (1995), the removal of overlying sediments and exhumation of some salt diapirs within the basin enabled late salt activity.

There have been several studies describing the timing of active diapir rise within the Nordkapp Basin (Gabrielsen et al., 1990; Koyi et al., 1995; Nilsen et al., 1995; Bugge et al., 2002; Grimstad, 2016) and the Norvarg-, Samson- and Svalis domes (Gabrielsen et al., 1990; Breivik et al., 1995; Mattos et al., 2016). The influence and feedback from salt tectonics on erosion and vice versa is not very well understood, but the timing and spatial variation of these processes is essential to the late Cenozoic development of the Barents Sea region.

# 1 Introduction

## 1.1 Objectives

The main ambition of this thesis is to study the late Cenozoic development of the southwestern Barents Sea, with an emphasis on the relation between erosion and salt tectonics and how these processes influence one another. Some key objectives are listed below:

- Interpret the shallow seismic stratigraphy above the Upper Regional Unconformity (URU).
- Investigate and understand the relationship between erosion and salt tectonics, and how these processes have influenced the late Cenozoic evolution of the southwestern Barents Sea.
- Compare the salt diapirs in the Nordkapp Basin to the Svalis, Samson and Norvarg domes to identify differences in how erosion has affected the salt diapirs, and vice versa.

## 1.2 Study area

The Barents Sea is an epicontinental, shallow sea bounded to the west and north by passive continental margins, and by surrounding landmasses to the south and east. Geographically the Barents Sea is bordered by the Norwegian and Russian coastline in the south, Novaya Zemlya to in the east and the Svalbard and Franz Josef Land archipelagos to the north (Figure 1.1 a)) (Smelror et al., 2009). The study area is located in the southwestern Barents Sea and covers approximately 49800 km<sup>2</sup>. It comprises the Nordkapp Basin, Bjarmeland Platform, as well as the Svalis, Samson and Norvarg domes (Figure 1.1 b)). The study focuses on the shallowest stratigraphy (Figure 1.2), primarily the URU and the glacial sediments above.

# 1 Introduction

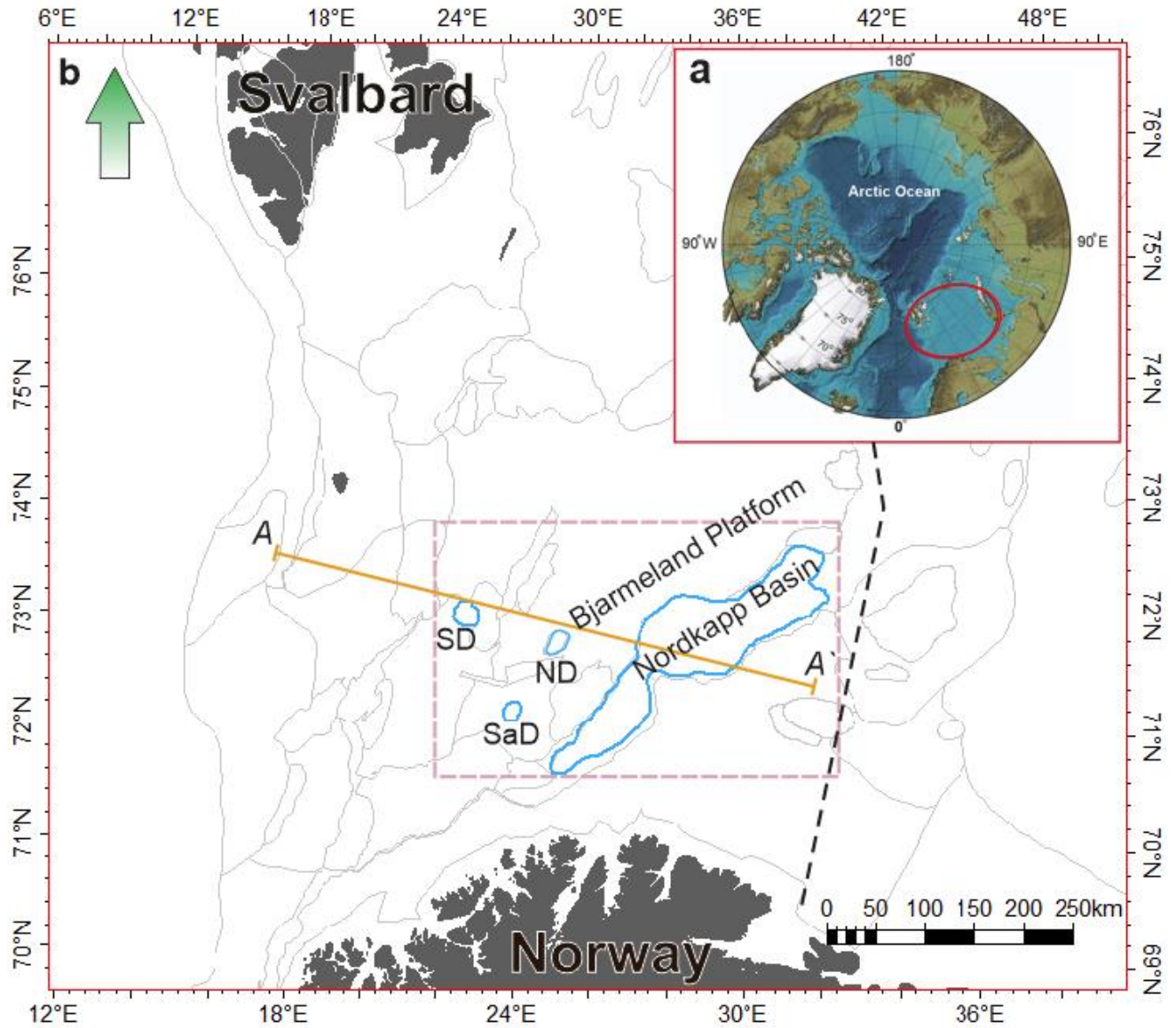


Figure 1.1: Map showing the location of the study area. a): Bathymetrical map of the Arctic waters, with the Barents Sea outlined by a red circle. b): Map showing the main structural elements within the study area (purple dotted rectangle) outlined in blue. SD = Svalis Dome, SaD = Samson Dome, ND = Norvarg Dome. The position and orientation of the profile in fig. 1.2 is shown by the orange line. The marine border towards Russian territory is delineated by the black dashed line. Base map provided from the Norwegian Petroleum Directorate (NPD). Map in figure a) modified from IBCAO version 3.0 (Jakobsson et al, 2012).

# 1 Introduction

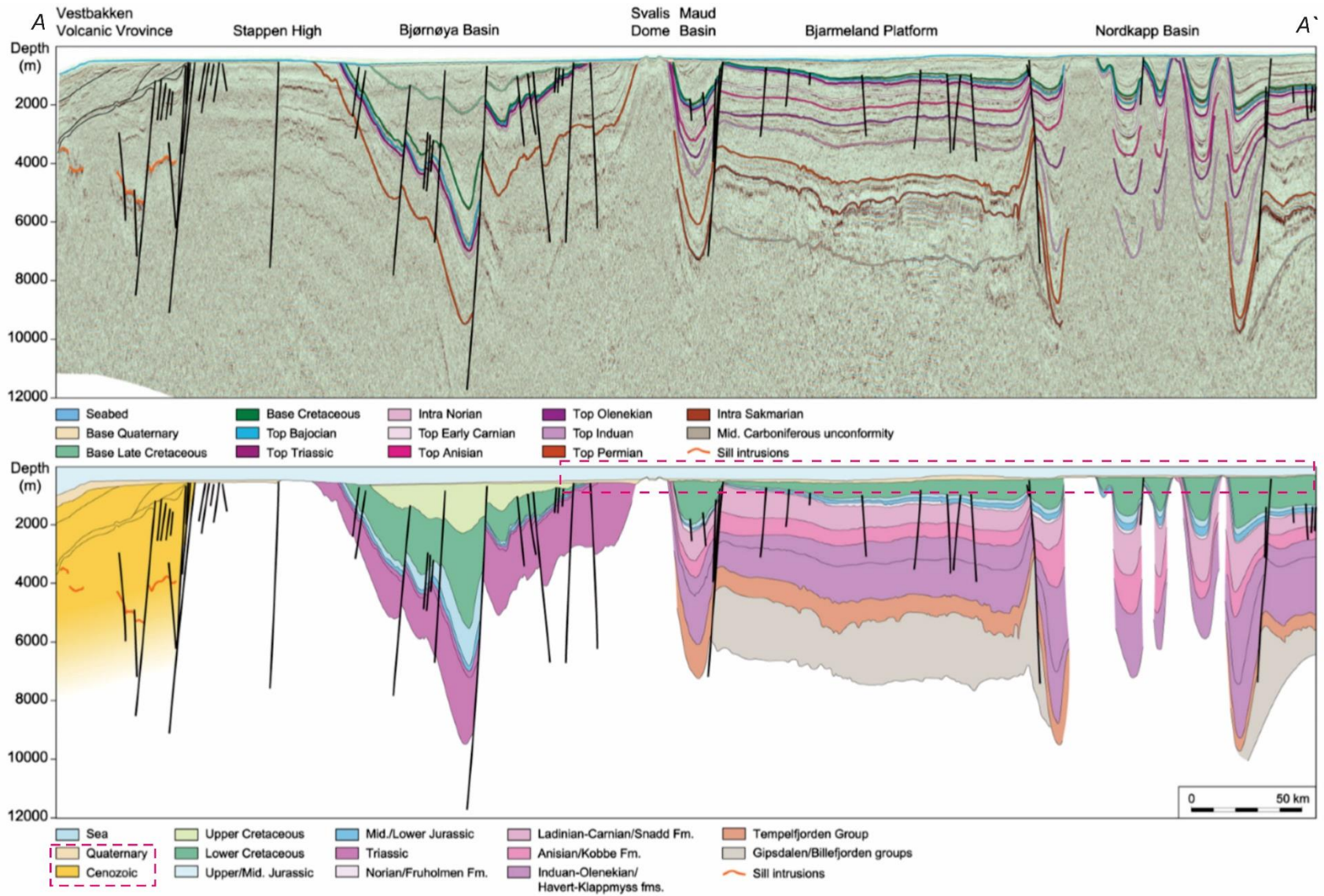


Figure 1.2: Profile through the study area showing the stratigraphy and main structural elements. The dotted purple rectangles outline the part of the stratigraphy targeted in the study. Figure modified from Henriksen et al. (2011a).

## 1 Introduction

### 1.3 Salt

#### 1.3.1 Deposition

Salt is an evaporite mineral, precipitated during evaporation of water, when the concentration of ions in the solution increases, relative to the amount of water. The chemical composition of evaporites is dependent of the water chemistry, temperature and the salinity at the time of precipitation (Nichols, 2009). Thus, the mineral composition reflects the environment in which they were precipitated (James & Dalrymple, 2010). The physical properties of the most common evaporite minerals are listed in table 1.1.

Table 1.1: Physical properties of the most common evaporite minerals. After Jones & Davidson (2014).

<i>Mineral</i>	<i>Composition</i>	<i>Hardness</i> ( <i>Mohs</i> )	<i>Density</i> ( <i>kg/m<sup>3</sup></i> )	<i>Seismic velocity</i> ( <i>m/s</i> )
<i>Halite</i>	NaCl	2.5	2200	4500
<i>Gypsum</i>	CaSO <sub>4</sub> 2H <sub>2</sub> O	1.5-2	2300	5700
<i>Anhydrite</i>	CaSO <sub>4</sub>	3.5	2900	6500
<i>Dolomite</i>	CaSO <sub>4</sub> MgCO <sub>3</sub>	3.5-4	2870	6300
<i>Sylvite</i>	KCl	1.5-2	1990	4110

#### 1.3.2 Salt migration

Salt is incompressible relative to surrounding rocks and its density is constant with depth (Jenyon, 1986). At a certain depth, the density of the overburden will exceed that of the buried salt, enabling it to become plastic and migrate upwards. It requires relatively little added pressure, with only a few hundred meters of overburden necessary for it to act plastic (Fossen, 2010). The plastic salt will migrate upwards through thin or weak zones in the overburden, resulting in deformation and fracturing of the strata (Figure 1.3) (Nichols, 2009). The mobility of the salt is influenced by its chemical composition (James & Dalrymple, 2010). As the salt pierces through the overburden and migrates from its original position, the adjacent overburden will subside to fill the space left behind by the salt, generating rim synclines (Trusheim, 1960; Giles and Rowan, 2012; Rojo and Escalona, 2018). The subsidence of the overburden is commonly compensated by infilling of new sediments above. The different structures resulting from the migration of salt and subsequent deformation of strata are collectively termed salt diapirs, and these are classified according to their shape by, as linear structures (salt canopy, wall, anticline, and roller) and circular structures (salt pillows, stocks, glaciers and sheets) (Figure 1.4) (Fossen, 2010).

# 1 Introduction

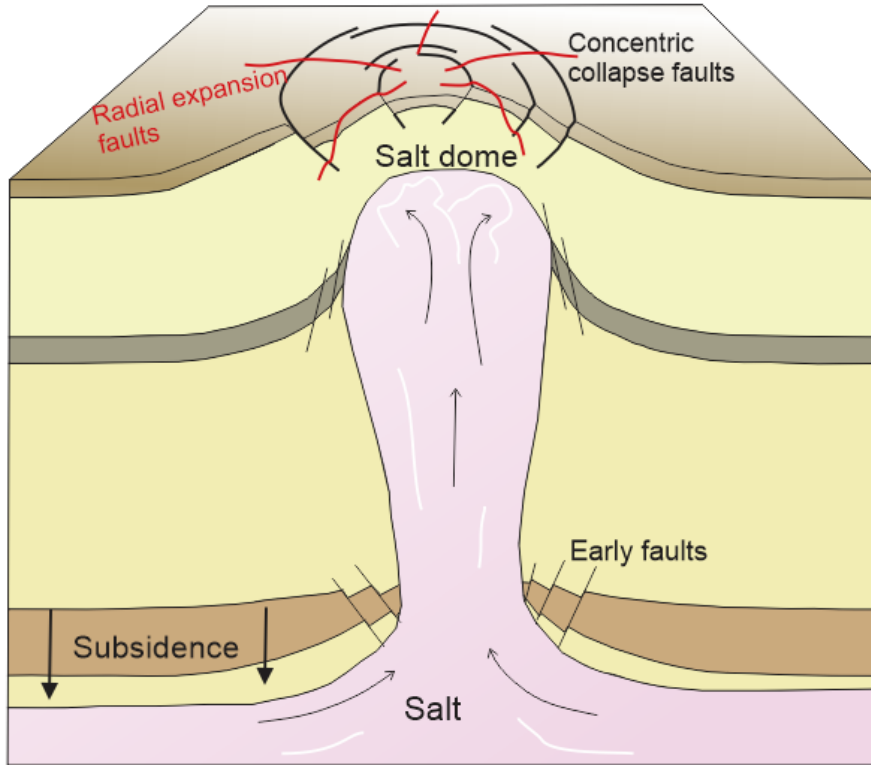


Figure 1.3: Illustration of salt migrating to form a salt diapir and the most common adjacent structures. Figure modified from Fossen (2010).

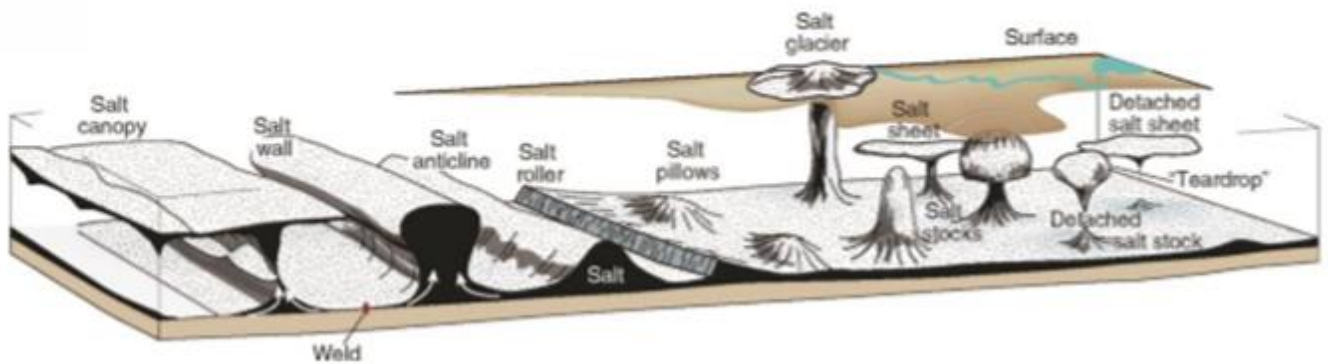


Figure 1.4: Classification of salt structures from their morphology. Circular structures are shown to the right, while linear structures are shown to the left. Figure from Fossen (2010).

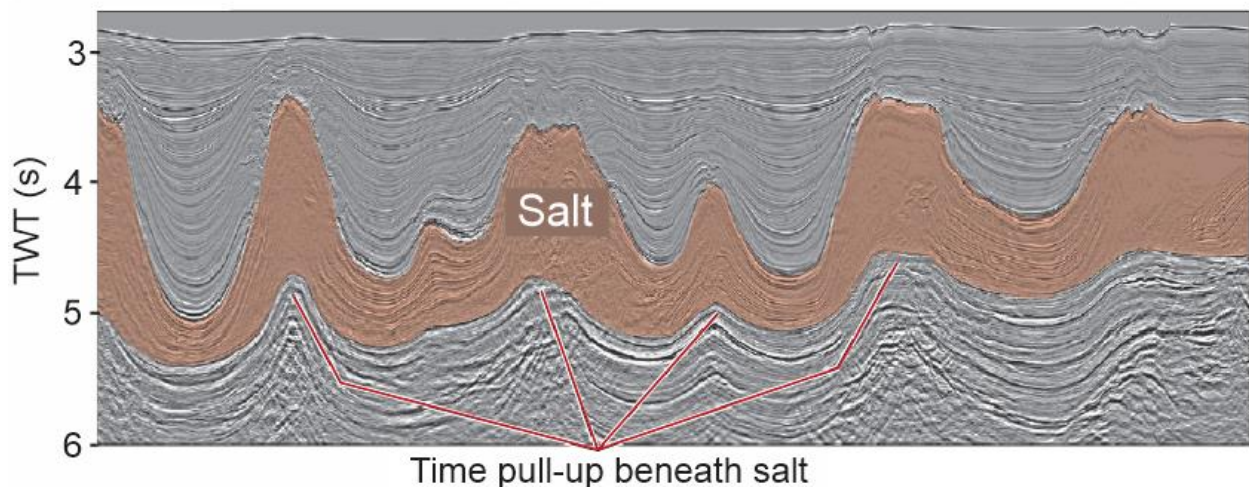


## 1 Introduction

### 1.3.3 Seismic imaging

The visualization of salt in seismic data presents some challenges, and though the seismic acquisition and processing techniques have been vastly improved the last decades, there are still some challenges. A salt body has a constant density and velocity with increasing depth, with the P-wave velocity of halite and anhydrite being 4500 m/s and 6500 m/s respectively (Fossen, 2010). Though there may be some impurities in the salt, the velocity is generally much higher than that of the surrounding water saturated shales and sandstones (1500-2000 m/s). The large contrast may cause velocity distortions in the seismic data, such as pull-up effects. When the seismic waves propagate through the salt body at such a high speed, the interface at the strata below the salt may appear at a shallower depth than the adjacent sediments in the time domain (Figure 1.5) (Jackson & Hudec, 2017).

There are also several challenges with imaging and interpreting salt bodies, related to their complex morphology. The morphology of the diapir may change a lot laterally, giving uncertainties during interpretation, especially if the area is poorly imaged. In addition, the interface between the salt body and the surrounding rocks or sediments is commonly quite steeply dipping (Figure 1.3). This complicates the seismic imaging of the salt structure (Jackson & Hudec, 2017). Fault complexes around and above the salt diapirs are also common, and may cause uncertainty for interpretation near the salt body (Fossen, 2010), and need to be considered when interpreting seismic images. Variations in stress and pore pressure in the sediments surrounding the salt body may cause seismic velocity anisotropy, something that may be challenging to correct for during processing of the seismic data (Jackson & Hudec, 2017).



*Figure 1.5: Seismic section illustrating the pull-up effect that salt bodies may cause seismic data to have in the time-domain. The interface below the salt appears at a shallower depth than what the reality is due to the high velocity of the salt. Figure modified from Jackson & Hudec (2017).*



## 2 Geological background

### 2.1 Tectonic development

#### 2.1.1 Paleozoic

The Paleozoic tectonic development of the Barents Sea is defined by two main events; the Caledonian orogeny (Late Silurian – Early Devonian) and the extensional regime that followed. Converging plates and compressional tectonics resulted in the collision of the Laurentian (present day Greenland and North America) and Baltic (present day Norway) tectonic plates. The subsequent closing of the Iapetus Sea and collision of continental margins resulted in the formation of the Caledonian orogenic belt (Dorè, 1995; Gabrielsen et al., 1990; Worsley, 2008). Following the orogeny, an extensional collapse and rifting during Late Devonian to Mid-Permian formed several fault-bounded basins and highs in western parts of the Barents Sea shelf, such as the Tromsø, Bjørnøya, Nordkapp, Fingerdjupet, Maud and Ottar basins (Faleide et al., 2015).

#### 2.1.2 Mesozoic

At the onset of the Mesozoic, the landmasses on Earth were gathered in the Pangaea supercontinent. The Barents Sea was at this time located at approximately 50-55°N, in the northern region of the supercontinent (Ryseth, 2014). The rifting that started in Late Devonian continued into the Early Triassic, but other than the subsidence related to this, the period from Early Triassic to Mid-Jurassic is defined as a tectonically calm period in the western Barents Sea (Glørstad-Clark et al., 2010; Smelror et al., 2009). Passive, regional subsidence has been described on the Bjarmeland and Finnmark platforms (Henriksen et al., 2011a).

From Mid-Jurassic to Early Cretaceous regional extension continued, resulting in further opening of the basins formed during the Paleozoic (Faleide et al., 1993). Fragmentation of Pangaea that began during the Triassic reached a maximum during the Jurassic, forming new continents and basins as the supercontinent split up. Due to sea floor spreading between the Canada and Makarov basins in relation to the opening of the Amerasian basin in the Arctic Ocean, the high Arctic underwent several stages of rifting, magmatism and sedimentation during this time (Dorè, 1995; Corfu et al., 2013).

During Barremian to Aptian times, the Barents Sea shelf was dominated by magmatic activity, leading to the development of the High Arctic Large Igneous Province (HALIP) (Corfu et al., 2013). Cretaceous igneous rocks from this period have been found on Svalbard, Franz Josef Land and in the subsurface of the adjacent shelf (Nejbert et al., 2011). Evidence of the HALIP in the form of igneous rocks have also been found in the northeastern and southeastern Barents Sea, showing the large extent of the province (Polteau et al., 2015). The extensional regime and magmatic activity during the Early Cretaceous resulted in uplift of the northern Barents Sea shelf, tilting the strata southwards.

## 2 Geological background

### 2.1.3 Cenozoic

The Barents Seas complex development during the Cenozoic is highly influenced by rifting and extension related to the opening of the Norwegian Greenland Sea (Faleide et al., 2008; Lasabuda et al., 2018a). Rifting along the Norwegian margin spread northwards during this time, resulting in transform movement and later extension along the western Barents Sea margin (Kristoffersen & Talwani, 1977). The western Barents Sea margin saw transpression, extension and transtension during the early stages of the opening of the Norwegian Greenland Sea (Nøttvedt et al., 1988; Faleide et al., 2008). Simultaneously, the eastern and northern Barents Sea shelf experienced uplift (Smelror et al., 2009). The onset of spreading is estimated to be the Paleocene-Eocene transition, based on magnetic polar reversals (Talwani & Eldholm, 1977).

In the early Oligocene, reorganization of the spreading plates caused the Greenland and north-American plates to move in the same direction, leading to extension and subsequent seafloor spreading along the Norwegian-Greenland margin. In Miocene, the Barents shelf was tectonically quiescent (Ryseth et al., 2003), while the sea floor spreading opened the Fram Strait (Kristoffersen et al., 1990; Engen et al., 2008).

## 2.2. Stratigraphy and depositional environment

### 2.2.1 Paleozoic

During the rifting that occurred from the Late Devonian, syn- and post-rift sedimentation occurred, filling the newly formed basins. Later, during the late Carboniferous and early Permian the depositional environment was dominated by shallow marine and subaerial settings. Carbonates were deposited during high stand, while during low stand large areas were left exposed, resulting in deposition of thick evaporite successions (Figure 2.1) (Worsley, 2008). As the Barents Sea moved further north due to continental drift, the depositional environment transitioned from a warm water carbonate platform to a cold one closer to the Late Permian.

## 2 Geological background

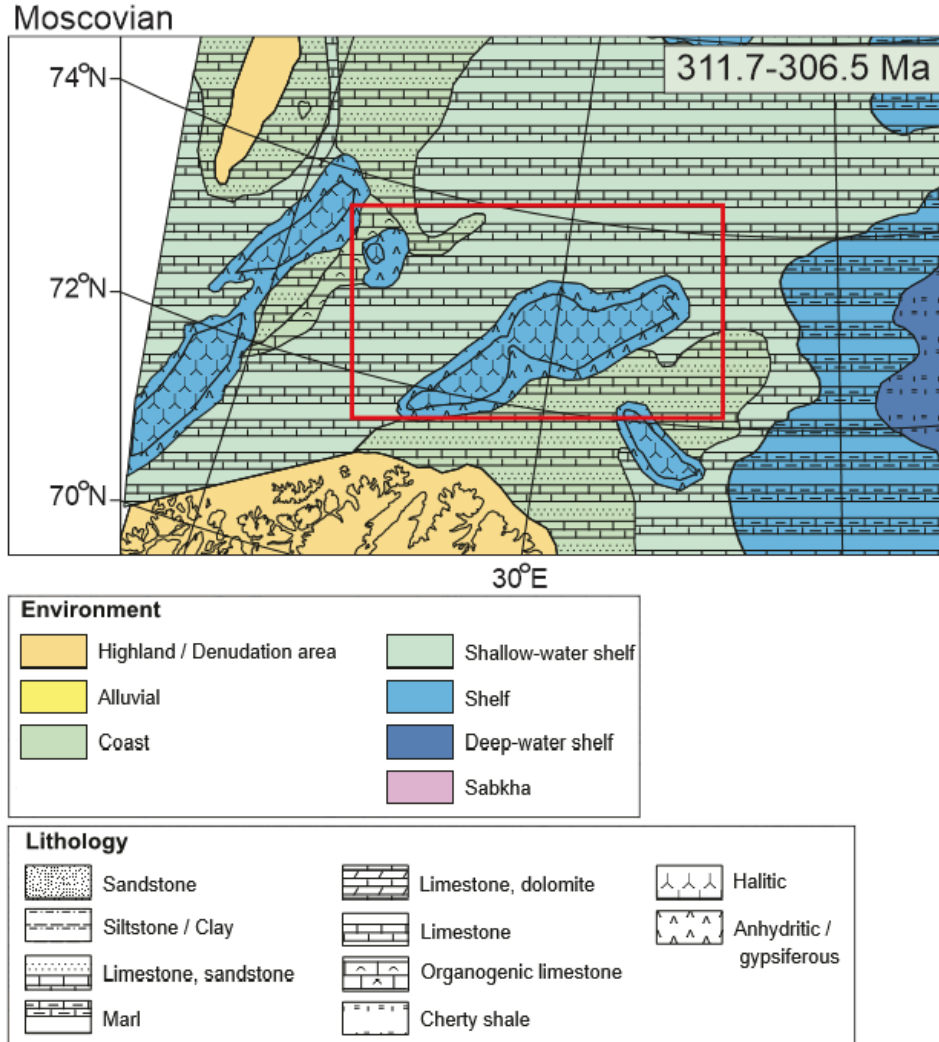


Figure 2.1: Paleo-map of the southwestern Barents Sea shelf showing the depositional environment during late Carboniferous, when the study area (outlined in red) experienced shallow water conditions with evaporitic deposition. Modified from Smelror *et al.* (2009).

### 2.2.2 Mesozoic

The Barents Sea saw several cycles of regressions and transgressions related to the tectonic development of the region during the Mesozoic, which heavily influenced the sea level and sediment supply. In the Triassic period, high subsidence and sedimentation rates dominated the shelf. The uplifted Uralian highlands, Novaya Zemlya and the Fennoscandian shield supplied the shelf with sediments, that prograded towards the basins in the west (Riis *et al.*, 2008), while the south was an area of denudation (Figure 2.2). The transition from Upper Triassic to Lower Jurassic is marked by observably more condensed sediment successions in the southwestern Barents Sea. The Upper Triassic was characterized by high subsidence and sedimentation rates, while the rates were lower during deposition of Lower Jurassic (Smelror *et al.*, 2009; Ryseth, 2014).

## 2 Geological background

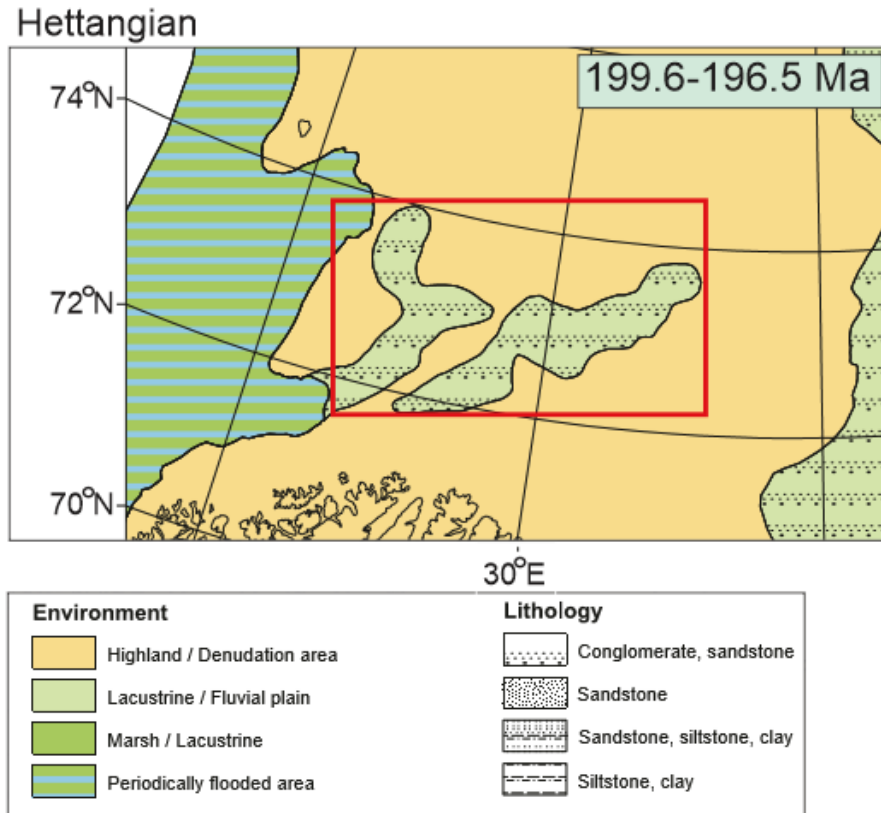


Figure 2.2: Paleo-map of the southwestern Barents Sea shelf during Lower Jurassic, showing how large parts were areas of denudation, while parts of the study area (outlined in red) was dominated by lacustrine clastic deposition. Modified from Smelror et al. (2009).

A shift in depositional environment occurred throughout the Jurassic, starting with a Norian flooding in the Late Triassic which was followed by a shoreline regression in the Early Jurassic. This resulted in widespread deltaic and eventually alluvial depositional environments (Klausen et al., 2017). The regression reached its maximum during the Hettangian-Sinemurian and was followed by a regional transgression that dominated the Middle Jurassic. During this time, the shoreline retreated landwards (Klausen et al., 2017). The sea level continued to fluctuate through the Middle and Late Jurassic. A regression in Middle Jurassic exposed the shelf to erosion, resulting in an unconformity observable on seismic data across large parts of the central and western Barents Sea (Smelror et al., 2009). Another transgression followed towards the end of the Jurassic, establishing a marine environment across the Arctic (Sømme et al., 2018). During the Jurassic-Cretaceous transition, the uplift of the northern Barents Sea caused a forced regression in the Svalbard region (Gjelberg & Steel, 1995; Worsley, 2008). The uplift was related to the opening of the Amerasia Basin and development of the HALIP. As a result, eroded sediments from the uplifted highland prograded southwards were a shelf-environment dominated (Figure 2.3) and were deposited as clinofolds (Worsley, 2008; Glørstad-Clark, 2011).

## 2 Geological background

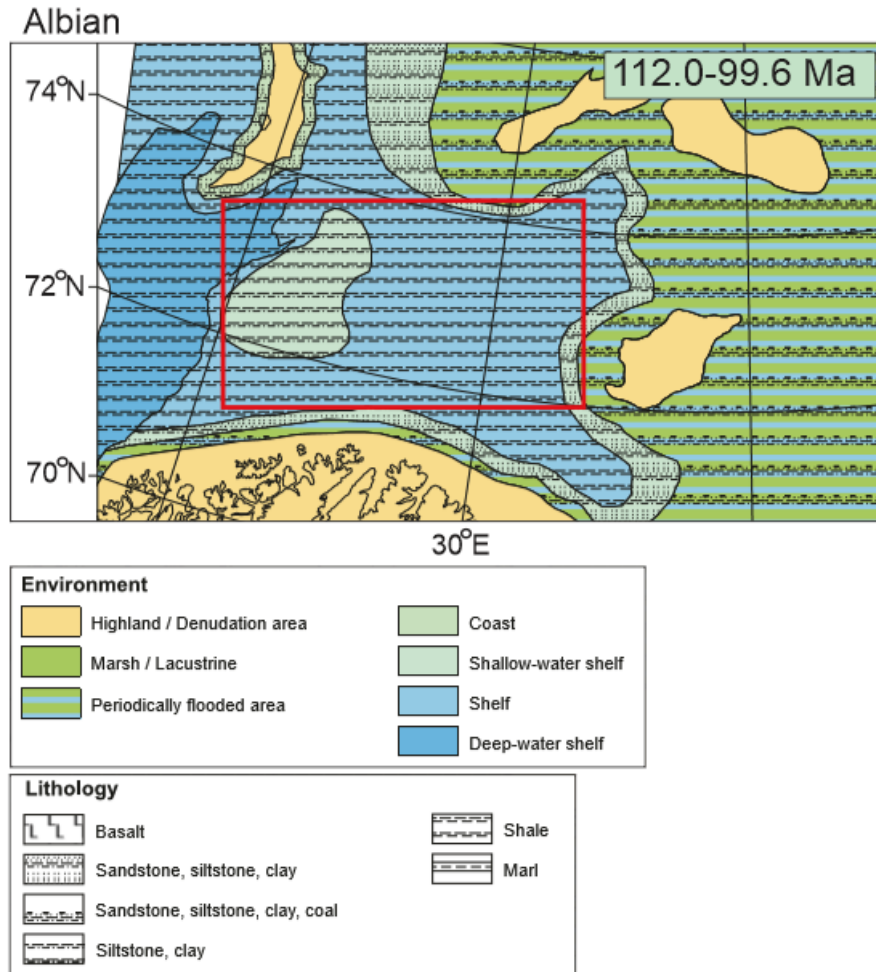


Figure 2.3 Paleo-map showing the depositional environments on the Barents Sea shelf during the end of the Lower Cretaceous, where the study area (outlined in red) experienced a shelf-environment during this period. Modified from Smelror et al. (2009).

Overall, the evolution of the Barents Sea shelf is complex, and the region was influenced by a combination of different depositional environments and climatic conditions. The main stratigraphy and evolution of the study area on the shelf is summarized in figure 2.4 below, along with the main phases of halokinesis. The salt-related evolution of the study area is described in more detail in chapter 2.4.

## 2 Geological background

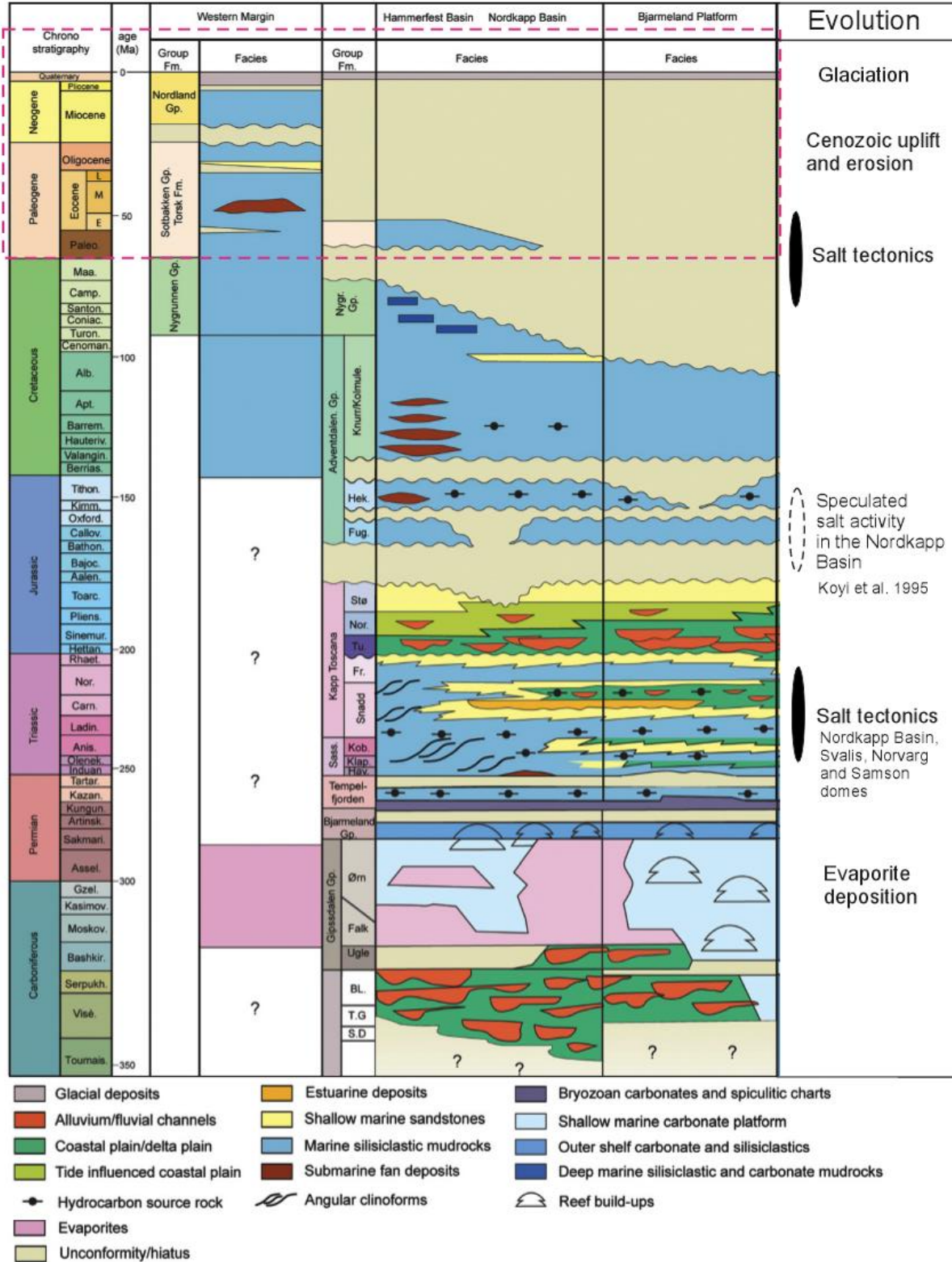


Figure 2.4: Stratigraphic chart showing the main events and depositional environments of the southwestern Barents Sea, as well as the main stages of halokinesis. Modified from Henriksen et al. (2011a). The part of the stratigraphy that is the focus of this study is outlined by the dotted purple rectangle. Note the pronounced unconformity after the Cretaceous deposition.



## 2 Geological background

### 2.3 Cenozoic uplift and erosion

The early Cenozoic depositional environment of the Barents Sea shelf was greatly influenced by the opening of the Norwegian-Greenland Sea to the west. Seafloor-spreading gradually expanded northwards along the margin and extension furthered basin-development on inner parts of the southwestern shelf (Lasabuda et al., 2018a). During the Eocene, most of the shelf was a highland exposed to erosion, while the southwestern shelf was a low relief area that received large sediment quantities from the uplifted highland (Rasmussen and Fjeldskaar, 1996; Butt et al., 2002). In the Oligocene and Neogene, the northwestern Barents Sea experienced increased uplift, and became the main sediment source to subsiding basins near the western margin (Smelror et al., 2009; Faleide et al., 2015; Lasabuda et al., 2018a). The highland supplied thick successions to the shelf, consisting of relatively unconsolidated and easily erodible sediments (Laberg et al., 2012). These sediments were mostly removed during late Cenozoic glacial erosion, and thus the present distribution of Cenozoic strata is limited to the westernmost basins. Paleogene strata have been observed in the Nordkapp Basin, but are eroded on adjacent platforms (Henriksen et al., 2011a).

Several studies have presented estimations of the total average Cenozoic erosion in the wider Barents Sea (Henriksen et al. 2011b; Ktenas et al. 2017). Henriksen et al. (2011b) presented a net erosion map for the wider Barents Sea, suggesting a total erosion between 900-1400 meters in the southwestern Barents Sea region. The majority of the erosion is suggested to be due to glaciations during the Late Cenozoic (Vorren et al., 1991; Knies et al., 2009; Laberg et al., 2010). This is inferred from trough mouth fans along the shelf edge comprising large amounts of glacial sediments (Vorren et al., 1991; Faleide et al., 1996; Laberg et al., 2010). However, a considerable amount of pre-glacial sediments overlying the oceanic crust along the shelf edge indicates a significant pre-glacial erosion component (Vorren et al., 1991; Fiedler and Faleide et al., 1996; Hjelstuen et al., 1996).

#### 2.3.1 Pre-glacial erosion

The pre-glacial erosion of the shelf is suggested to have a tectonic and thermal origin (Wood et al., 1989), related to the opening of the Norwegian-Greenland Sea (Smelror et al., 2009). During the Paleocene, the Stappen and Loppa highs and parts of the Bjarmeland Platform were exposed to erosion and supplied sediments to the developing continental slope in the west (Figure 2.5a) (Vorren et al., 1991; Lasabuda et al., 2018a). Meanwhile, shallow marine to shelf conditions dominated in the Nordkapp Basin (Figure 2.5a). From the Paleocene-Eocene transition, the structural highs and the margin west of Svalbard served as sediment sources. The southwestern source area is assumed to have expanded eastwards, with larger parts of the Bjarmeland and also Finnmark Platform experiencing erosion and shedding sediments to adjacent basins (Figure 2.5b) (Vorren et al., 1991; Lasabuda et al., 2018a). At the end of the Eocene, the Nordkapp Basin was surrounded by exposed highs, but still experienced a shallow marine setting (Figure 2.5b).

## 2 Geological background

The basin experienced more uplift during the Oligocene, and by the end of the period the northeastern part of the basin became an area of non-deposition (Figure 2.5c). Erosion of the adjacent highs continued during the Oligocene and into Miocene, with an increase in erosion of the northwestern margin (Vorren et al., 1991; Lasabuda et al., 2018a). Lasabuda et al. (2018b) found the erosion rate in the northwestern Barents Sea to be two times higher than in the southwestern region, implying a more tectonically active northwestern margin, with more extensive erosion. Therefore, a general northwards increase of pre-glacial erosion is inferred (Lasabuda et al., 2018b).

The Neogene erosion of the shelf is assumed to have been focused within the same areas as during the Oligocene (Figure 2.5d) (Lasabuda et al., 2018a). The study area experienced significant erosion, including the Loppa High and the Bjarmeland Platform. The northeastern Nordkapp Basin was also an exposed area of non-deposition, while the southwestern part was a fluvial or coastal plain that experienced some sediment accumulation (Figure 2.5d). Paleogene sediments have been found within the Nordkapp Basin, but are eroded across the adjacent platforms (Henriksen et al., 2011a).

Vorren et al. (1991) suggested an average of 600-1200 meters of pre-glacial erosion in the southwestern Barents Sea during Eocene-Miocene, which was later also concluded in a study by Richardsen et al. (1993). Recent studies by Lasabuda et al. (2018a) found the average pre-glacial erosion to be between 858-1362 meters.

## 2 Geological background

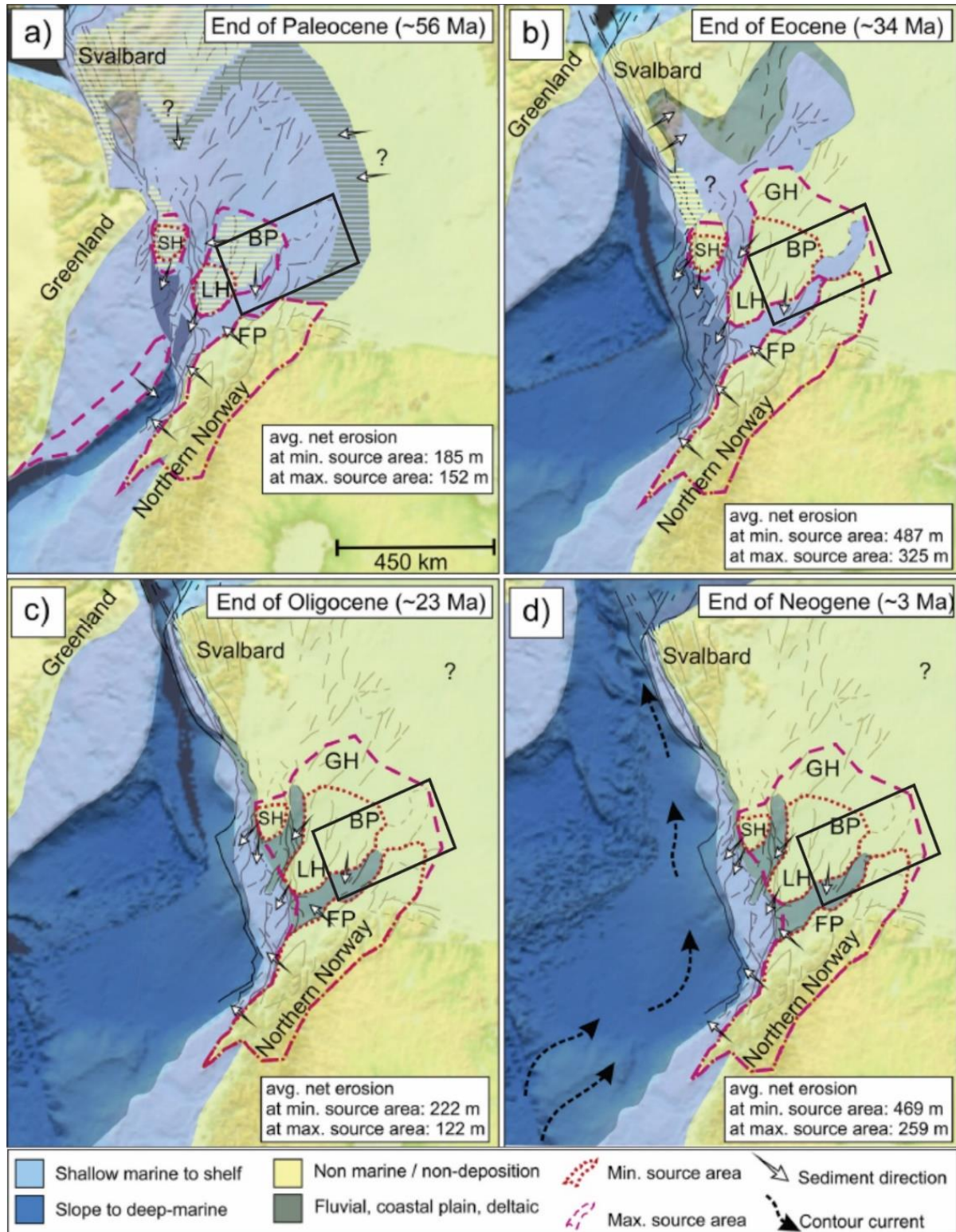


Figure 2.5: Paleoenvironmental reconstruction of the southwestern Barents Sea during the Cenozoic. Please note that maximum size of the source area corresponds to the minimum estimate of average erosion, and vice versa. Study area outlined by the black rectangle. Figure modified from Lasabuda et al. (2018a). BP = Bjarmeland Platform, FP = Finnmark Platform, GH = Gardarbanken High, SH = Stappen High, LH = Loppa High.

## 2 Geological background

### 2.3.2 Glacial history

#### *Plio-Pleistocene glaciations*

The erosion of the shelf during the Plio-Pleistocene was predominantly from glacial activity, where ice sheets repeatedly reached the shelf edge in the Barents Sea (Vorren et al., 1989; Laberg & Vorren, 1996; Dowdeswell & Cofaigh, 2002). Three major glacial phases have been identified in the Barents Sea during the Pliocene-Pleistocene period (Knies et al., 2009; Smelror et al., 2009).

The first phase lasted from 3.5-2.4 Ma, during which the glacial cover was restricted to Svalbard and Novaya Zemlya, and only reaching the coastline and shelf edge in the northern Barents Sea (Figure 2.6a) (Knies et al., 2009; Smelror et al., 2009). The second phase occurred between 2.4-1 Ma, and during this period the ice sheets repeatedly expanded on the Barents Sea shelf (Figure 2.6b) (Knies et al., 2009).

During the third and last phase, glaciations were more extensive and the ice sheet covered the entire shelf (Figure 2.6c). The glaciations had a 100,000 year frequency during the last 1 Ma and it is suggested that the Barents Sea experienced at least five to six shelf edge glaciations the last 800 Ka (Smelror et al., 2009, Knies et al., 2009).

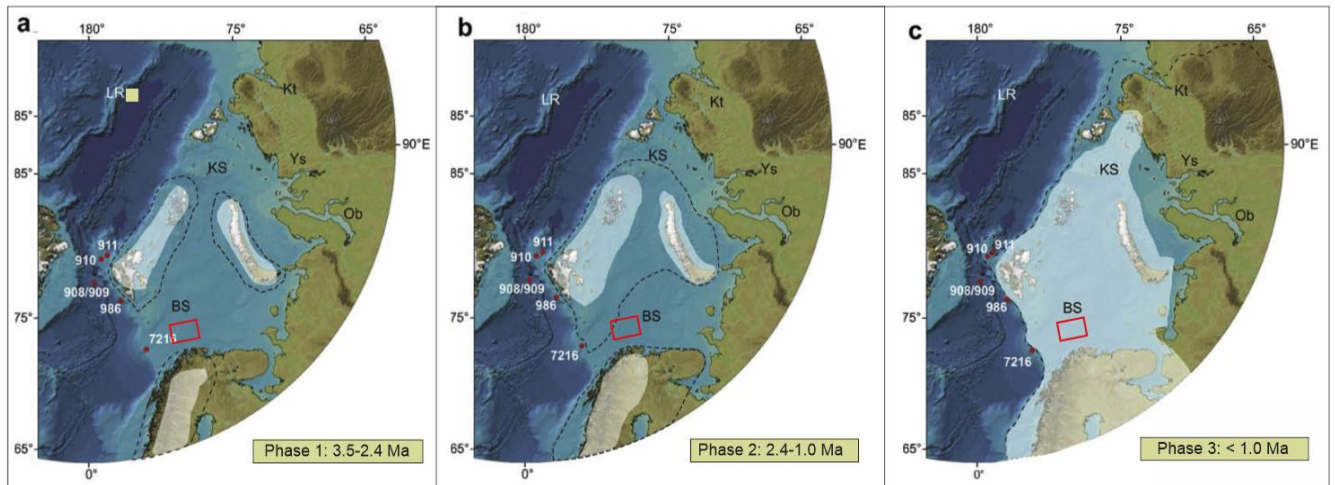


Figure 2.6: Reconstruction of timing and extent of ice sheets during the Late Cenozoic. Three phases of glaciations with various extent are illustrated: a) 3.5-2.4 Ma, b) 2.4-1.0 Ma, c) < 1.0 Ma. The study area is outlined in red. Modified from Knies et al. (2009).

## 2 Geological background

### *The last Ice age – Weichselian*

The last ice age in the Barents Sea region has been divided into three major phases of glaciation (Mangerud et al., 1998; Svendsen et al., 2004a; Svendsen et al., 2004b) during the early, middle and late Weichselian. There are however some discrepancies regarding the timing and extent of glacial activity. Larsen et al., (2006) suggested four major glaciations, dividing the mid-Weichselian in two phases.

The early Weichselian phase occurred from approximately 100-90 Ka (Larsen et al., 2006). During this phase, there was an extensive ice coverage above Svalbard, Novaya Zemlya and the Kara Sea in the east, while Scandinavian Ice Sheet was mostly land-based (Figure 2.7a). The two ice sheets were separated by a passage of open water, leaving the central Barents Sea relatively ice free. The second glacial phase lasted from approximately 70-65 Ka, and during this time both ice sheets experienced growth, resulting in one large ice sheet covering the entire Barents Sea (Figure 2.7b) (Larsen et al., 2006). A third glaciation is suggested to have occurred from 55-45 Ka, where the shelf was again ice free while Scandinavia and the Kara Sea was covered by ice sheets (Figure 2.7c). The last phase in the late Weichselian lasted from 25-10 Ka and was the most extensive glaciation in the region during the last ice age. The ice sheet covered Svalbard, Scandinavia, the entire Barents Sea shelf and extended across parts of the British Isles (Figure 2.7d) (Larsen et al., 2006). The ice is estimated to have reached the shelf edge on at least two occasions during this time (Laberg and Vorren, 1995; Laberg and Vorren, 1996) and ice sheet modelling suggests a maximum thickness of anywhere between 1000 (Siegert and Dowdeswell, 2002) and 2000 meters on the Barents sea shelf (Landvik et al., 1998).

## 2 Geological background

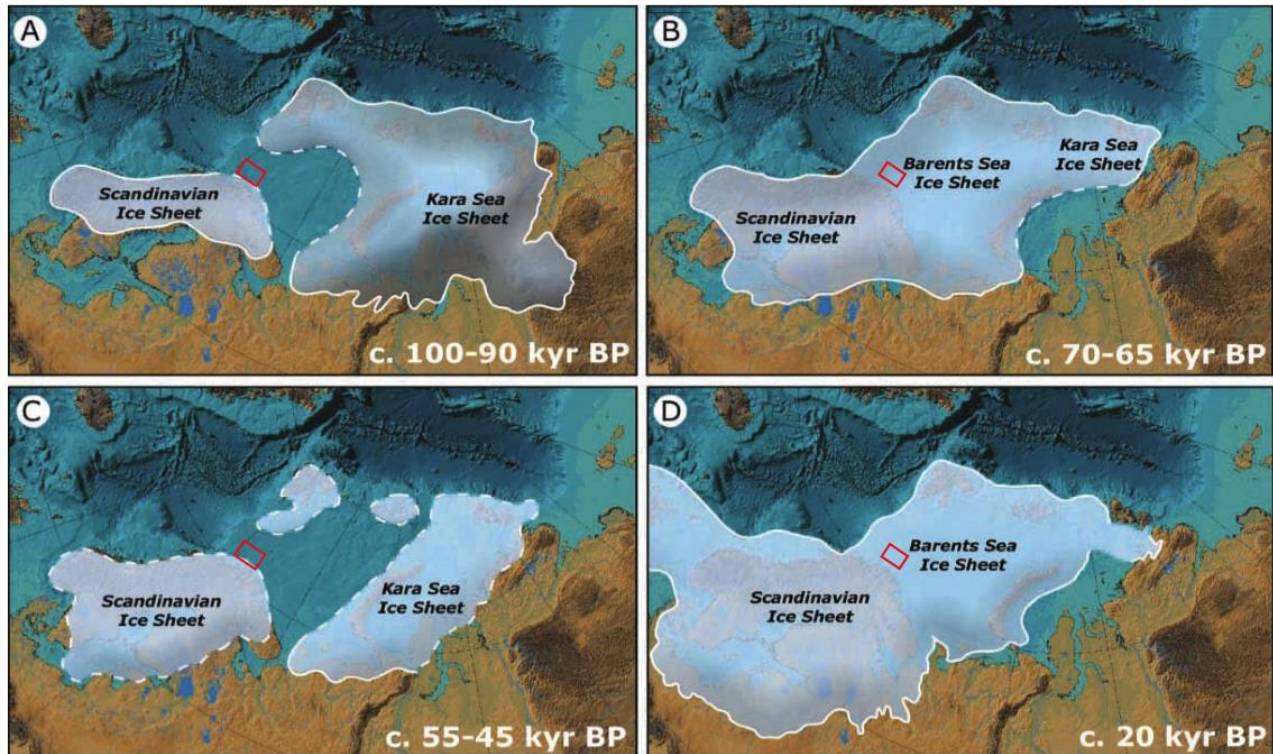


Figure 2.7: Reconstruction of ice sheet extent during Weichsel. a) 100-90 ka BP, b) 70-65 ka BP, c) 55-45 ka BP, d) ca. 20 ka BP. Study area is marked by the red square. Modified from Larsen et al. (2006).

### Glacial erosion

Extensive glacial erosion of the Barents Sea shelf during the late Cenozoic is evidenced by trough mouth fans on the continental slope along the western shelf margin (Lasabuda et al., 2018a), which comprise large volumes of glacial sediments (Vorren and Laberg, 1997; Laberg et al., 2010). The sediments were mainly eroded by fast-flowing ice streams, which drained the ice sheet that periodically covered the shelf (Laberg et al., 2010). Deep erosion occurred beneath the ice streams, forming cross-shelf troughs on the seafloor that characterize the present bathymetry of the Barents Sea shelf (Laberg et al., 2010). The ice streams were separated by areas of more stagnant ice, where the erosion was less efficient, forming shallow banks between the deeper troughs (Andreassen et al., 2007; Ottesen et al., 2008). The largest of the Weichselian ice streams was the Bear Island Ice stream (Figure 2.8), which eroded a deep cross-shelf trough on the seafloor.

There are multiple studies presenting estimates of the total net glacial erosion in the Barents Sea (e.g. Vorren et al., 1991; Laberg et al., 2010; Laberg et al., 2012; Henriksen et al., 2011b). Glacial erosion of the shelf during the Pleistocene can be divided in three phases with different erosional processes as the main influence on the shelf. In the early Pleistocene, the Scandinavian continent and the Svalbard archipelago were the areas most subjected to erosion (Vorren et al., 1991), and the main process on the shelf from 2.7-1.5 Ma was glaciofluvial erosion (Laberg et al., 2012). It was concentrated in the southwestern part of the shelf

## 2 Geological background

(Figure 2.9a) and resulted in 170-230 m erosion (Laberg et al., 2012). From 1.5-0.7 Ma subglacial erosion beneath paleo ice streams dominated and affected an area of  $\sim 575,000 \text{ km}^2$  (Laberg et al., 2012). Erosion was highest beneath ice streams, but also affected the banks, as ice flow was not strictly restricted to troughs on the shelf. An estimate of 330-420 m of erosion occurred on the southwestern shelf during this time (Figure 2.9b). During the last 0.7 Ma, erosion was concentrated in glacial troughs (Figure 2.9c and d) and resulted in the removal of 440-530 m of strata.

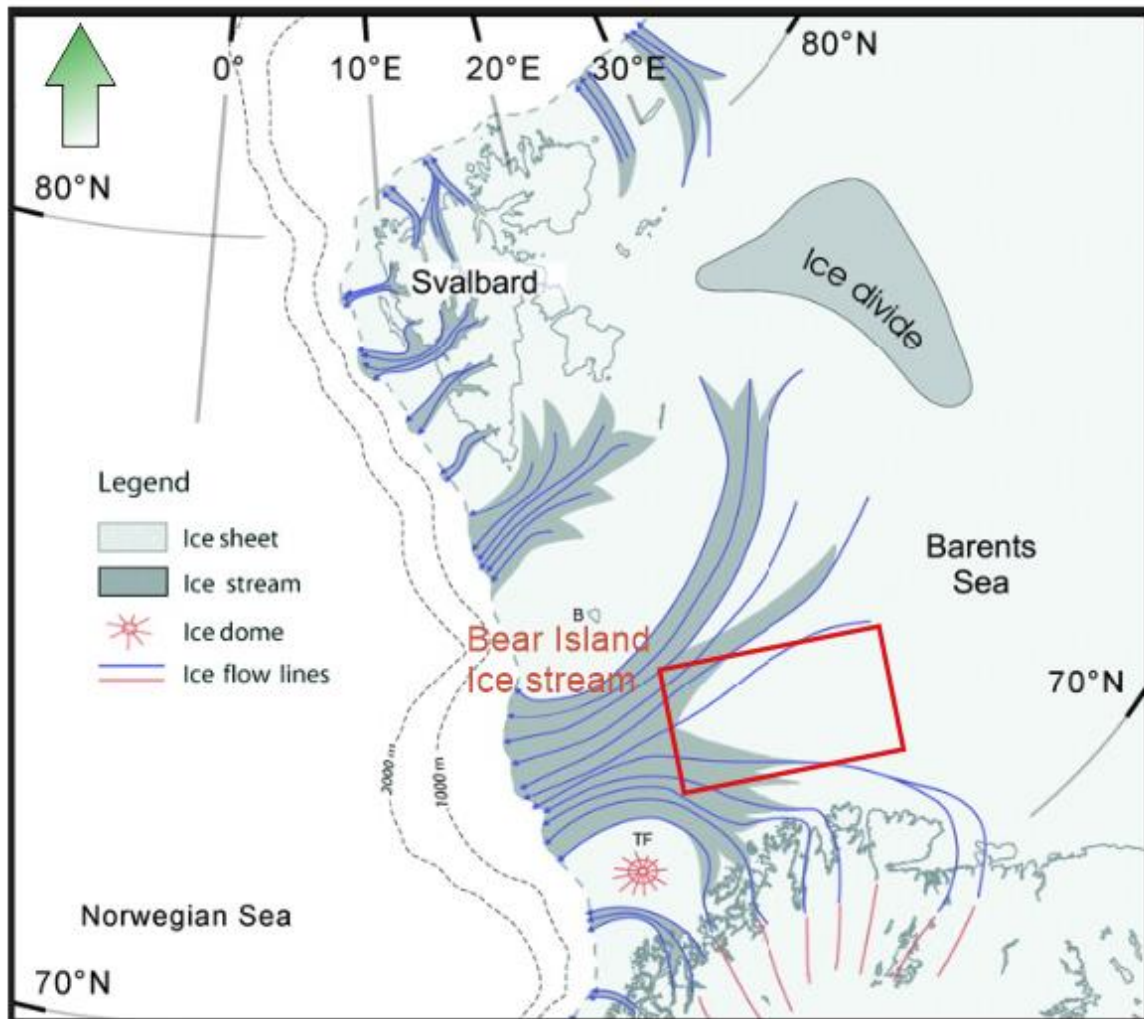


Figure 2.8: Illustration showing the late Weichselian Ice sheet flow-regime in the Barents Sea, with several ice streams separated by areas of stagnant ice dominated the shelf. The red square outlines the study area. Figure modified from Ottesen et al. (2005).

## 2 Geological background

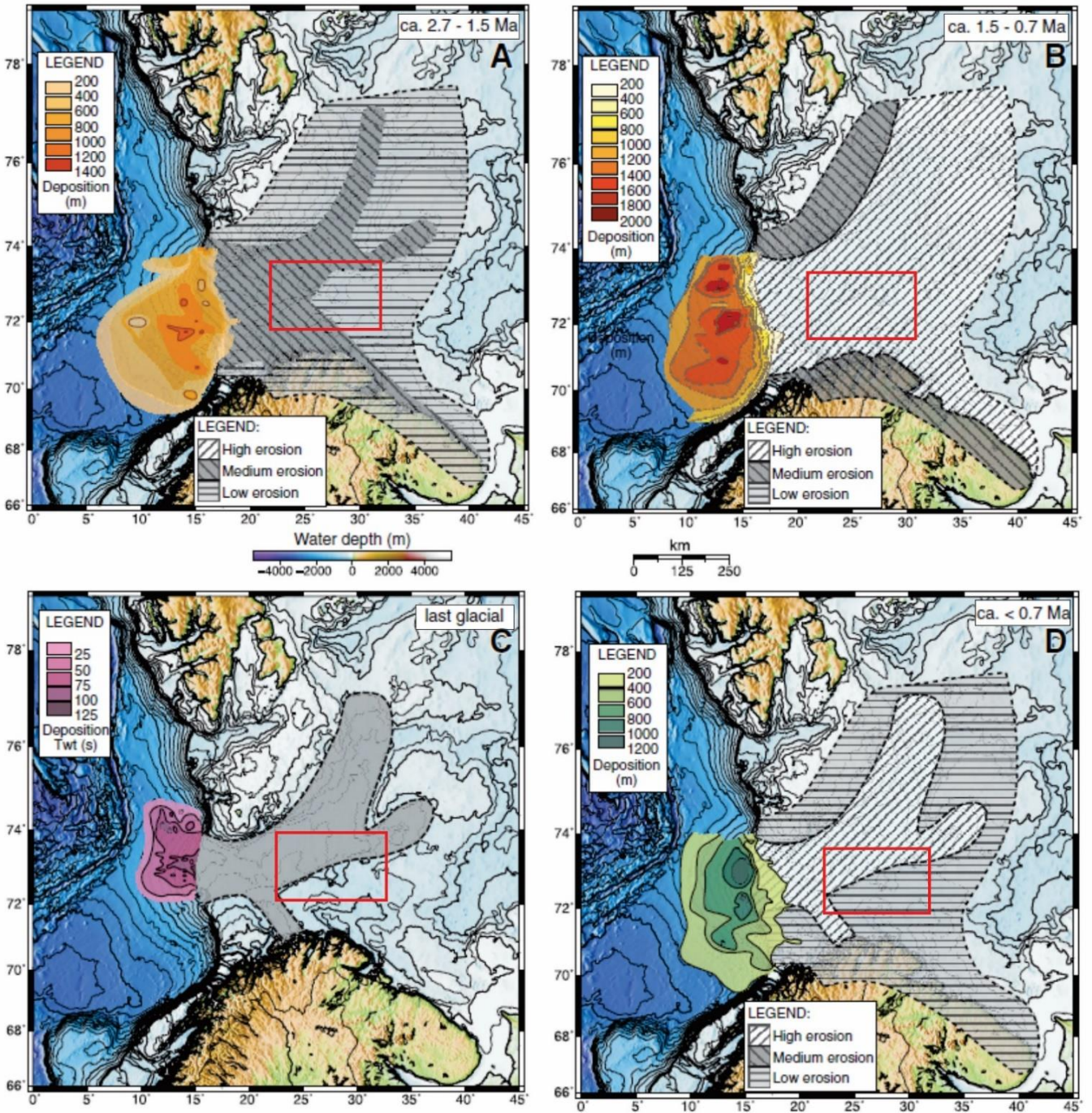


Figure 2.9: Model showing a) the areas affected by glaciofluvial erosion from 2.7-1.5 Ma, b) areas affected by subglacial erosion from 1.5-0.7 Ma, c) isopach map (from Laberg and Vorren, 1996) showing the amount of glacial deposition during the latest two glacial maximums and d) the areas of glacial erosion during the last 0.7 Ma, when erosion was confined to fast-flowing ice streams. The study area is outlined by the red square. Figure modified from Laberg et al. (2012).



## 2 Geological background

### 2.3.3 Late Cenozoic seismic stratigraphy

#### *Upper Regional Unconformity (URU)*

The Upper Regional Unconformity (URU) separates the Quaternary sediments from underlying strata in the Barents Sea (Vorren et al., 1986; Andreassen et al., 2007). The unconformity is a result of the uplift and extensive erosion of the entire Barents Sea, when sediments were re-deposited to the west (Vorren et al., 1991; Henriksen et al., 2011b). The unconformity represents the lowermost erosional surface for the glaciations on the Barents Sea shelf and cuts underlying strata, thus it is a pronounced reflector across most of the shelf on seismic data due to the contrast in acoustic impedance between the glacial sediments and underlying bedrock. Mesozoic strata sub-crops the unconformity from the eastern Hammerfest basin to the Pechora Sea in the east and are truncated on major structural highs across large areas on the shelf (Henriksen et al. 2011b). A detailed study of the unconformity by Lebesbye and Vorren (2000) found that the URU comprises three main morphological elements: troughs and depressions, large low-relief plains, and terrace-like landforms of glacial origin. The unconformity is diachronous, varying in age laterally, as it represents the lowermost erosion of the glaciations.

#### *Glacigenic sediments*

Above the Upper Regional Unconformity, glacigenic sediments were deposited underneath and in front of the Quaternary ice sheets. The glacial sequence varies in thickness, ranging from 0-300 meters on the shelf, up to 1000 meters at the shelf edge (Vorren et al., 1991). On the continental slope, the glacial deposits can be several kilometers in thickness, reaching up to 4.5 km thickness in the Storfjorden Fan (Hjelstuen et al., 1996). The spatial distribution and internal structures also varies, depending on what glacial-related process deposited the sediments. Glacigenic sediments are usually poorly sorted and deposited in a chaotic matter. Some internal horizons may be recognized, representing erosional truncations within the sequence, but glacial deposits are generally seismically transparent due to a lack of significant structures.

## 2 Geological background

### 2.4 Structural setting

#### 2.4.1 Nordkapp Basin

The Nordkapp Basin is a deep, narrow salt basin located in the southwestern Barents Sea (Figure 2.10). It is divided into a southwestern and northeastern sub-basin, respectively. The basin is inferred to have formed during Early-Middle Carboniferous following the Caledonian orogeny, based on observed graben-and half-graben structures in the basement (Stemmerik and Worsley, 1989; Dengo and Røssland, 1992; Gabrielsen et al., 1992; Smelror et al., 2009).

The basin was a depocenter during the Carboniferous and Permian, and evaporite and carbonate successions were deposited in large quantities during this time. The thickness of the evaporite successions is estimated to vary from 2.0-2.5 km in the southwestern sub-basin to 4.0-5.0 km in the northeastern one, where the basement subsidence was greater (Bergendhal, 1989; Jensen and Sørensen, 1992). Late Permian carbonates and Triassic siliciclastic deposits buried the evaporites (Gabrielsen et al., 1992; Jensen and Sørensen, 1992). The added load on the salt caused it to start migrating and form salt diapirs (NPD, 2013).

The timing of active diapir rising in the basin has been discussed in several studies (Gabrielsen et al., 1990; Koyi et al., 1995; Nilsen et al., 1995; Bugge et al., 2002; Grimstad, 2016) and is probably related to regional tectonics. Koyi et al. (1995) suggest that the diapirs extruded as salt overhang during the Jurassic, and that they were subsequently buried during the Cretaceous, before being reactivated during the Cenozoic. Grimstad (2016) presents an opposing view, with no salt movement occurring in the basin during the Jurassic and Early Cretaceous, but rather that the sedimentary successions were affected by reactivation of the diapirs during Late Cretaceous-Cenozoic. The exact timing of active diapir rise in the Cenozoic is especially difficult to identify due to the extensive glacial erosion in the Quaternary, when approximately 2000 meters of sediments are estimated to have been removed from the Nordkapp Basin and adjacent areas (Worsley, 2008; Smelror et al., 2009).

## 2 Geological background

### 2.4.2 Bjarmeland Platform

The Bjarmeland Platform is located north of the Nordkapp and Hammerfest basins (Figure 2.10) and bordered to the north by the Sentralbanken and Gardarbanken highs. The Loppa High and the Fingerdjupet Sub-basin define the western border of the platform (Gabrielsen et al., 1990). The platform has been tectonically stable since the Late Paleozoic, and was formed during the Late Carboniferous and Permian. The exception is during the Paleogene tectonism that tilted Paleozoic and Mesozoic sequences, causing southwards dipping of the strata (NPD CO<sub>2</sub> Storage Atlas, 2014). The Bjarmeland Platform is generally characterized by having relatively few structures. It does however comprise some structural elements such as minor highs and sub-basins influenced by salt tectonics (Gabrielsen et al., 1990; NPD CO<sub>2</sub> Storage Atlas, 2014) as the Samson and Norvarg domes.

### 2.4.3 Samson Dome

The Samson Dome is a structural high within the loosely defined Ottar Basin, located in the southwestern part of the Bjarmeland Platform (Figure 2.10) (Breivik et al., 1995). It formed due to Middle to Late Triassic halokinesis, after the basin acted as a Carboniferous and Permian evaporite and carbonate depocenter (Gabrielsen et al., 1990). It is one of two domes in the basin, the other one being the Norvarg Dome. Seismic data shows a lenticular body of salt at the base of the dome (Gabrielsen et al., 1990; Breivik et al., 1995) at approximately 8.5 km depth. The reason for the halokinesis is assumed to be an added sediment load, as a thick Late Paleozoic overburden is identified above the Upper Paleozoic evaporites (Breivik et al., 1995). Mattos et al. (2016) suggest that the main stage of halokinesis and anticline development occurred during the Late Cretaceous and early Cenozoic, causing radial faulting around the dome and uplift of the strata. However, the diapir did not reach the surface. At a later stage, salt dissolution caused subsidence of the diapir roof, as the overburden caused the structure to collapse. Extensive Cenozoic erosion later removed much of the overburden.

### 2.4.4 Norvarg Dome

Situated on the southwestern Bjarmeland Platform near the northeastern margin of the Swaen Graben (Figure 2.10), the Norvarg Dome is a structural high with a salt core (Gabrielsen et al., 1990). The evaporites at the core of the dome are estimated to be of late Carboniferous to early Permian age, similar to the ones of the Samson Dome (Gabrielsen et al., 1990). Periods of pre-Cretaceous doming are identified in the Mesozoic sediment sequences. The Cretaceous sequence is also domed and truncated by the Cenozoic Upper Regional Unconformity. Therefore, a reactivational doming of Late Cretaceous or early Cenozoic age is assumed (Gabrielsen et al., 1990; Breivik et al., 1995).

## 2 Geological background

### 2.4.5 Svalis Dome

Located in the southwestern Maud Basin, the Svalis Dome is a diapiric structure forming a positive relief on the seafloor relative to surrounding areas (Gabrielsen et al., 1990; NPD, 2013). The dome is bounded by the Loppa High to the south and west (Figure 2.10). Around the dome, Upper Paleozoic and Mesozoic rocks outcrop at the seafloor or beneath a cover of Quaternary sediments (Bugge and Fanavoll, 1995; Mørk and Elvebakk, 1999). The dome was rising actively in the Late Mesozoic, forming an anticline above the salt body. The present day positive relief is suggested to be due to a cap of Paleozoic silicified shales and carbonates, protecting the salt body from erosion, as they are more resistant than the surrounding softer Mesozoic siliciclastic rock (Nilsson et al., 1996; NPD, 2013). It is suggested that a continuous rise of active salt may contribute to the positive seafloor relief (NPD, 2013).

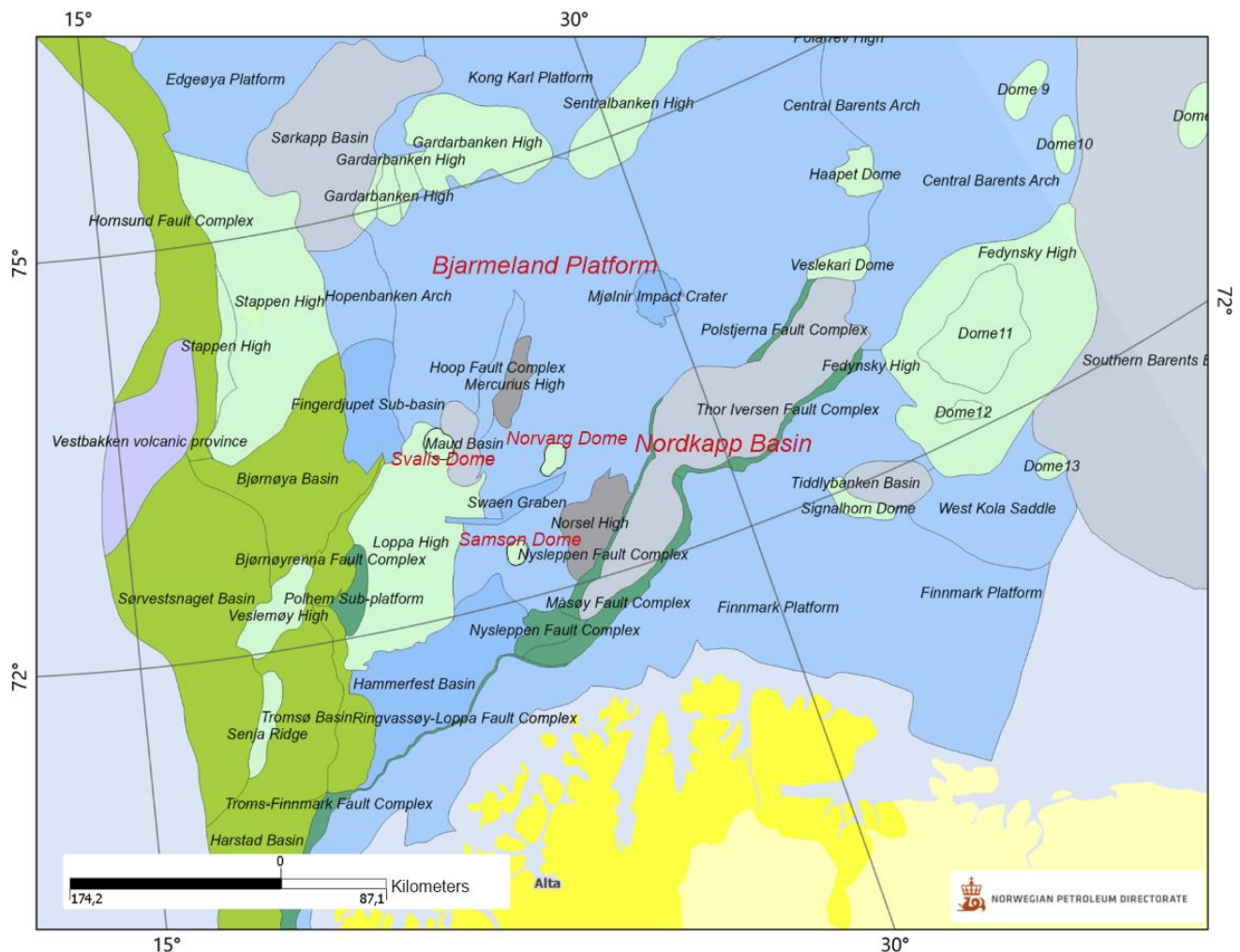


Figure 2.10: Illustration showing the structural elements of the Barents Sea shelf. The main structural elements of the study area are highlighted in red. Map from NPD (2019).

## 3 Data and methodology

### 3.1 Data

The seismic interpretation of this study is based on 2D and 3D seismic data. The 2D seismic data was acquired in the period from 2006-2014 by Fugro Seacore on behalf of the Norwegian Petroleum Directorate (NPD). The data sets cover most of the southern Barents Sea within Norwegian territory (Figure 3.1). In the western part of the study area, the line density of the overlapping data sets is relatively high (Figure 3.2), while there is slightly more distance between lines in the east, especially in the central Nordkapp Basin. General information about the 2D surveys is listed in table 3.1.

The 3D seismic data was acquired during the period from 1994-2010 by Equinor and are located in the Nordkapp Basin. ST0811 and ST0624 are located in central parts of the basin, while ST0309, ST9403R01 and ST10011 are located in the southwestern sub-basin. The ST0820 dataset covers the transition from the Nordkapp Basin to the Bjarmeland Platform towards the northwest (Figure 3.3). General information about the 3D surveys is listed in table 3.2.

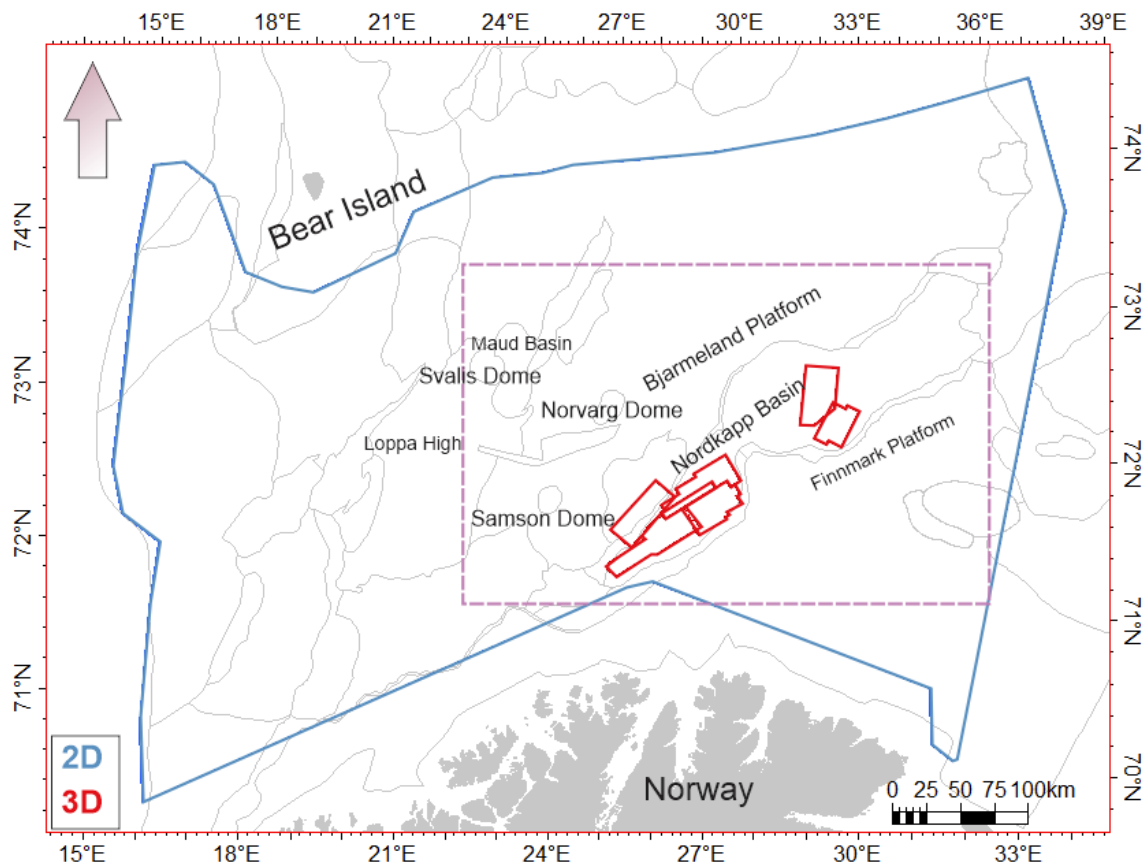


Figure 3.1: Map showing the structural elements of the Barents Sea shelf. The outline of 2D survey line coverage is shown in blue, while the location of 3D data sets is shown in red. The general study area is outlined as by the dotted purple line. Structural element base map provided by NPD.

### 3 Data and methodology

Table 3.1: General information about the 2D surveys used in this study. Note that the numbers behind “NBR” represent the year the seismic acquisition was completed. Example: NBR06 acquired in 2006. Average line spacing calculated from measured distance between the closest and most distant lines of each data set.

Survey name	Line number	Line spacing average (km)	Data quality
NBR06	20	57.5	Medium
NBR07_RE09	31	36.5	Good
NBR08	63	37.5	Good
NBR09	50	52	Good
NBR10	60	27	Medium
NBR11	56	54	Medium
NBR12	50	21.75	Good
NBR14	58	26.75	Medium
BSSE14RE	98	19.5	Medium

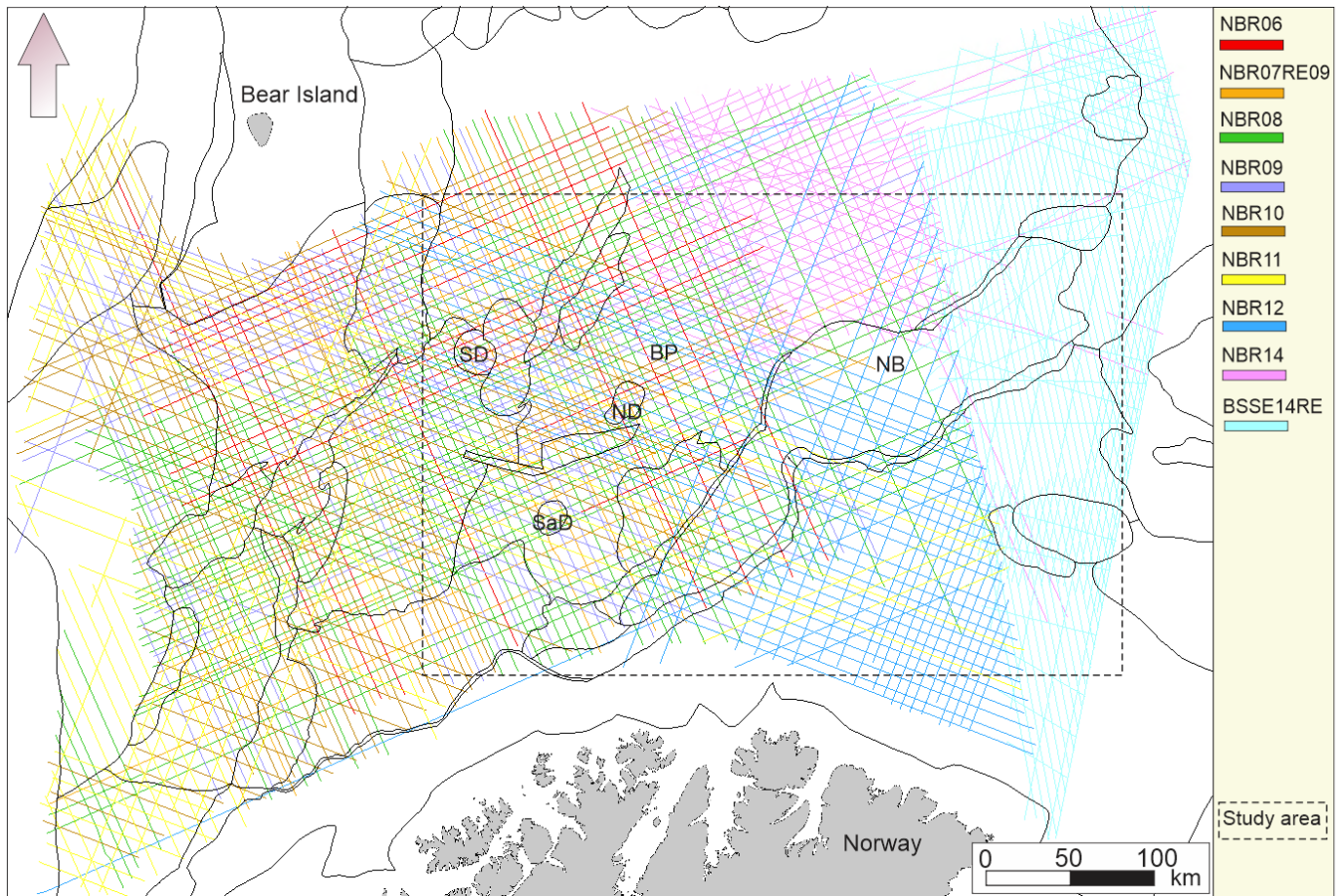


Figure 3.2: Map showing the location and line spacing of the respective 2D data sets used in the study. The black dashed rectangle delineates the study area. Note the relatively poor coverage within the central Nordkapp Basin relative to the more dense line spacing across the Bjarmeland Platform and the more dense coverage across the Svalis and Norvarg domes compared to the Samson Dome.

### 3 Data and methodology

Table 3.2: General information of the 3D seismic cubes used in this study. Note that the first two numbers after “ST” represent the year the seismic acquisition was completed. Example: ST0309 acquired 2003.

Survey name	Area (km <sup>2</sup> )	Inline number	Inline interval	Data quality	Orientation
ST0309	930	909	25.02	Good	SW-NE
ST0624	620	1186	18.77	Good	SSW-NNE
ST0811	938	961	25.03	Good	SSW-NNE
ST0828	959	816	25.0	Medium	SW-NE
ST10011	1350	969	25.02	Good	SW-NE
ST9403R01	876	959	25.02	Good	SW-NE

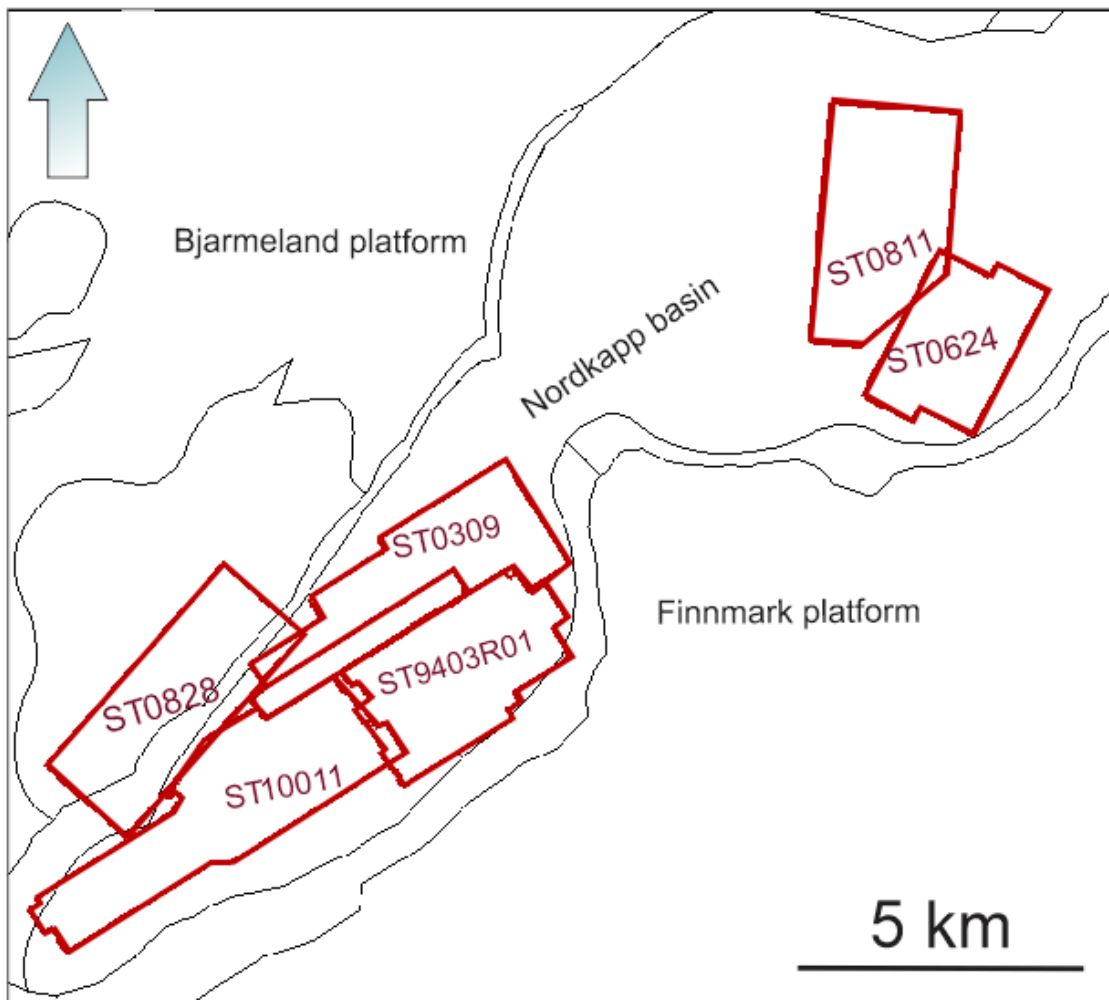


Figure 3.3: Map showing the location of respective 3D data sets used in the study. Four data sets are located in the southwestern Nordkapp Basin, while two are located in the central northeastern part.

### 3 Data and methodology

#### 3.2 Seismic reflection theory

The main principle of all seismic methods is the generation of elastic waves by a controlled seismic source, utilized to acquire an image of the subsurface (Kearey et al. 2002). The generated seismic pulses are sent from the source downwards into the subsurface and partially reflected at the seafloor and at deeper interfaces (reflectors) with a sufficient contrast in acoustic impedance (Badley, 1985). The acoustic impedance ( $Z$ ) of a material is a product of its density ( $p$  ( $kg/m^3$ )) and sound velocity ( $v$  ( $m/s$ )):

$$Z = p * v$$

The amplitude of the reflected seismic wave at an interface is dependent on the contrast in acoustic impedance, which is determined by the properties of the rock above and below the interface. The amplitude is described by the reflection coefficient ( $R$ ) (Reynolds, 2011):

$$R = \frac{(Z_2 - Z_1)}{(Z_2 + Z_1)} = \frac{(p_2v_2 - p_1v_1)}{(p_2v_2 + p_1v_1)}$$

The Reflection coefficient has a value between 1 and -1, depending on whether the acoustic impedance is higher or lower below the interface where the seismic wave is reflected. If the acoustic impedance above and below an interface are equal ( $Z_2=Z_1$ ), no energy will be reflected and the reflection coefficient will be zero (Kearey et al., 2002). The seismic reflection method is utilized to visualize structural and stratigraphic features in the subsurface and is predominantly applied for hydrocarbon exploration or academic purposes (Kearey et al. 2002; Reynolds 2011).

##### 3.2.1 Seismic resolution

Seismic resolution is defined as the ability to distinguish between two closely spaced objects, both laterally and vertically, so they appear as separate (Kearey et al., 2002). The resolution describes how large an objects or unit needs to be in order to be resolved in the seismic section. It is determined by the relationship between the seismic wave's frequency ( $f$ ), velocity ( $v$ ) and wavelength ( $\lambda$ ) and also influenced by how the data is collected and processed (Brown, 1999; Kearey, 2002). The relationship between frequency ( $f$ ), velocity ( $v$ ) and wavelength ( $\lambda$ ) is given by:

$$\lambda = \frac{v}{f}$$



### 3 Data and methodology

Seismic resolution tends to decrease with depth, as the frequency of the seismic wave decreases, and the velocity and wavelength of the wave increases (Kearey et al., 2002) (Figure 3.4). As the wave travels downwards energy is attenuated due to absorption and the higher frequencies are lost in the recorder data. The resolution at which the impedance contrasts of the subsurface interfaces can be imaged, applies to both vertical and horizontal conditions.

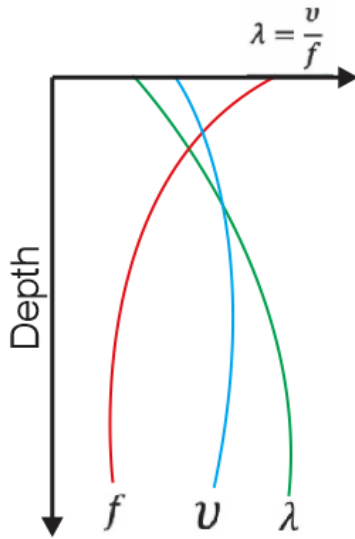


Figure 3.4: Graph showing the relationship between frequency, velocity and wavelength with increasing depth. As the seismic wave travels downwards, the wavelength increases, while the frequency decreases. Figure modified from Brown (1999).

#### Vertical resolution

Vertical resolution ( $Vr$ ) is given in meters, and is a measure of how closely separate reflectors can be spaced in the subsurface and still be detected in the seismic section (Kearey et al., 2002). It is given by:

$$Vr (m) = \frac{\lambda}{4}$$

Where,

$Vr$  = vertical resolution

$\lambda$  = wavelength

The vertical resolution is given in the spatial domain as the quarter of the wavelength of the seismic wave, but corresponds directly to half a period in the time domain. In physical terms, the resolution is tied to how thickness in the subsurface is related to the seismic section.

### 3 Data and methodology

#### Seismic tuning effect

The top- and bottom interfaces of a layer in the subsurface will appear as separate as long as the layer thickness is equal to or exceeds the half the wavelength of the seismic wave. If the thickness of the layer is between half and a quarter of the wavelength, the signals will begin to overlap (Figure 3.5). If the thickness of the subsurface layer is less than what corresponds to a quarter of the wavelength of the seismic wave, the wavelets will fully overlap, resulting in constructive or destructive interference (Figure 3.5).

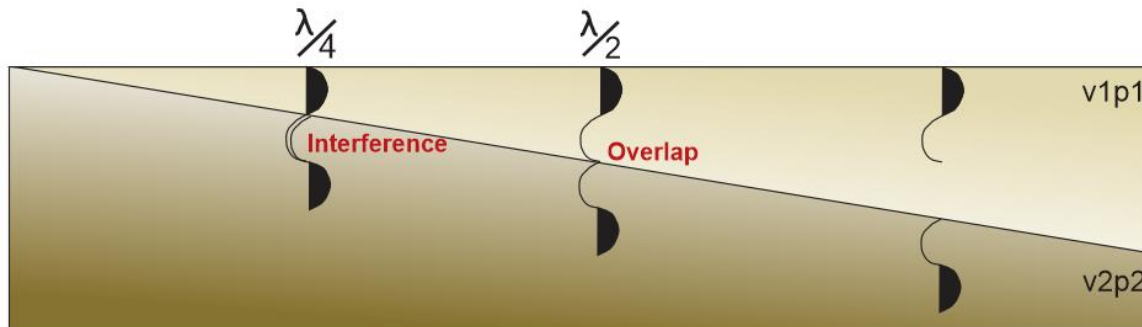


Figure 3.5: Illustration of how the vertical resolution varies with layer thickness. Note how there is signal overlap and constructive interference when the layer thins, resulting in the top-and bottom layer interfaces not being properly resolved. Figure modified from Kearey et al. (2002).

#### Horizontal resolution

When a seismic wave is generated, it travels in all directions from the shot point. The wave front propagates spherically, expanding with increasing distance. Due to this spreading, the seismic energy does not reflect from a single point on an interface, but from a circular zone on its surface. The extent of the zone where the energy is reflected determines the horizontal resolution of unmigrated seismic sections, and is termed the Fresnel zone (Figure 3.6) (Brown, 1999; Kearey et al., 2002). Migrated seismic data, especially 3D data, will have a smaller Fresnel zone, providing a better resolution (Figure 3.7). Objects smaller than the zone will not be resolved and will not be visible on the seismic section. The radius of the Fresnel zone for unmigrated seismic data ( $R_f$ ) is given by:

$$R_f (m) = \frac{v}{2} \sqrt{\frac{t}{f}}$$

Where,

$R_f$  = Radius of the Fresnel zone (m)

$v$  = Average propagating speed on the incident wave (m/s)

### 3 Data and methodology

t = Two-way travel time (s)

f = Frequency (Hz)

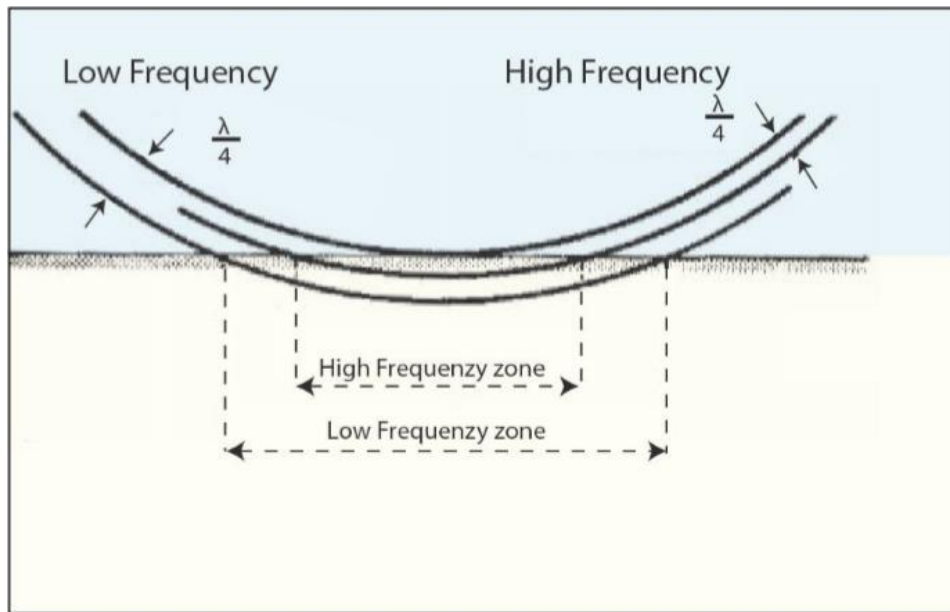


Figure 3.6: Illustration of the Fresnel zone for high and low frequencies. The Fresnel zone is larger for low frequencies than for higher. Thus, objects are resolved more poorly by low frequencies. Figure modified from Sheriff (1985).

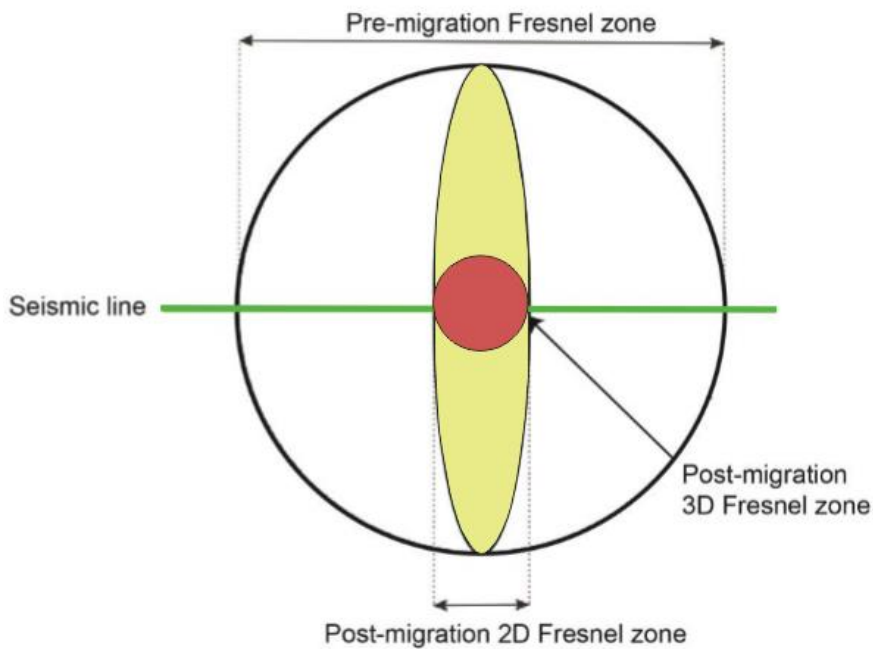


Figure 3.7: Illustration of the Fresnel zone before and after migration for 2D and 3D seismic data. Figure modified from Brown (1999).

### 3 Data and methodology

The vertical and horizontal resolution of the 2D and 3D surveys were calculated, to determine how well sequences are resolved in the data. The 3D cubes were cropped in the Z-direction, to make the frequency spectrum representative of only the shallow stratigraphy. Velocity is generally not recorded in wells at the depth of the stratigraphy in focus. The velocity of 2000 m/s used for resolution-calculation is defined in Andreassen et al. (2007) where characteristics of the glacial sediments above the URU in the Barents Sea were presented. Note that the velocity is an average value that will vary with the degree of consolidation of the sediments. Also note that the equation used for the horizontal resolution is for unmigrated seismic data. The data of this study is migrated, and will ideally have a horizontal resolution similar to the vertical one, at a quarter of the wavelength of the data (Sheriff, 1977). The respective resolutions of 2D and 3D surveys are listed in tables 3.3 and 3.4. The vertical resolution of the 2D data sets is found to be between 12.3-20 meters and between 12.5-26.3 meters for the 3D data sets, meaning subsurface features must exceed this thickness to be properly resolved.

*Table 3.3: Below are the calculated vertical and horizontal resolutions of the 2D data sets. Note that the average depth of 400 ms to the seafloor was used to calculate horizontal resolution.*

Survey name	Average velocity (m/s)	Peak frequency (Hz)	Wavelength (m) (v/f)	Vertical resolution (m)	Horizontal resolution (m) (unmigrated)
NBR06	2000	40	50	12.5	100
NBR07_RE09	-	29	69	17.3	117.4
NBR08	-	41	49	12.3	98.8
NBR09	-	37	54	13.5	104
NBR10	-	25	80	20	126.5
NBR11	-	30	65	16.3	115.5
NBR12	-	32	62.5	15.6	111.8
NBR14	-	25	80	20	126.5
BSSE14RE	-	34	59	14.8	108.5

*Table 3.4: The vertical and horizontal resolution of the 3D data sets are shown below. Note that the average depth of 400 ms to the seafloor was used to calculate horizontal resolution.*

Survey name	Average velocity (m/s)	Peak frequency (Hz)	Wavelength (m) (v/f)	Vertical resolution (m)	Horizontal resolution (m) (unmigrated)
ST0309	2000	40	50	12.5	100
ST0624	-	19	105	26.3	145.1
ST0811	-	20	100	25	141.4
ST0828	-	25	80	20	126.5
ST10011	-	22	91	22.8	134.8
ST9403R01	-	38	53	13.3	102.6

### 3 Data and methodology

The resolution of the 2D and 3D surveys is relatively similar, but there is a slight trend of better resolution in the 2D data. More reflections of thinner layers are therefore visible in the subsurface on 2D lines (Figure 3.8). Additionally, the 3D data generally displays higher amplitude reflections, especially by the top of salt diapirs.

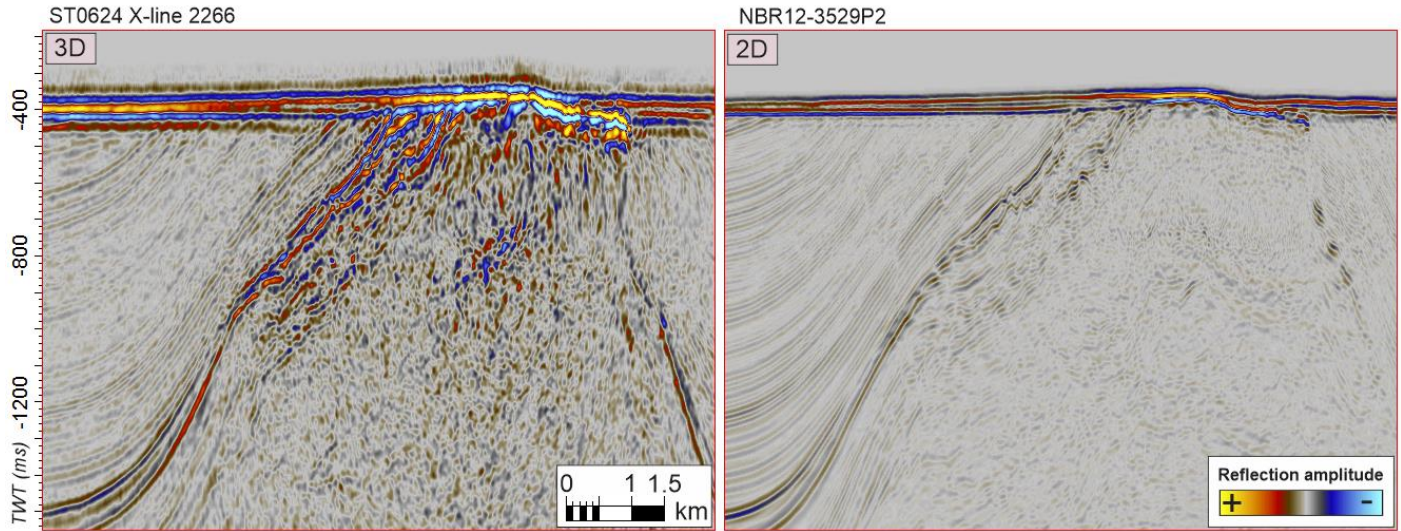


Figure 3.8: Side by side comparison of a seismic profile through the same salt diapir on 3D and 2D seismic data. Note the higher amplitude reflections on the 3D data set, and the better resolution of the dipping reflections to the left of the salt on the 2D data.

#### 3.2.2 Phase and polarity

The phase and polarity of the surveys was determined according to the SEG polarity standard set by Sheriff (2002). All surveys display a zero phase signal, showing a trough-peak-trough shape along the seafloor reflection on the seismic lines, where the traces also show a normal polarity (Figure 3.9) and positive reflection coefficient.

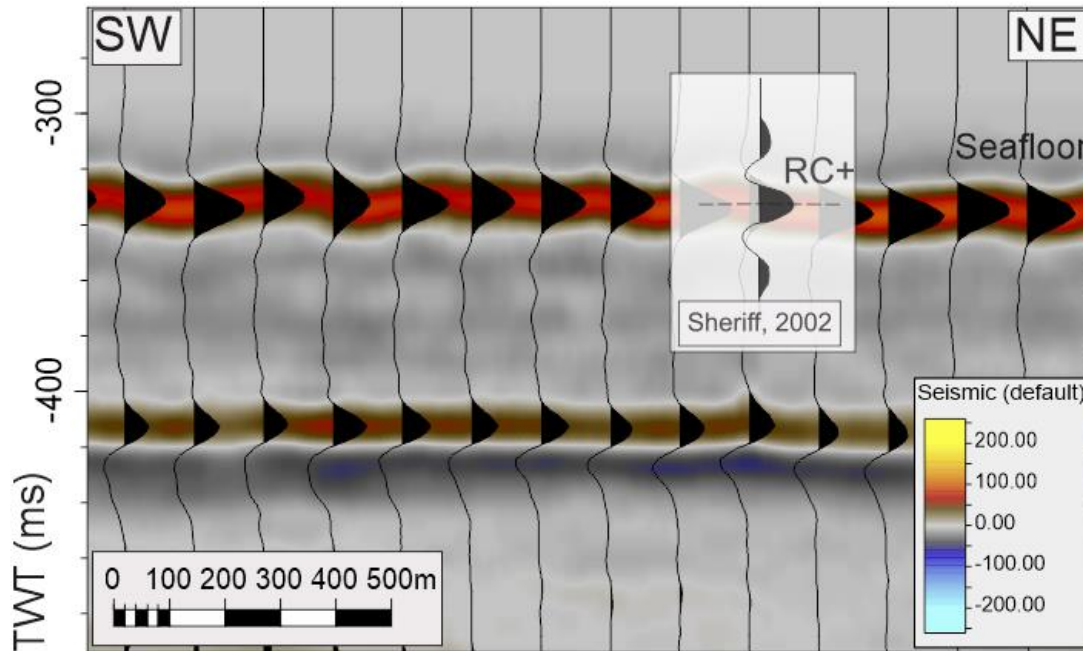


Figure 3.9: Seismic inline from 3D data set ST10011. The seafloor reflection displays a zero phase shape and a normal polarity according to the Sheriff (2002) convention.

### 3.2.3 Artefacts and noise

Any observable features in the seismic section not originating from the geology in the subsurface is referred to as an artifact. Noise is a term describing any recorded seismic signal other than primary reflections, such as multiples and diffractions (Badley, 1985). While noise may obscure the features in a seismic image, artefacts appear to be features but are not. They are a result of acquisition technique or processing, and need to be noted when working with seismic data, as they may be misinterpreted to represent real structures in the subsurface. Due to the uplift and extensive erosion of the Barents Sea shelf, high velocity rocks are present below the glacial deposits and URU. The sharp transition in acoustic impedance in the strata makes acquisition and processing more difficult, which may result in noise and artefacts on the data. In this study, acquisition footprint artefacts are observed on some of the surfaces generated from interpretation of 3D surveys, appearing as lines parallel to the inline direction (Figure 3.10).

### 3 Data and methodology

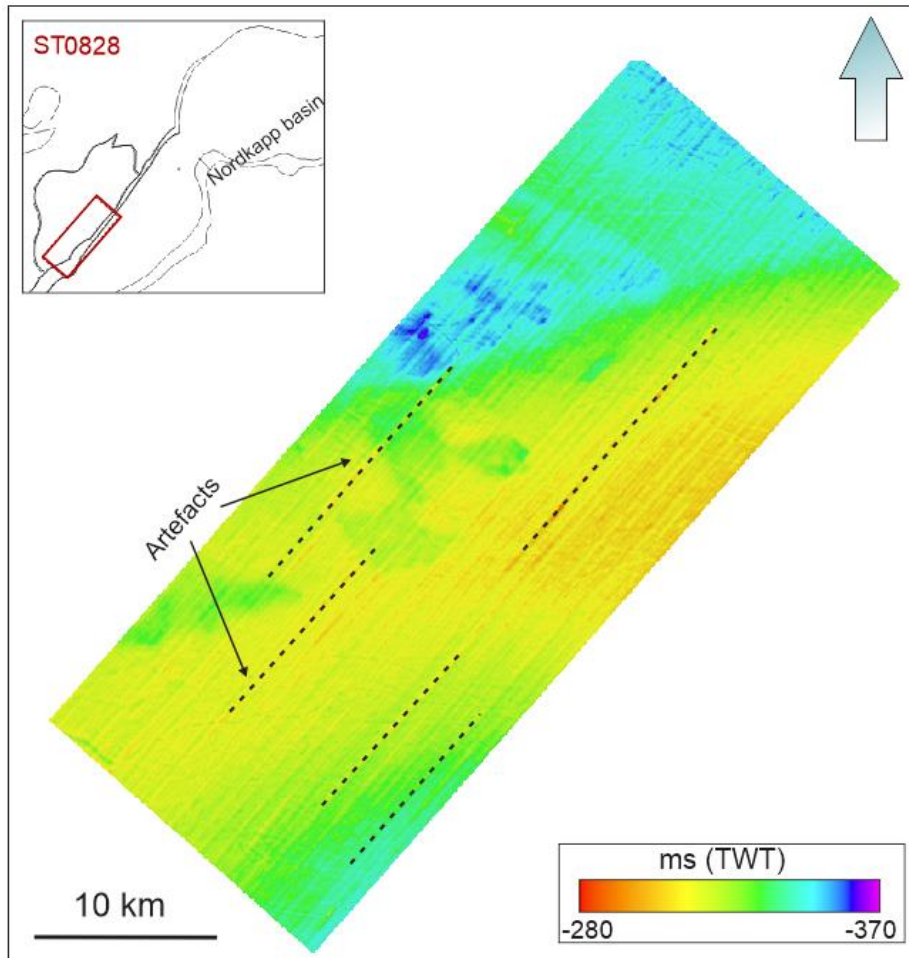


Figure 3.10: Seafloor horizon from 3D data set ST0828 with acquisition footprint artefacts visible as linear features parallel to the inline direction.

### 3.3 Interpretation methodology

#### 3.3.1 Seismic Interpretation

Petrel E&P Software Platform (2016 version) was used for seismic interpretation. The software was developed by Schlumberger, and serves as a tool for seismic interpretation and visualization for geoscientists. The seafloor and upper regional unconformity were identified, and interpreted as horizons on the 2D and 3D data. The seafloor horizon, identified as the uppermost reflection, was tracked using the manual, seeded and automatic tracking tool. The URU was identified on the seismic data by its truncational relationship with underlying reflections, due to its erosional origin (Figure 3.11). The reflection is also distinguishable by its relatively high amplitude, due to the contrast in acoustic impedance between the glacial sediments and consolidated strata below. The polarity of the unconformity reflection varies according to the acoustic properties of the strata below relative to the sediments above, and may be both positive and negative compared to the seafloor reflection after the Sheriff (2002) convention.

### 3 Data and methodology

In 3D seismic data sets ST0624 and ST0811, URU was interpreted on a peak reflection. In data sets ST0309, ST0828, ST10011 and ST9403R01 it was interpreted on a trough reflection, due to better continuity. From the horizons tracked in the 2D and 3D surveys, surfaces were produced in Petrel. Additionally, seismic time slices visualizing lateral differences in amplitude at certain depths (ms (TWT)) were used to determine the depth and shape of salt bodies.

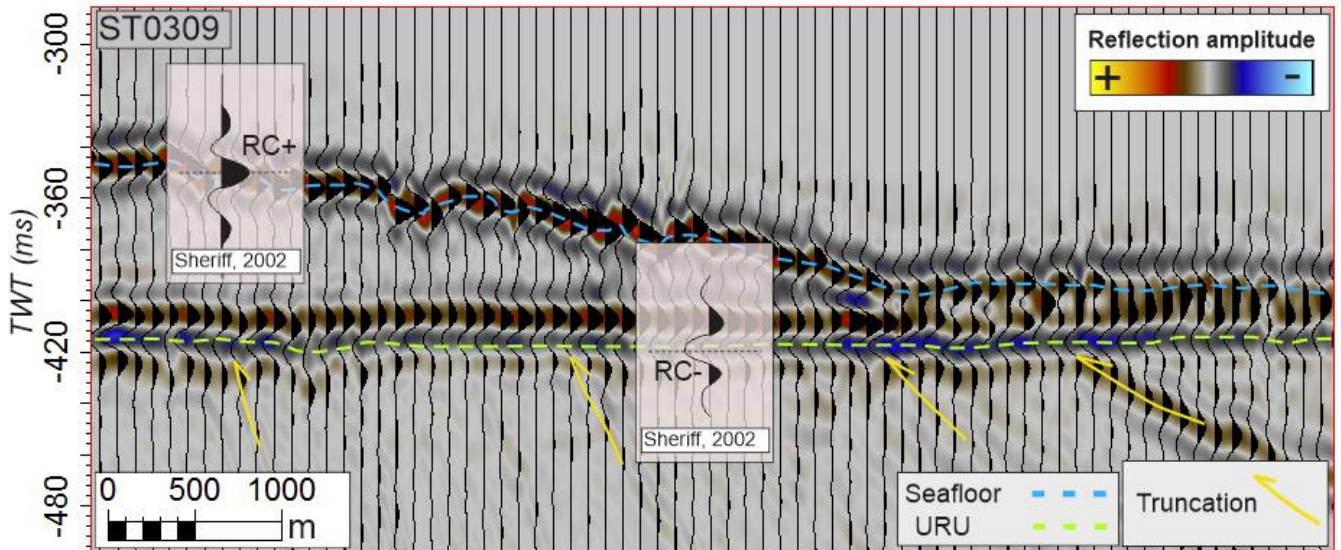


Figure 3.11: Example of the appearance of the seafloor and URU in seismic data. Note how the reflections below the URU terminate abruptly against the reflection.

#### 3.3.2 Seismic stratigraphy

Seismic stratigraphy is used to group and correlate a series of seismic reflections in units corresponding to distinctive chronostratigraphic depositional intervals (Mitchum et al, 1977; Vail, 1987). Studies of seismic stratigraphy and depositional facies interpreted from seismic data is utilized to reconstruct paleo-environments.

##### *Seismic sequence analysis*

Seismic sequence analysis is an important tool when interpreting the depositional environment from seismic sequences. It is based on reflection terminations (Mitchum et al., 1977; Vail, 1987), and describing the geometric relationship between reflections and the stratigraphic surface they terminate against (Catuneanu, 2006). There are four main defined reflection terminations used for identifying stratigraphic surfaces, respectively named onlap, toplap, downlap and truncation (Figure 3.12).

Onlap is recognized by the termination of reflections against a steeper stratigraphic surface, resulting in the younger strata progressively overstepping underlying deposits (Veeken, 2007). Toplap is the termination of inclined strata with a clinoform geometry against an overlying surface. The overlying truncating surface



### 3 Data and methodology

generally has a lower angle than the reflections terminating against it. The sequence boundary is a result of sedimentary bypass with a minor erosional influence (Catuneanu, 2006). Downlap refers to a downwards termination of inclined strata against an underlying stratigraphic surface. Similar to toplap, the surface generally has a lower angle than the reflections that terminate against it (Catuneanu, 2006). Truncation describes the termination of reflections against an overlying truncational surface, generally an unconformity, representing an erosional surface (Catuneanu, 2006).

In this study, sequence analysis is important for interpreting and describing the URU and any internal horizons found within the glacialic sediments above. The sequence analysis is used to describe various terminations of internal horizons in the glacial deposits against the unconformity, especially around the salt domes within the study area, and to describe the relationship between the URU and underlying stratigraphy.

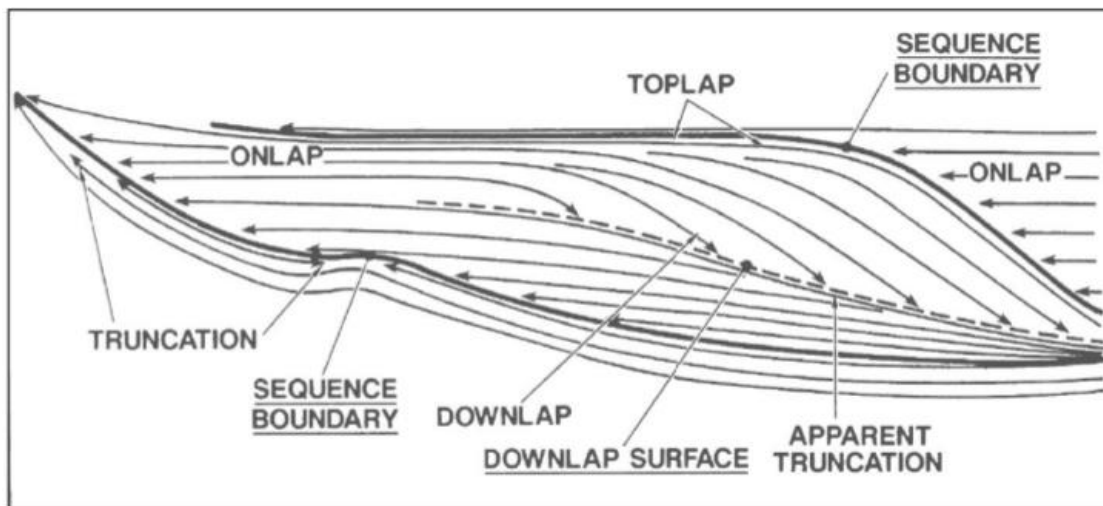


Figure 3.12: Schematic illustration of an idealized seismic sequence with the main reflection terminations used in sequence stratigraphy analysis. Figure modified from Vail (1987).

#### *Seismic facies*

Seismic facies are determined by a multitude of parameters concerning the appearance of reflections on the seismic section and was defined by Mitchum et al. (1977) as the description and geological interpretation of these. Among the parameters used are reflection configuration, continuity and amplitude. Seismic facies provide information about the subsurface geology and reflect parameters surrounding the depositional environment. Figure 3.13 shows examples of how different reflection configurations may appear on seismic data.

### 3 Data and methodology


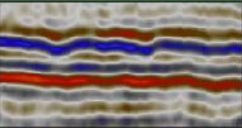

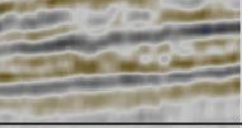






Reflection geometry	Reflection amplitude	Seismic facies (after Veeken, 2007)	Seismic facies in this study
Parallel continuous	High amplitude		
Parallel continuous	Medium amplitude		
Parallel continuous	low amplitude		
Subparallel discontinuous	low-medium amplitude		
Chaotic	low amplitude		

Figure 3.13: Table showing the appearance of some common seismic facies from Veeken (2007) and from this study.

#### 3.3.3 Seismic attributes

Attributes are measurable properties of seismic data that may give complementary information to the interpretation and may be used to increase the understanding of the geological features in the subsurface. In this study, attributes were applied to the surfaces to better understand the properties of the shallow strata in the study area.

##### *Root mean square (RMS)*

This attribute calculates the square root of the sum of squared amplitudes divided by the number of samples (Koson et al., 2014). It shows areas within a volume or across a surface with high amplitude anomalies, and is useful for visualization of lateral amplitude variations in a seismic volume. In this study, RMS maps were produced from surfaces and volumes in Petrel to illustrate the lateral variation in amplitude along the seafloor- and URU surfaces, and internally in the glacial sediments.

##### *Time-thickness map (Isochore map)*

The vertical thickness in two-way-travel time between surfaces was calculated in Petrel to produce isochore maps. The maps show the lateral variation in time thickness between two surfaces, and were used to estimate the thickness of the glacial sediment sequence between the seafloor and the Upper Regional Unconformity.

## 4 Results

In this chapter, the results of the seismic interpretation are presented in chronological order, beginning with an overview of the regional trends of the interpreted surfaces in the study area. Following this, the late Cenozoic stratigraphy in the study area is presented, with a focus on the Svalis, Samson and Norvarg domes as well as the Nordkapp Basin and the relationship between the salt diapirs and the overlying stratigraphy.

### 4.1 Regional overview

The upper regional unconformity (URU) and the seafloor are regional horizons and have been mapped across the entire study area. In addition, above and adjacent to some salt diapirs the Quaternary sediment package is locally thick enough to enable seismic stratigraphic mapping of the interval. Intra Quaternary horizons are distinguishable on the Loppa High adjacent to the Svalis Dome. In addition, they are interpreted within an arcuate sediment ridge found in the southwestern Nordkapp Basin, and in a sediment accumulation in the northeastern Nordkapp Basin. The horizons are not correlated between the three areas due to lacking data coverage and resolution. An overview of the interpreted reflections is given in figure 4.1.









Seafloor 		
Intra Quaternary horizons		
Loppa High	Nordkapp Basin SW	Nordkapp Basin NE
A2 	B2 	C2 
A1 	B1 	C1 
Upper Regional Unconformity (URU) 		

Figure 4.1: Schematic overview of the horizons interpreted in the study area.

#### 4.1.1 Upper Regional Unconformity (URU)

The URU is the lowest stratigraphic horizon interpreted in this study. The horizon is represented by a medium to high amplitude reflection, which is overall continuous, though there are differences in the quality between the seismic surveys. On 2D seismic data sets, URU is mainly visible as a positive reflection that truncates underlying strata. In the 3D seismic data sets ST0624 and ST0811, URU is interpreted on a peak reflection, while it was interpreted on a trough in ST0309, ST0828, ST10011 and ST9403R01. In further descriptions, the depth is given in ms two-way travel time (TWT).

## 4 Results

Regionally in the SW Barents Sea, the URU surface mirrors the seabed bathymetry. The unconformity reaches up to 800 ms (TWT) depth within the Bear Island Trough (Figure 4.2) and more than 1000 ms towards the western margin. The unconformity is shallowest above the northeastern Nordkapp Basin, where it is mapped at 350 ms (TWT) depth (Figure 4.2).

The depth of the URU is relatively uniform across the southern Bjarmeland Platform. It is relatively flat above both the Samson and Norvarg domes, and the depth increases towards more central parts of the platform (Figure 4.2 and 4.6). Across the central and southwestern Nordkapp Basin, the depth is also fairly uniform, with an average depth of 425 ms (TWT). The unconformity is cut by a local elongated seafloor depression in the central basin (Figure 4.2). Some local depressions and highs associated with deeper located salt occur (Figure 4.4 and 4.5). Some of these are described in more detail in chapter 4.5.2.

The unconformity is elevated around the flanks of the Svalis Dome, relative to above the adjacent Maud Basin and Bjarmeland Platform (Figure 4.2). There is a significant difference in depth of the unconformity between the western and eastern side of the dome: in the east the URU has a depth of around 600 ms and west of the dome the depth increases to up to 800 ms (TWT) (Figure 4.2 and 4.5). It is truncated by the seafloor near the crest of the dome, at a depth of 500 ms (TWT) (Figure 4.2 and 4.4). Thus, the URU displays a positive relief of 300 ms (TWT) by the dome.

## 4 Results

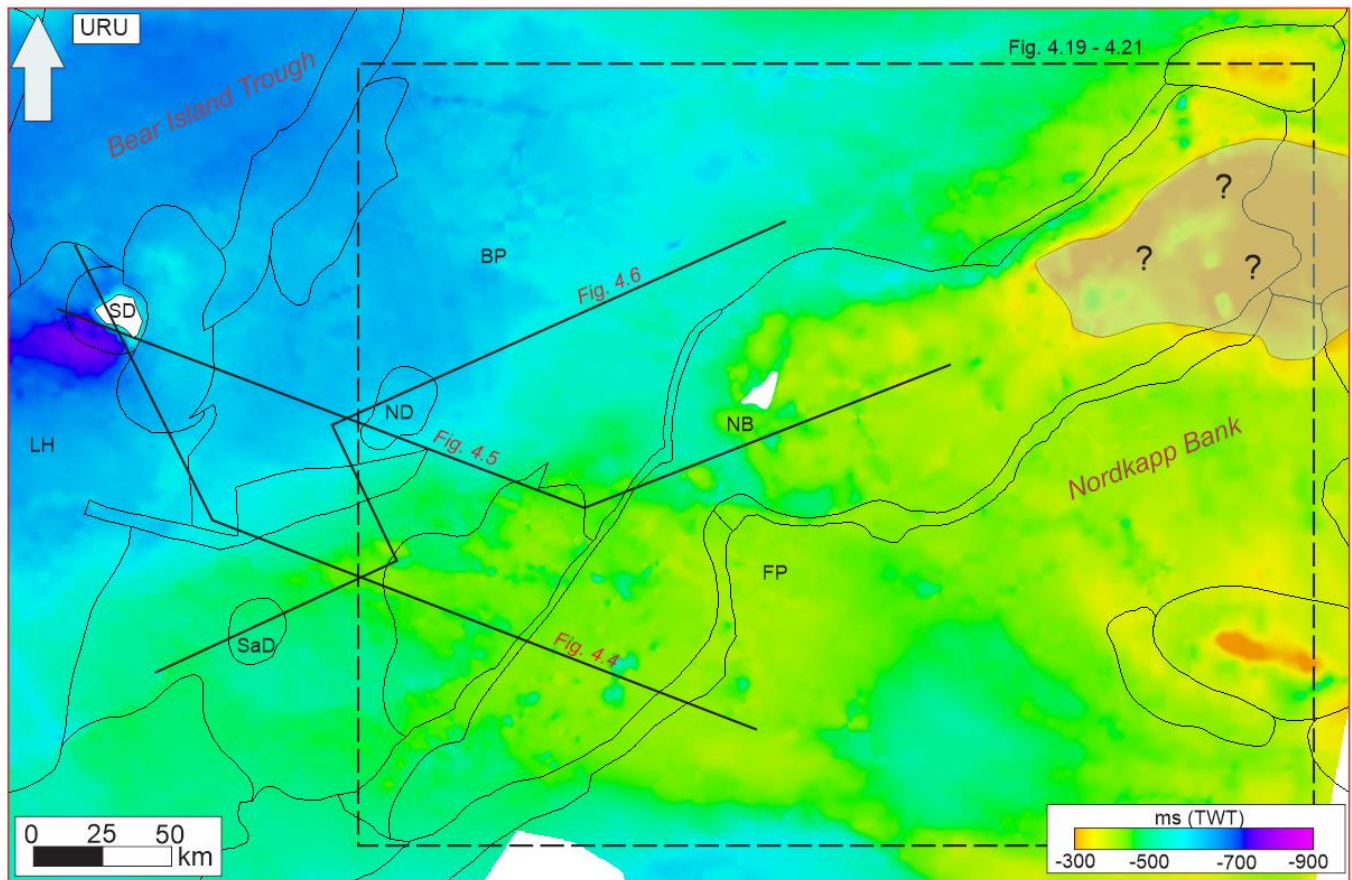


Figure 4.2: Regional surface showing the depth in ms (TWT) of the URU on the SW Barents Sea. The positions and orientations of profiles in fig. 4.4-4.6 are given by the black lines. The dashed square outlines fig. 4.19-4.21 which provide a more detailed look of the unconformity in the Nordkapp Basin. Note how the URU is not present above the Svalis Dome and locally in the central Nordkapp Basin. The presence of the unconformity is also uncertain in the northeastern Nordkapp Basin. LH = Loppa High, HB = Harstad Basin, SD = Svalis Dome, ND = Norvarg Dome, MB = Maud Basin, SaD = Samson Dome, BP = Bjarmeland Platform, NB = Nordkapp Basin, FP = Finnmark Platform. Structural element base map provided by NPD.

## 4 Results

### 4.1.2 Seafloor

In the seismic data the seafloor is represented by a continuous and high amplitude peak reflection (Figure 4.4b). The main bathymetrical features on the seafloor in the study area are the Bear Island Trough to the northwest and the Nordkapp Bank to the southeast. The trough reaches 600 ms (TWT) depth in the study area, and increases in depth towards the western shelf-margin (Figure 4.3). The Svalis Dome is a local high within the trough, and is elevated with up to 200 ms (TWT) relative to the adjacent seabed (Figure 4.12). The Nordkapp Bank is a shallower feature, with depths of down to 250 ms (TWT) (Figure 4.3). The bank covers the central and southeastern part of the study area (Figure 4.3). An elongated arcuate ridge is a dominant feature on the southern part of the bank, across the southwestern Nordkapp Basin. The arcuate ridge is approximately 120 km long and 30 km wide and is located at the distal end of the Djuprenna trough (Figure 4.3). The ridge is located in one of the shallowest parts of the study area, with a depth of 250 ms (TWT) across the top.

Above the rest of the Nordkapp Basin, the average seabed depth is approximately 400 ms (TWT). It decreases to less than 250 ms (TWT) above some of the salt diapirs in the northeastern part of the basin (Figure 4.3). Several smaller local depressions are found along the northern central margin of the basin, and in between some of the salt diapirs. The relationship between the seafloor and the underlying salt diapirs in the basin is described in more detail in chapter 4.5.2.

## 4 Results

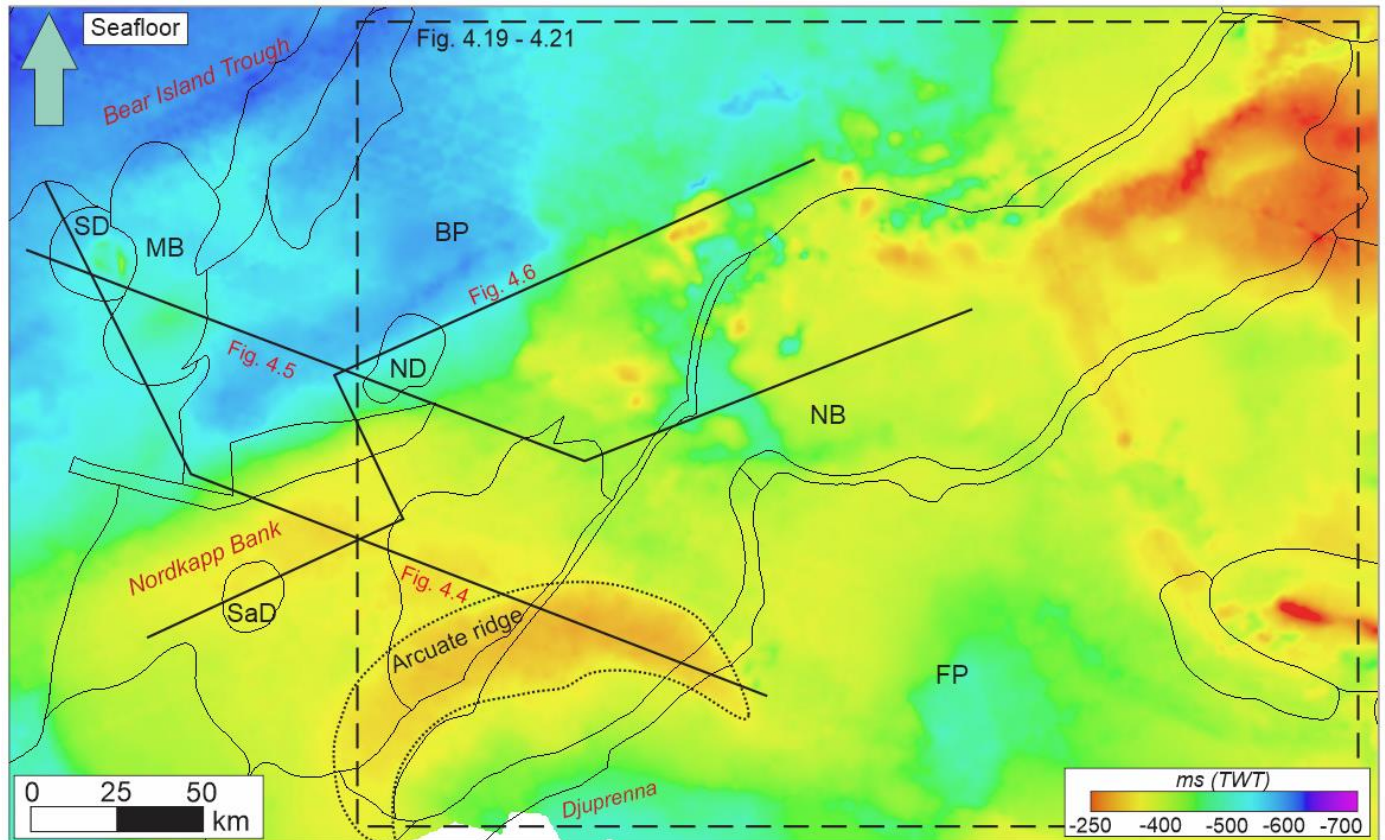


Figure 4.3: Regional surface showing the depth in ms (TWT) of the seafloor in the study area. The positions and orientations of profiles in fig. 4.4-4.6 are given by the black lines. The dashed square outlines fig. 4.19-4.21 which provide a more detailed look of the seafloor in the Nordkapp Basin. SD = Svalis Dome, MB = Maud Basin, SaD = Samson Dome, ND = Norvarg Dome, BP = Bjarmeland Platform, NB = Nordkapp Basin, FP = Finnmark Platform.

#### 4 Results

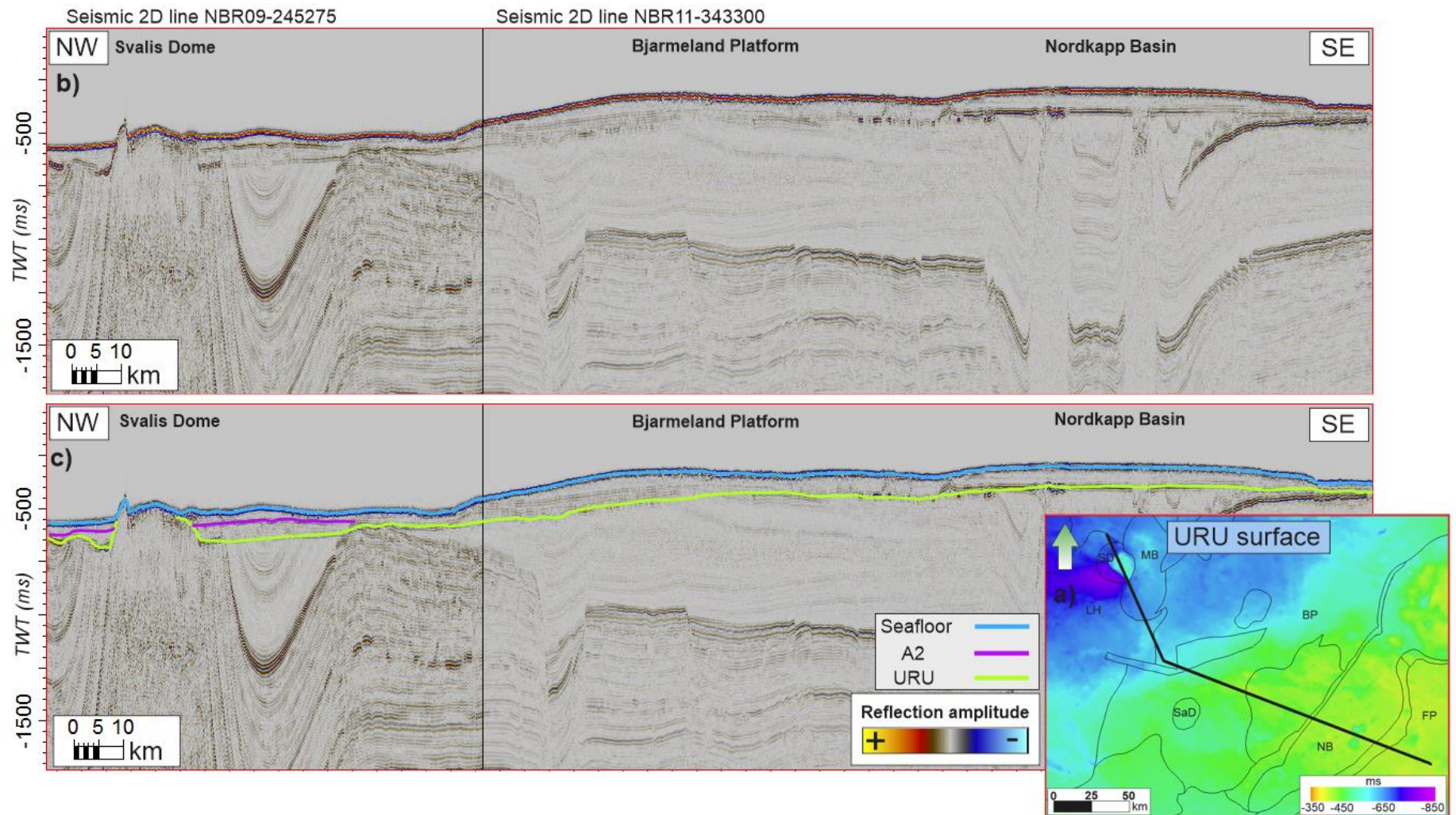


Figure 4.4: Composite 2D line showing a) the depth of the URU in the study area and an uninterpreted (b) and interpreted (c) seismic profile with the URU and seafloor surfaces marked, as well as intra quaternary horizon A2. The black vertical line on the profiles marks the intersection of the 2D lines where the profile changes direction. LH = Loppa High, SD = Svalis Dome, MB = Maud Basin, SaD = Samson Dome, BP = Bjarmeland Platform, NB = Nordkapp Basin, FP = Finnmark Platform.



## 4 Results

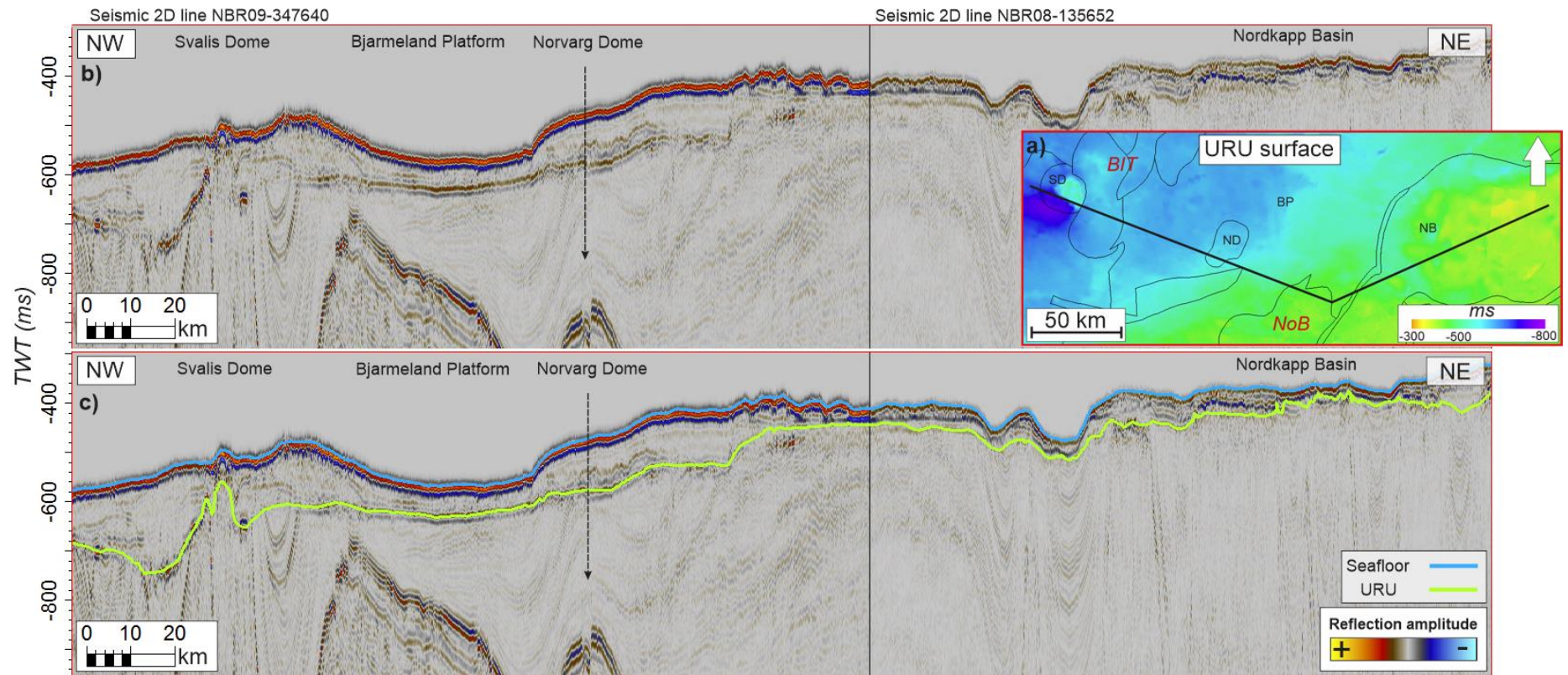


Figure 4.5: Composite line showing a) the depth of the URU, b) an uninterpreted and c) an interpreted seismic profile with the URU and seafloor surfaces. The vertical line on the profile marks the intersection of the two 2D lines. Note that compression of the line exaggerates changes in depth (TWT). BIT = Bear Island Trough, NoB = Nordkapp Bank, SD = Svalis Dome, ND = Norvarg Dome, BP = Bjarmeland Platform, NB = Nordkapp Basin.

## 4 Results

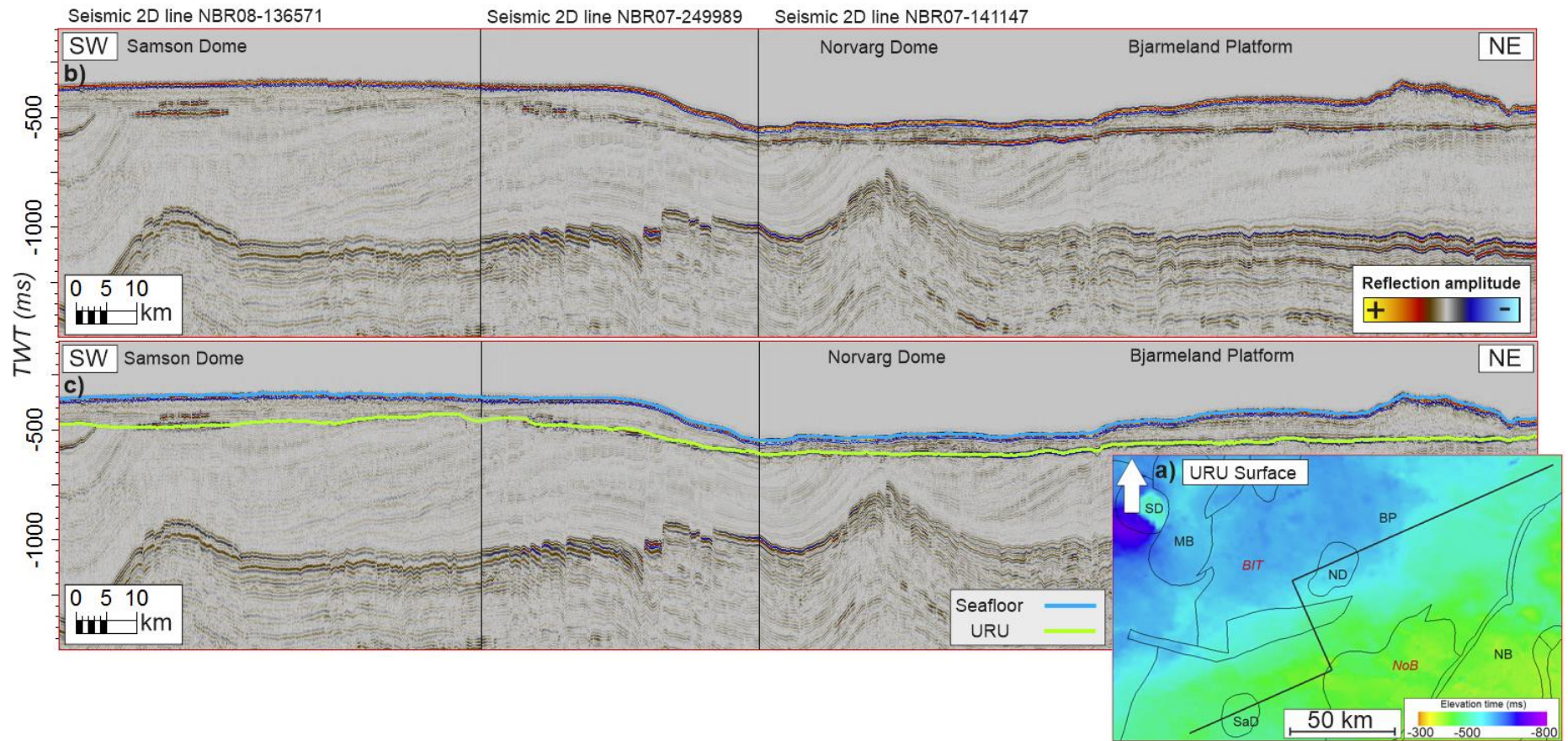


Figure 4.6: Composite line through the Samson and Norvarg domes showing a) the depth of the URU, b) an uninterpreted and c) an interpreted seismic profile with the URU and seafloor surfaces. Note the truncation of underlying strata by the URU above the Norvarg Dome. The vertical lines on the profile marks the intersection where the lines change direction.. BIT = Bear Island Trough, NoB = Nordkapp Bank, SD = Svalis Dome, MB = Maud Basin, SaD = Samson Dome, ND = Norvarg Dome, BP = Bjarmeland Platform, NB = Nordkapp Basin.

## 4 Results

### 4.1.3 Quaternary sediments

The thickness of the Quaternary sediments is mainly between 150-50 ms , and there is a general thickening westwards (Figure 4.7). Above the eastern part of the Nordkapp Basin, the sediment package is less than 50 ms thick, and the sediment package thickens towards the northwestern margin of the bank (Figure 4.7), where it locally reaches up to 200 ms thickness (Figure 4.8 and 4.9). In the Bear Island Trough in the northwest, the sediment package thickness averages between 50-100 ms. The sediment thickness is more than 250 ms west of the Svalis Dome, where there is a significant difference in thickness relative to the eastern side (Figure 4.7 and 4.9). Northeast of the dome the average thickness is 50-100 ms. The thickness increases locally to more than 250 ms southwest of the dome. Above the Samson Dome the glacial sediments are relatively uniform in thickness (Figure 4.10) at 150 ms (Figure 4.7), while there is an increase in thickness towards the northwest above the Norvarg Dome. There is a pronounced sediment accumulation above the southwestern part of the Nordkapp Basin, reaching up to 200 ms time-thickness locally (Figure 4.7 and 4.8b).

Intra Quaternary horizons were interpreted within three separate sediment accumulations; A1 and A2 southwest of the Svalis Dome, B1 and B2 within the arcuate ridge in the southwestern Nordkapp Basin, and C1 and C2 in an accumulation of sediments along the northern central margin of the basin (Figure 4.7). The configuration of the horizons is described further in chapters 4.2.2 (A1 and A2) and 4.5.2 (B1 and B2, C1 and C2), respectively.

## 4 Results

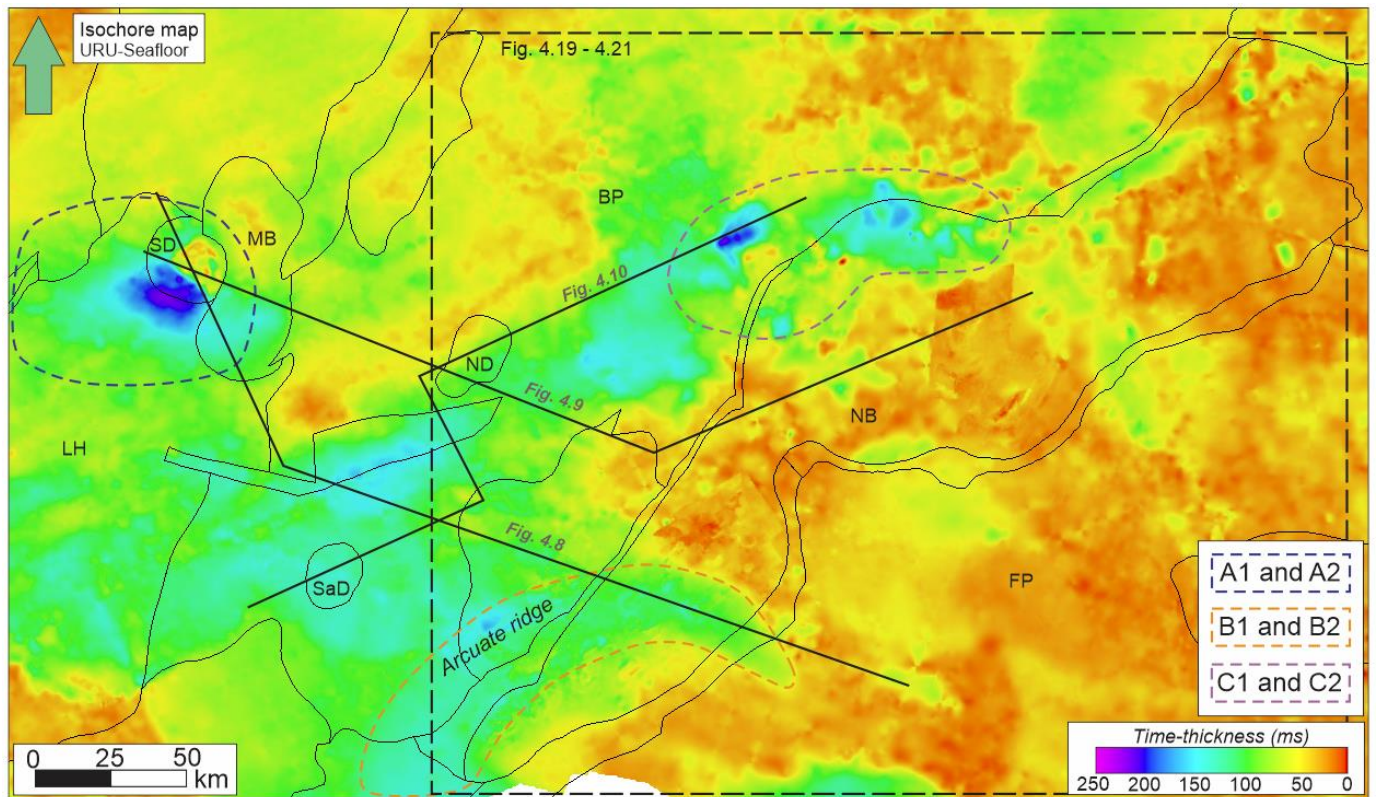


Figure 4.7: Isochore map showing the vertical time-thickness of the Quaternary deposits in the study area. Note the three areas where intra Quaternary horizons have been interpreted within the glacial sediments. LH = Loppa High, SD = Svalis Dome, MB = Maud Basin, SaD = Samson Dome, ND = Norvarg Dome, BP = Bjarmeland Platform, NB = Nordkapp Basin, FP = Finnmark Platform.

#### 4 Results

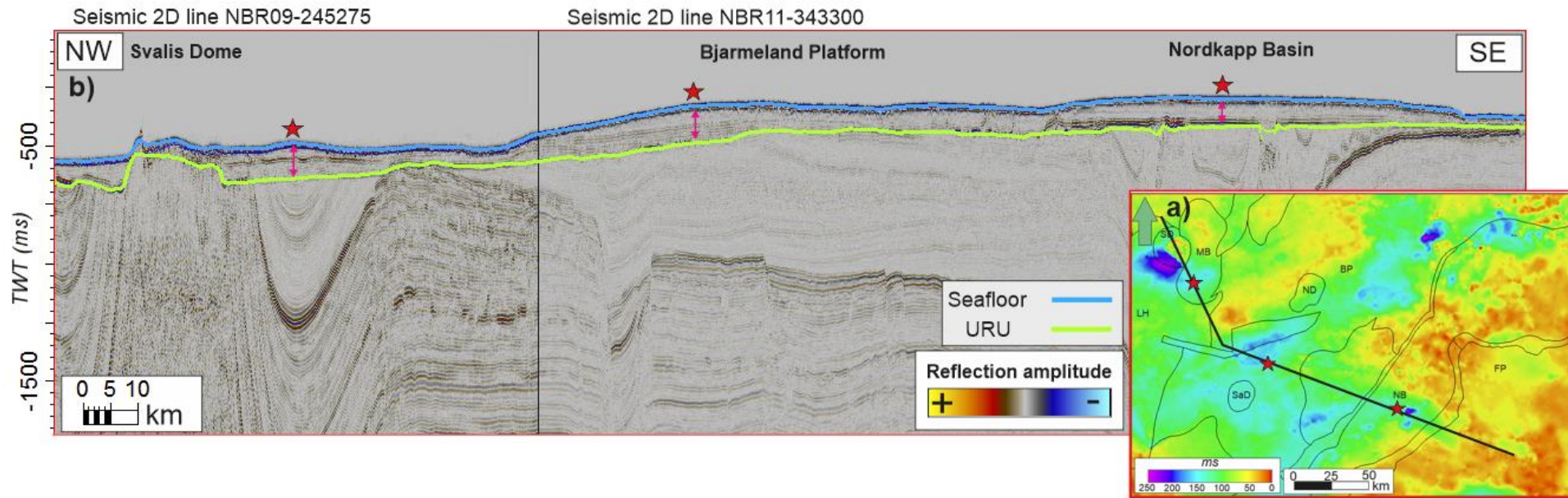


Figure 4.8: a) Isochore map and b) composite 2D line across the study area showing the variations in time-thickness of the Quaternary sediments between the URU and the seafloor. LH = Loppa High, SD = Svalis Dome, MB = Maud Basin, SaD = Samson Dome, ND = Norvarg Dome, BP = Bjarmeland Platform, NB = Nordkapp Basin, FP = Finnmark Platform. The red stars on the profiles correspond to the locations marked with stars on the map.

## 4 Results

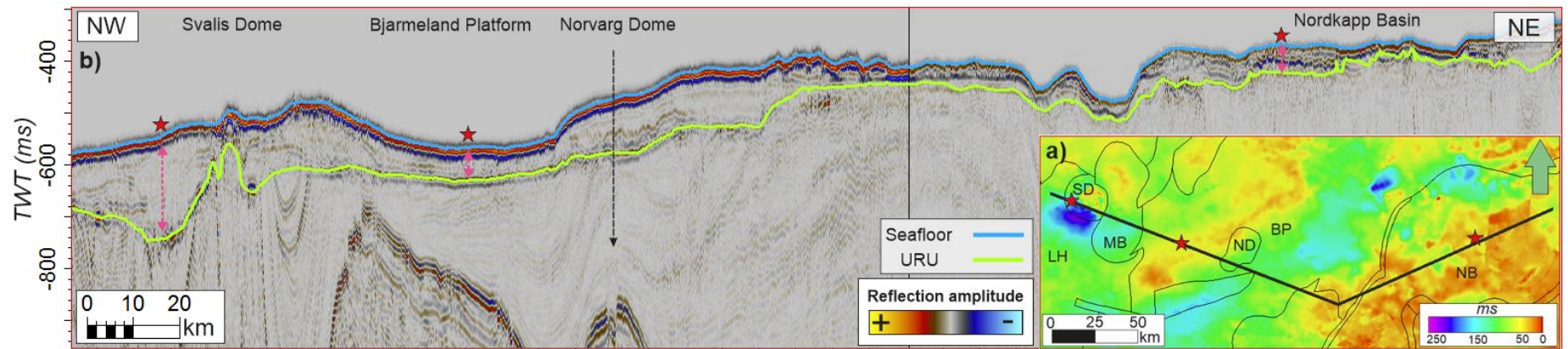


Figure 4.9: a) Isochore map and b) composite 2D line across the study area showing the variations in thickness of the Quaternary sediments. LH = Loppa High, SD = Svalis Dome, MB = Maud Basin, SaD = Samson Dome, ND = Norvarg Dome, BP = Bjarmeland Platform, NB = Nordkapp Basin. The red stars on the profiles correspond to the locations marked with stars on the map.

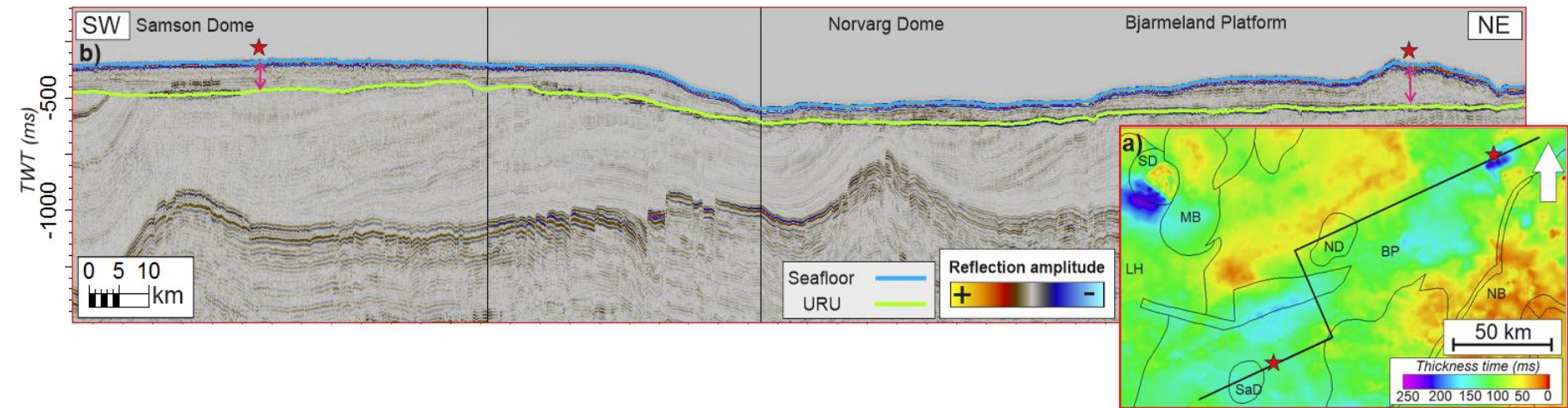


Figure 4.10: a) Isochore map and b) composite 2D line across the Samson and Norvarg domes and the Bjarmeland Platform showing the variations in time-thickness of the Quaternary sediments. LH = Loppa High, SD = Svalis Dome, MB = Maud Basin, SaD = Samson Dome, ND = Norvarg Dome, BP = Bjarmeland Platform, NB = Nordkapp Basin. The red stars on the profiles correspond to the locations marked with stars on the map.

## 4 Results

### 4.2 Svalis Dome

#### 4.2.1 Horizons

Adjacent to the Svalis Dome, the URU is distinguishable as a continuous high amplitude reflection with normal polarity. The strata below the URU is uplifted and steeply dipping reflections subcrop the unconformity with a high angle around the flank of the dome. The URU reflection is also uplifted on the flanks of the dome, and subcrops the seafloor reflection around the domes peak. The URU has a gentler dip on the eastern flank than on the western flank of the dome, where the depth of the unconformity increases abruptly, forming a depression filled with Quaternary sediments.

The seafloor is represented by a high amplitude peak reflection above and around the dome. It is elevated above the dome, as an anomalous high relative to the surrounding seafloor in the Bear Island Trough. The seafloor is elevated in several smaller peaks above the central part of the dome, with otherwise flat seafloor in between them.

#### 4.2.2 Quaternary sediments

The thickness of the Quaternary sediments varies around the Svalis Dome, i.e. they are thicker (more than 200 ms) and thinner (less than 100 ms) SW and NE of the dome, respectively (Figure 4.11). The average time thickness (TVT) in the deepest part of the “mini-basin” SW of the dome is 200 ms. Using the average velocity of 2000 m/s for glaciogenic sediments inferred from Andreassen et al. (2007), the thickness is calculated to approximately 200 meters. Assuming a relatively even thickness in this area, the volume of glaciogenic sediments in this part of the mini-basin would be approximately 90.7 km<sup>3</sup>. The sediment sequence comprises horizontal, subparallel reflections with low to medium amplitudes. The continuity of the reflections varies in the different 2D datasets.

Intra Quaternary horizon A1 is distinguishable as a low amplitude peak reflection above the URU. The reflection is slightly undulating but relatively even. The interpreted horizon onlaps the uplifted URU on the southwestern flank of the dome (Figure 4.12 and 4.14) and downlaps onto the unconformity along towards the western margin of the depression the sediments are accumulated in (Figure 4.14).

Horizon A2 is represented by an intra Quaternary low amplitude peak reflection that is continuous and slightly undulating. The depth of the horizon increases towards the northwest, where it downlaps onto the URU at approximately 680 ms (TWT) depth. It onlaps the uplifted URU along the flanks of the dome and downlaps onto the unconformity in the east (Figure 4.12, 4.13 and 4.15).

## 4 Results

The sequence between A1 and A2 southwest of the dome comprises low to medium amplitude reflections with varying continuity. The reflections display a hummocky and undulating pattern with some local high amplitudes. East of the dome there are less visible reflections, as the sequence is thinner and as the resolution varies in the different data sets. These reflections are less continuous and have an undulating form.

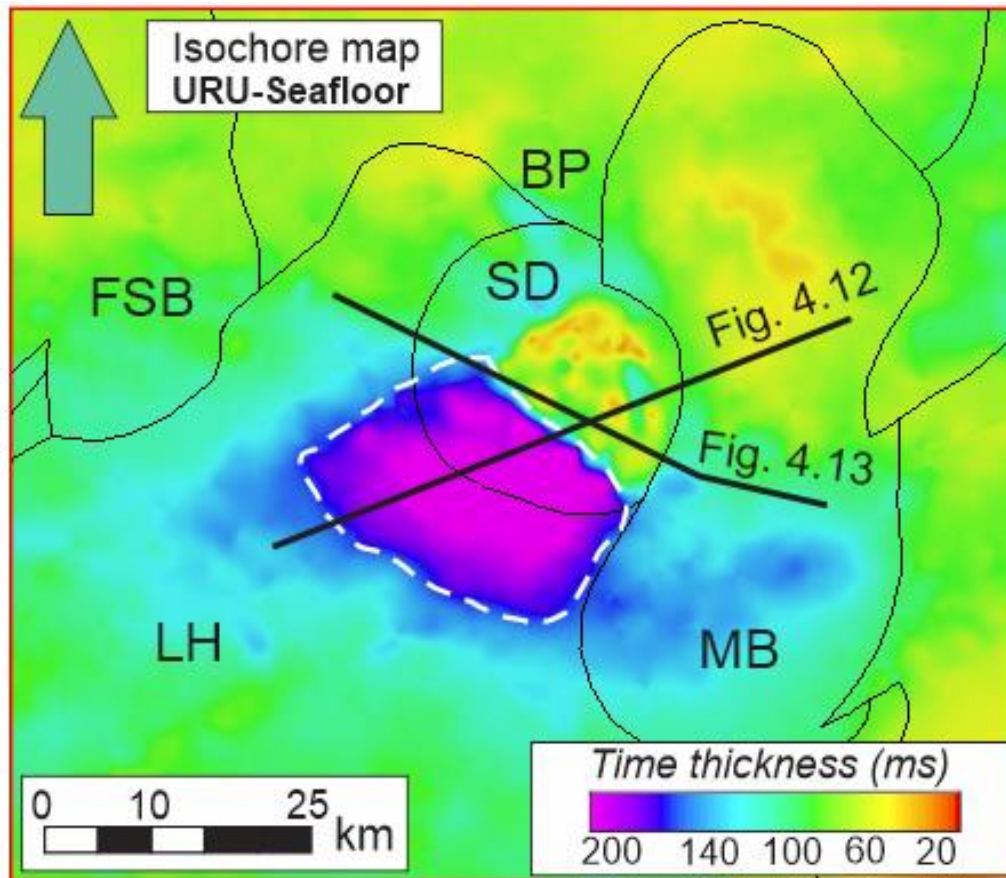


Figure 4.11: Isochore map showing the increase in time thickness of the Quaternary sediments southwest of the Svalis Dome. The black lines mark the position and orientation of the seismic profiles in figures 4.12 and 4.13. The white dotted line outlines the area where the volume of sediments was calculated. FSB = Fingerdjupet Sub-Basin, LH = Loppa High, SD = Svalis Dome, BP = Bjarmeland Platform, MB = Maud Basin.



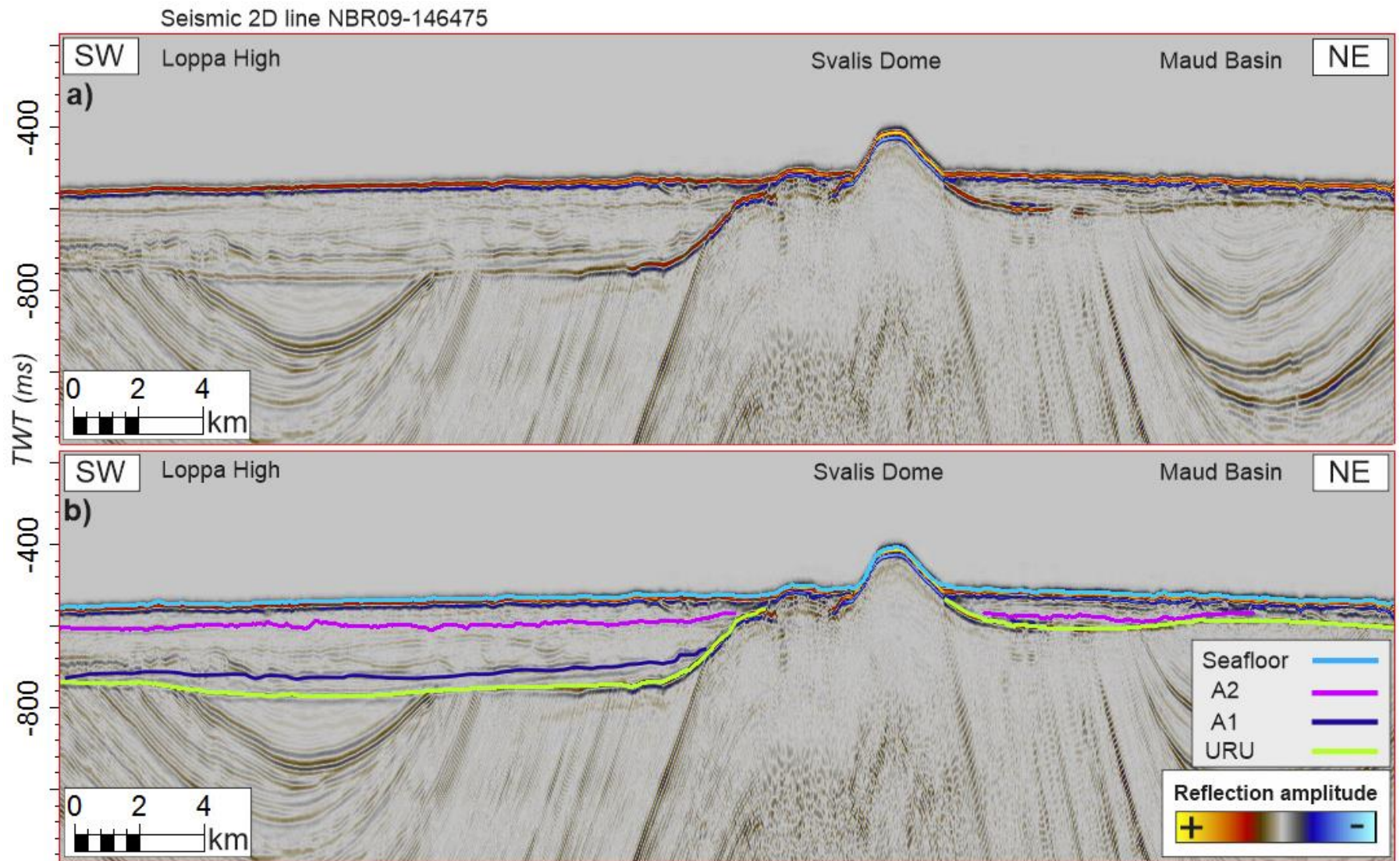


Figure 4.12: a) uninterpreted and b) interpreted seismic profiles showing the variations in depth of the URU and thickness of the Quaternary sediments by the Svalis Dome.

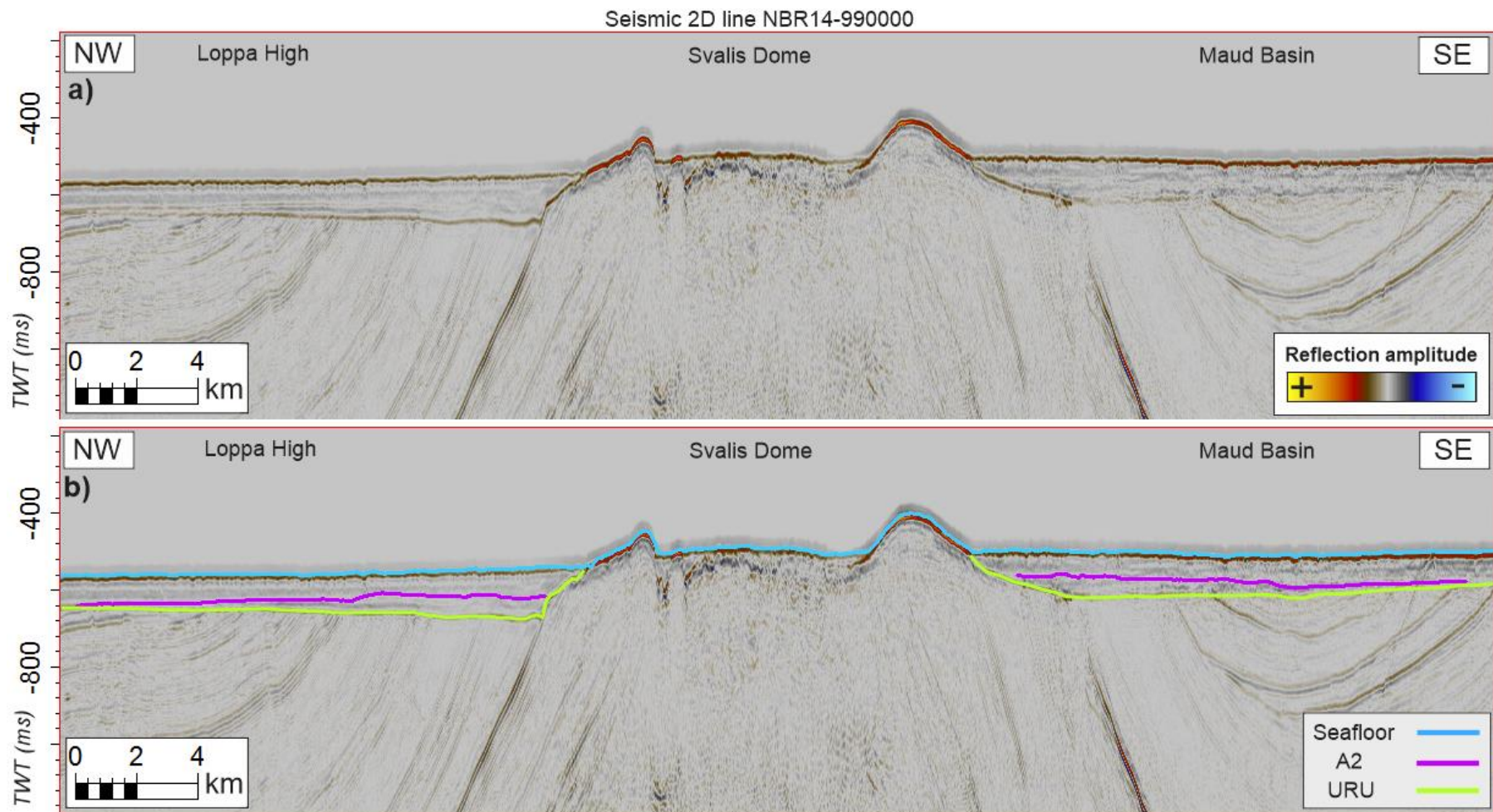


Figure 4.13: a) uninterpreted and b) interpreted seismic profiles through the Svalis Dome. Note how the URU is uplifted on the flanks of the dome and terminates against the seafloor near the top.

## 4 Results

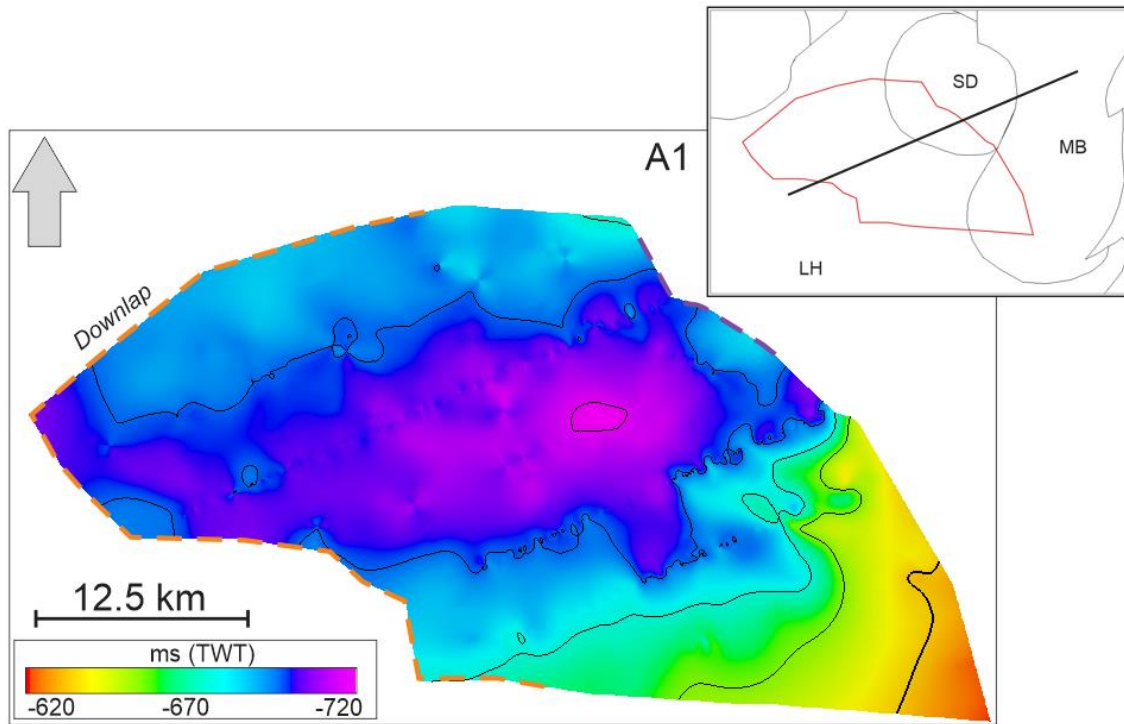


Figure 4.14: Extent (red polygon) and depth of Intra quaternary horizon A1. Contour line increment = 25 ms. LH = Loppa High, SD = Svalis Dome, MB = Maud Basin. The orange dotted line delineates where the horizon downlaps onto the URU and the purple dotted line marks where it onlaps the Svalis Dome.

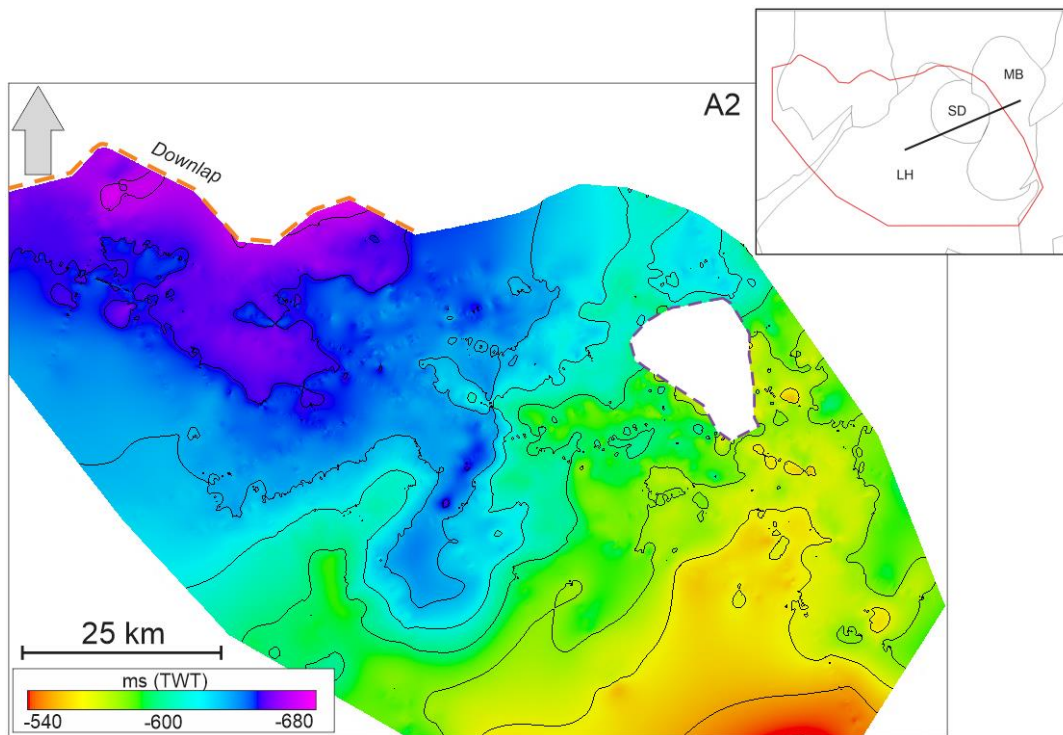


Figure 4.15: Extent (red polygon) and depth of Intra quaternary horizon A2. Contour line increment = 20 ms. LH = Loppa High, SD = Svalis Dome, MB = Maud Basin. The orange dotted line delineates where the horizon downlaps onto the URU and the purple dotted line marks where it onlaps the Svalis Dome.

### 4.3 Samson Dome

Above the Samson Dome, the URU reflection is represented by a medium amplitude peak reflection with high continuity. The unconformity is even above the dome and truncates the strata below that has been uplifted by the dome (Figure 4.16). Towards the southwest, the reflections underlying the URU subcrop it at a relatively steep angle, relative to the northern side. Towards the north and east it is difficult to distinguish where the underlying reflections subcrop the unconformity, as they have a more gentle angle. The URU reflection displays a prominent lateral increase in amplitude above the Samson Dome (Figure 4.16 and 4.17). The area of increased amplitude is located above the central and southern part of the dome, and extends approximately 10 km towards the south in a sub-circular shape (Figure 4.17a).

The quaternary sediment package is even in thickness above and adjacent to the dome and comprises low to medium amplitude subparallel reflections (Figure 4.17b and c). There is a local increase in amplitude of one of the intra quaternary reflections, displaying a peak signature above the unconformity in central parts of the dome (Figure 4.17). The dome is located below the Nordkapp Bank, and the seafloor is even above and adjacent to the dome with an average depth of 350 ms (TWT).

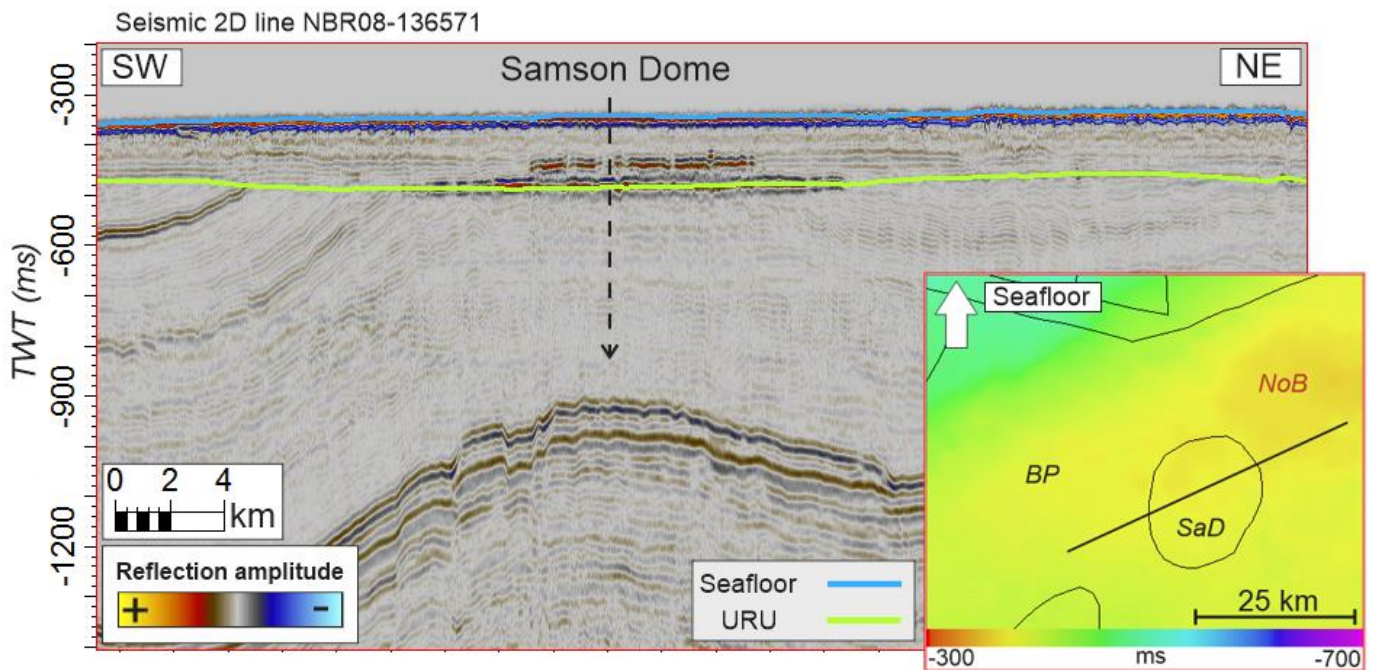


Figure 4.16: Seafloor surface and interpreted profile through the strata above the Samson Dome. BP = Bjarmeland Platform, SaD = Samson Dome, NoB = Nordkapp Bank.

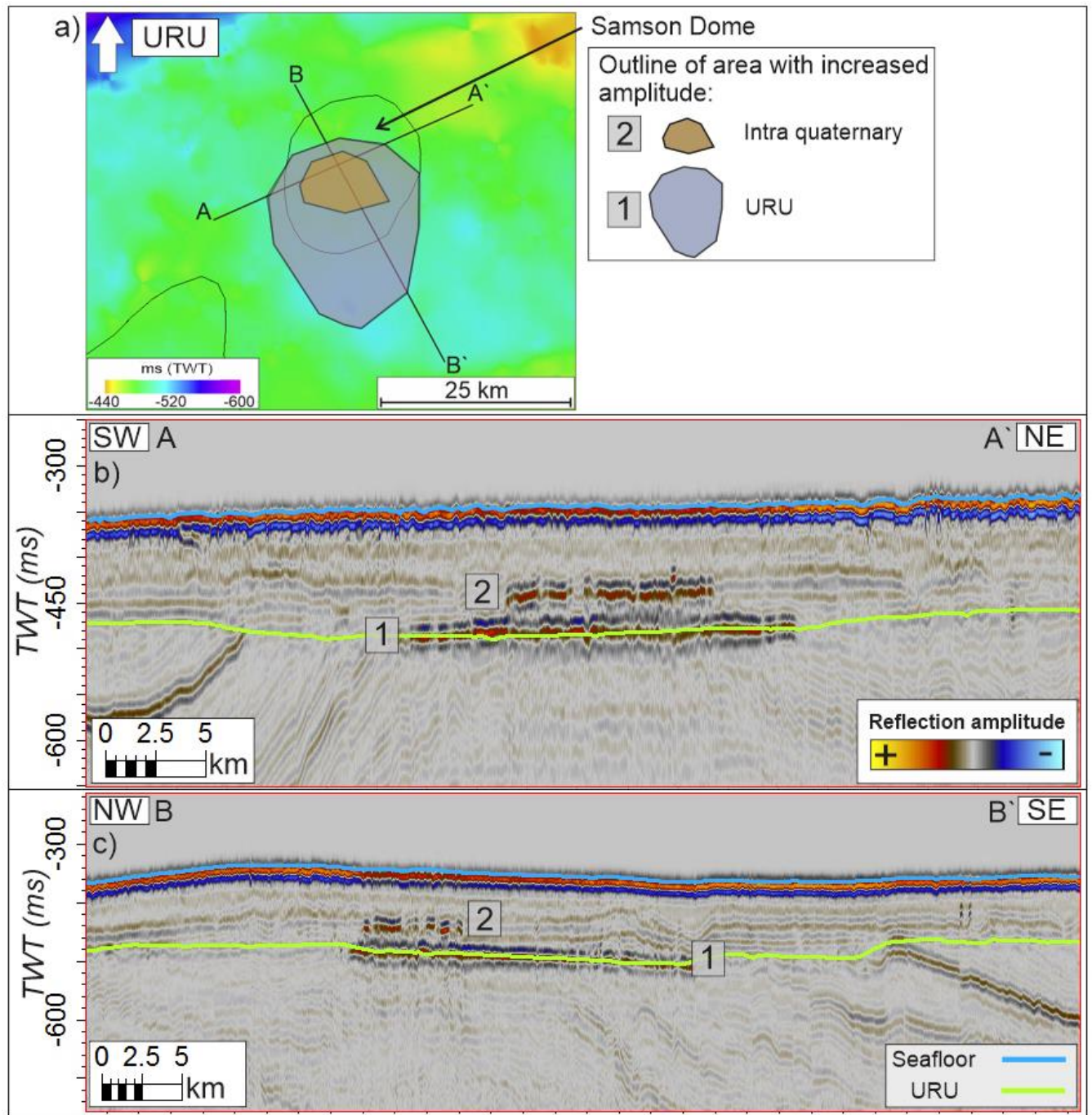


Figure 4.17: a) URU surface above the Samson Dome with the extent of the high amplitude zones along the URU and intra Quaternary horizon marked and two profiles showing the appearance of the zones on seismic data (b) and c).

## 4 Results

### 4.4 Norvarg Dome

Above and adjacent to the Norvarg Dome, the URU is relatively flat and has an even depth of approximately 600 ms (TWT). The unconformity is represented by a medium amplitude peak reflection. Directly above the dome, the URU reflection is slightly undulating and shows local variations in amplitude. The URU truncates the uplifted strata below, and the doming reflections above the dome subcrop the horizon at a relatively steep angle around the margin of the structure (Figure 4.18).

Below the unconformity, faulting of the strata is visible. The doming reflections of the uplifted strata above the deeper salt is vertically displaced by steep faults. Some of the faults reach the unconformity, and terminate against it (Figure 4.18).

The dome is located by the margin of the Bear Island Trough, and there is a decrease in water depth towards the southeast when moving from the trough up onto the Nordkapp bank. The depth decreases from almost 600 ms at the margin of the trough, to less than 500 ms towards the bank.

Above the dome, there is a southwards increase in sediment thickness towards the Nordkapp Bank. The sequence displays some low amplitude reflections with medium to poor continuity and a hummocky, undulating pattern (Figure 4.18).

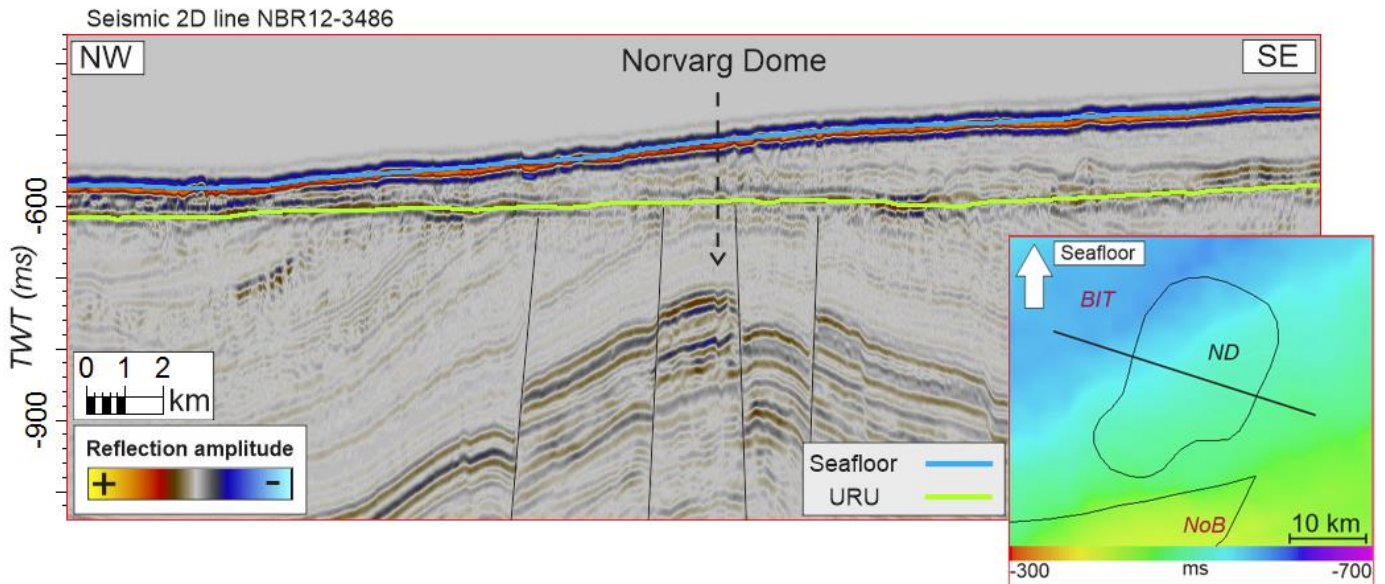


Figure 4.18: Seafloor surface and interpreted seismic profile through the strata above the Norvarg Dome. BIT = Bear Island Trough, ND = Norvarg Dome, NoB = Nordkapp Bank.

## 4 Results

### 4.5 Nordkapp Basin

#### 4.5.1 Horizons and sediments

Within the Nordkapp Basin, the depth of both the seafloor and URU varies locally in between the many salt bodies located within the basin. The unconformity has an average depth of 425 ms, and is shallowest towards the northeast at less than 300 ms, and deepest in the northern central part of the basin, at 575 ms (Figure 4.19). The presence of the URU is uncertain above the northeastern part of the basin. The seafloor displays a similar trend, and is at less than 250 ms depth in the northeastern part of the basin, where it is elevated above salt diapirs (Figure 4.20).

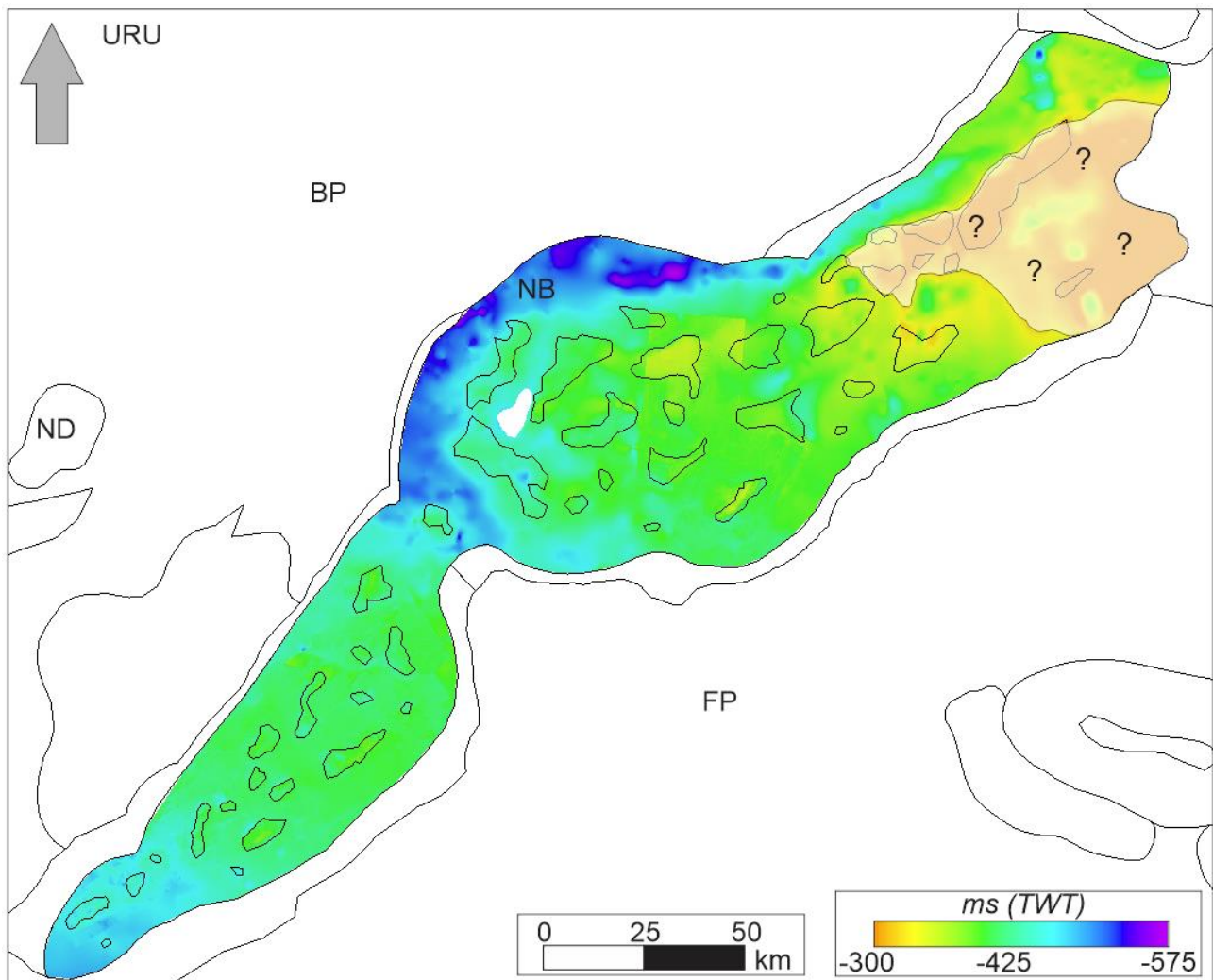


Figure 4.19: Map showing the depth in ms TWT of the URU horizon within the Nordkapp Basin. ND = Norvarg Dome, BP = Bjarmeland Platform, FP = Finnmark Platform.

## 4 Results

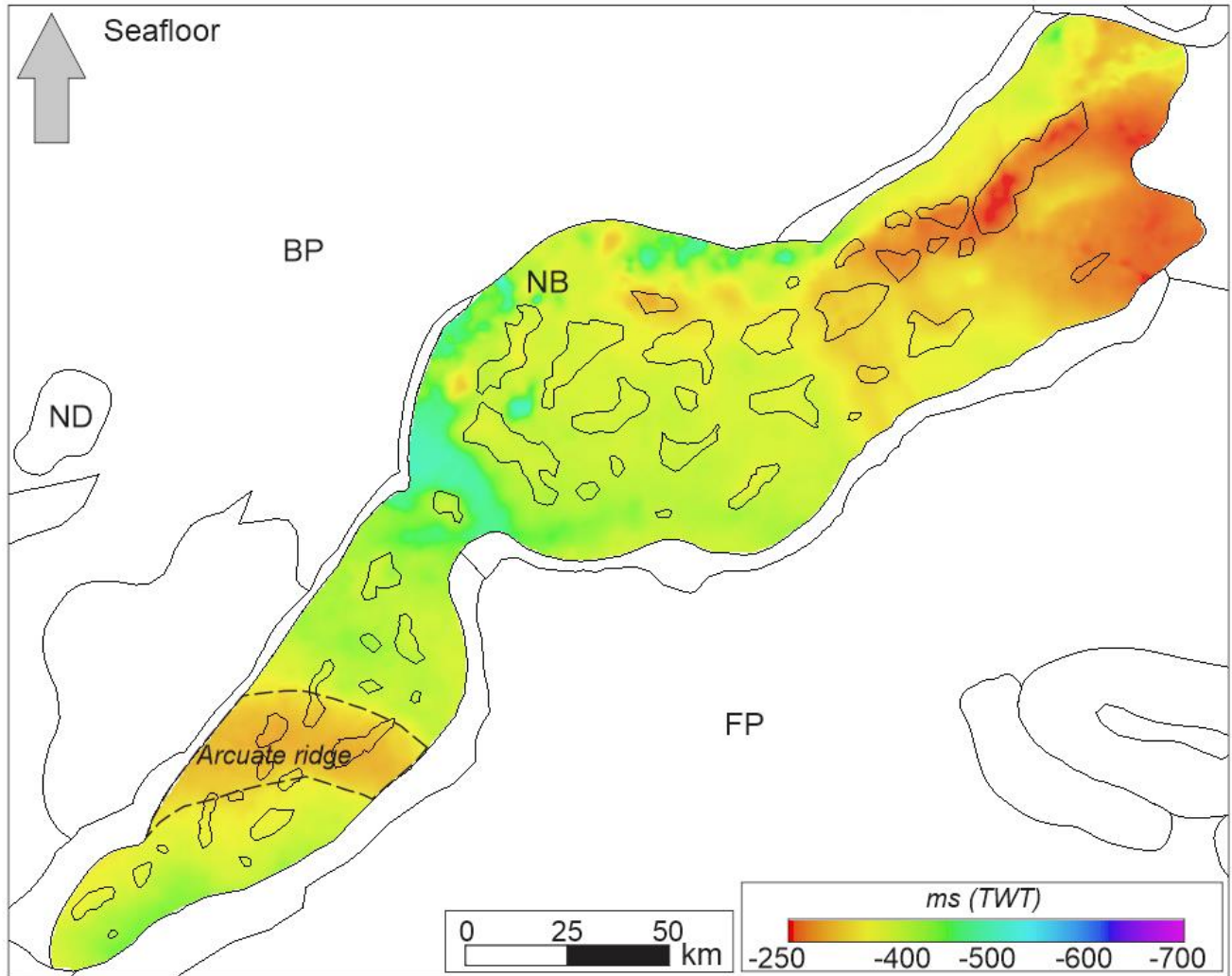


Figure 4.20: Map showing the depth in ms TWT of the seafloor horizon within the Nordkapp Basin. The Nordkapp arcuate ridge is outlined by the dashed black polygon. ND = Norvarg Dome, BP = Bjarmeland Platform, FP = Finnmark Platform.



## 4 Results

The quaternary sediment cover is relatively thin across large parts of the basin, with an average thickness of 40 ms (Figure 4.21). The sediment package is thinnest above central eastern and northeastern parts of the basin. Here the thickness is close to 0 ms across large areas, where the sediment package is either absent or too thin to be resolvable on the seismic data. The thickness increases towards the central northwestern margin of the basin, where it reaches more than 180 ms thickness (Figure 4.21). Here, the URU shows a depression while the seafloor is relatively flat or elevated (Figure 4.19 and 4.20). In the southwest, the sediment package thickness increases significantly where the previously described arcuate ridge located, and the shape of the ridge is distinguishable on the isochore map.

Several intra quaternary horizons have been interpreted within some of the sediment accumulations. Within the arcuate ridge in the southwest, reflection B1 and B2 were mapped (Figure 4.21) and are visible as a medium amplitude peak reflections with good continuity. They downlap onto the URU towards the northeast, near the margin of the ridge.

In the central northeast part of the basin, intra quaternary reflections C1 and C2 are mapped within the sediment sequence (Figure 4.21). Both reflections display a medium amplitude and are continuous. The horizons onlap the URU towards the southwest, where the URU is elevated above salt diapirs. Towards the northeast these intra quaternary horizons downlap towards the unconformity.

Internally, the sediment package is characterized by sub-parallel medium amplitude reflections. The continuity of the reflections varies greatly, and is also dependent on the quality of the seismic surveys. In the areas where the sediment thickness is low, it is not possible to distinguish the internal horizons. Thus, they have only been interpreted within large sediment accumulations. The seismic stratigraphy of the intra quaternary horizons in relation to some of the salt diapirs in the basin is described further in the next sub-chapter.

## 4 Results

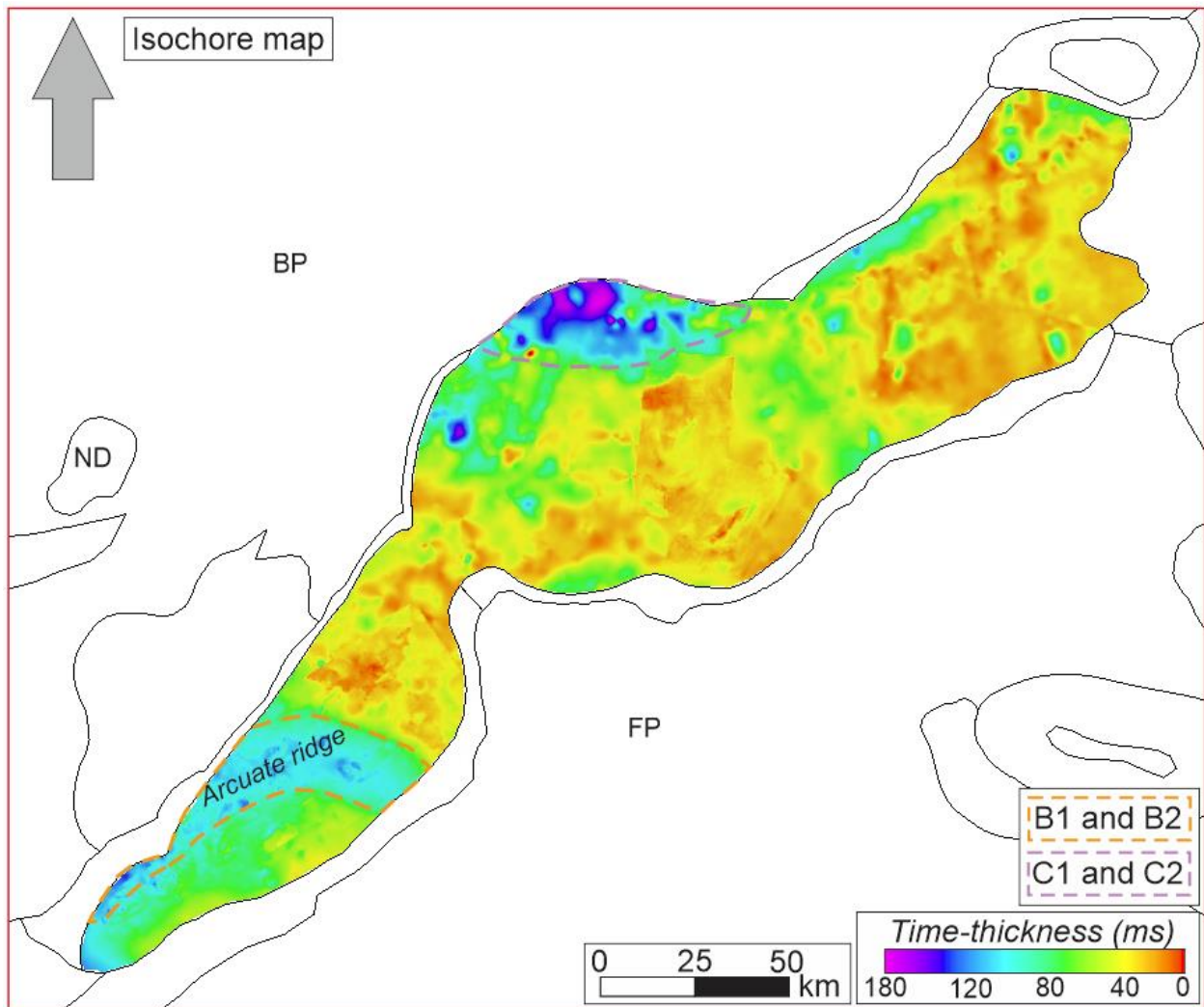


Figure 4.21: Isochore map showing the time-thickness (TVT- True Vertical Thickness) of the sediments above URU within the Nordkapp Basin. The dashed polygons outline the areas of sediment accumulation where intra Quaternary horizons were mapped. ND = Norvarg Dome, BP = Bjarmeland Platform, FP = Finmark Platform.

## 4 Results

### 4.5.2 Salt diapirs in the Nordkapp Basin

Forty-four salt diapirs in the Nordkapp Basin have been studied on 2D and 3D seismic data. The diapirs have been categorized based on the stratigraphic relationship between the salt bodies and the interpreted URU and seafloor surfaces overlying them. The numbering and positions of the different diapirs are shown in figure 4.22. The morphology and orientation of the diapirs and the interpreted depth to the top of the salt bodies are summarized in table 4.1. For systematic purposes, the basin is divided into a southwestern and northeastern sub-basin when describing the positions of the salt diapirs. Due to time constraints, not all diapirs could be studied and shown in detail. In the following chapter, some select diapirs representing different stratigraphic relationships are described, starting in the southwest and moving consequently toward the northeast.

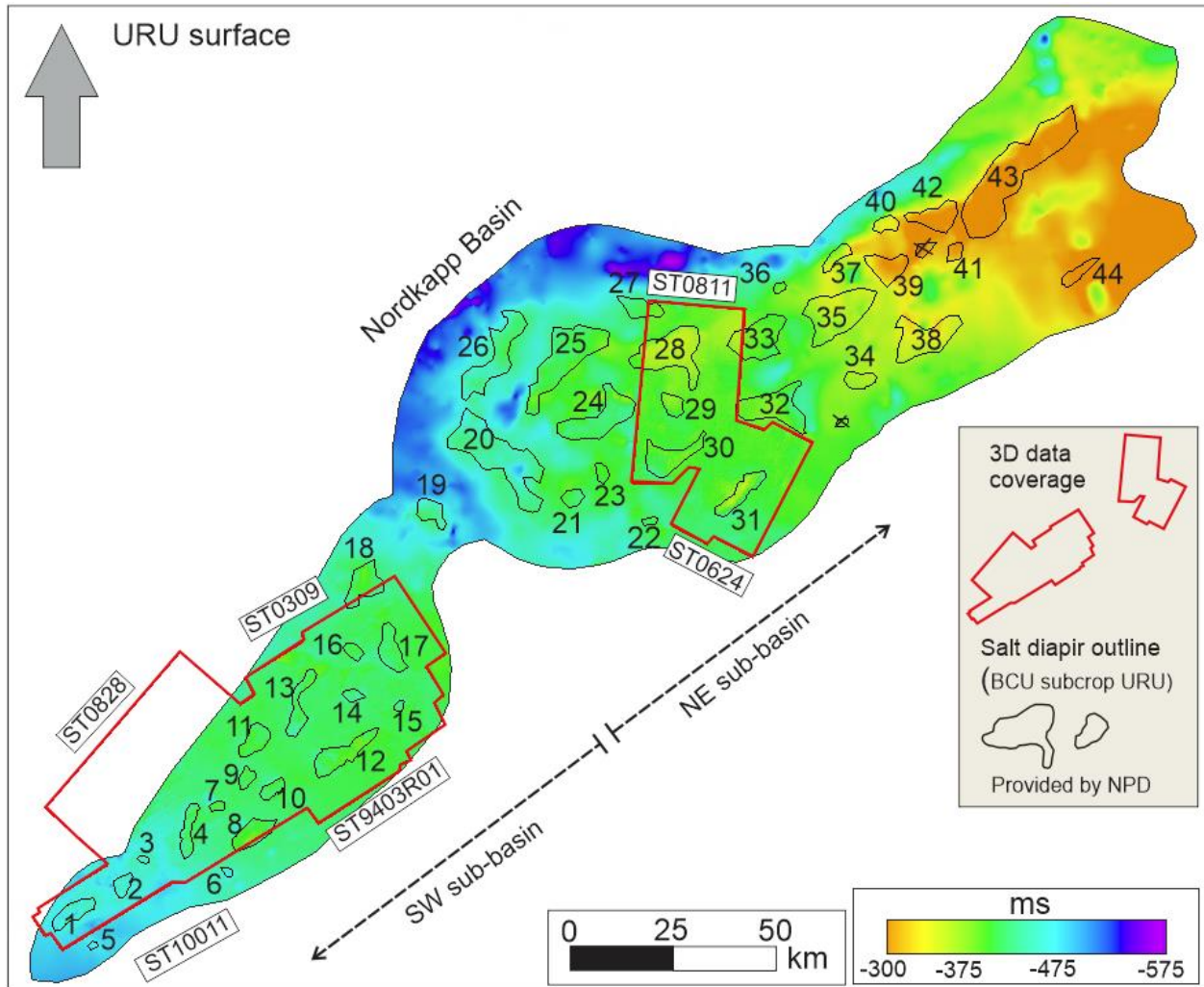


Figure 4.22: Overview of the numbering and positions of the salt diapirs studied within the Nordkapp Basin. The red polygons delineate the coverage of the 3D data sets and the dotted arrows indicate how the basin is divided into sub-basins for systematic and descriptive purposes.

## 4 Results

Table 4.1: General information about the salt diapirs in the Nordkapp Basin.

<b>Diapir Number</b>	<b>Top salt TWT (ms)</b>	<b>Shallow morphology</b>	<b>Orientation</b>
<b>Nordkapp Basin</b>			
1	480	Elongated	SW-NE
2	460	Sub-circular	Undefined
3	460	Circular	Undefined
4	450	Elongated	SSW-NNE
5	470	Circular	Undefined
6	700	Sub-circular	Undefined
7	500	Sub-circular	E-W
8	440	Elongated	SW-NE
9	420	Sub-circular	Undefined
10	420	Elongated	SW-NE
11	420	Elongated	SW-NE
12	500	Elongated	SW-NE
13	440	Elongated	SSW-NNE
14	430	Sub-circular	Undefined
15	430	Circular	Undefined
16	420	Sub-circular	NW-SE
17	410	Elongated	N-S
18	400	Sub-circular	Undefined
19	400	Sub-circular	Undefined
20	440	Elongated	NW-SE
21	430	Circular	Undefined
22	420	Elongated	E-W
23	700	Sub-circular	Undefined
24	400	Elongated	WSW-ENE
25	400	Elongated	SW-NE
26	420	Elongated	SW-NE
27	450	Elongated	W-E
28	390	Sub-circular	Undefined
29	400	Circular	Undefined
30	550	Elongated	SW-NE
31	400	Elongated	SW-NE
32	410	Elongated	W-E
33	400	Partly elongated	Undefined
34	380	Sub-circular	W-E
35	370	Partly elongated	SW-NE
36	400	Circular	Undefined
37	370	Elongated	SW-NE
38	360	Elongated	W-E
39	350	Large elongated salt wall system of multiple diapirs with a common stem	Oriented SW-NE
40	380		
41	350		
42	340		
43	300		
44	320	Elongated	SW-NE

## 4 Results

### *Southwestern sub-basin*

The relationship between the URU, seafloor and salt bodies of some selected diapirs have been studied in the southwestern Nordkapp sub-basin. The positions and orientations of the seismic profiles through the studied diapirs are shown in figure 4.23 below.

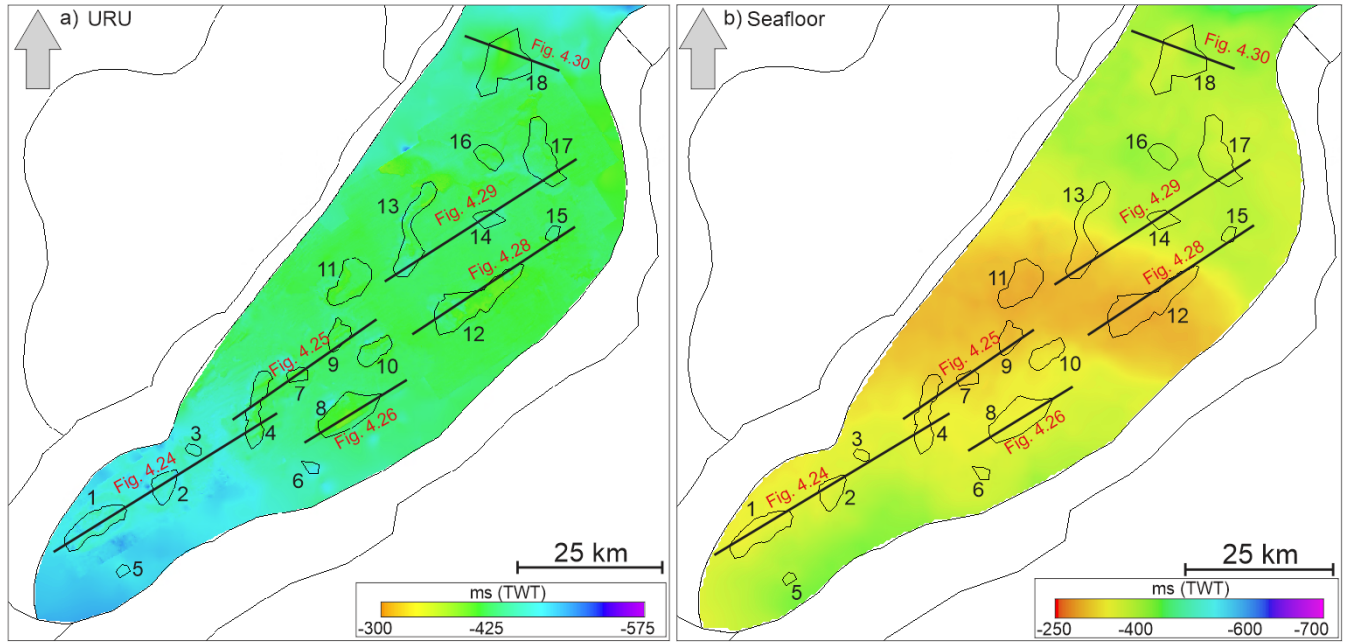


Figure 4.23: a) URU surface in the SW Nordkapp sub-basin. b) Seafloor in the SW Nordkapp sub-basin. The black lines mark the position and orientation of featured seismic profiles.

### Diapir 1-4

The top of the salt bodies is identified by local high amplitude peak reflections (Figure 4.24), in response to the increase in acoustic impedance. The salt body has a higher velocity than the overlying glacial sediments, with halite reaching a velocity of 4500 m/s (see table. 1.1) (Jones and Davidson, 2014). This causes a contrast in acoustic impedance and a positive reflection coefficient, giving the peak reflection. The top of the salt bodies is located between 480 and 450 ms (TWT) depth.

All diapirs are truncated by the URU, which overlies the diapirs represented by a continuous medium amplitude trough reflection (Figure 4.24). The unconformity is locally slightly elevated above the diapirs (Figure 4.24 and 4.25). The Seafloor horizon is uniform in depth above the diapirs and remains relatively flat (Figure 4.24). The sediment package above the URU displays some low amplitude reflections with poor continuity and has a uniform thickness of approximately 80 ms (TWT).

## 4 Results

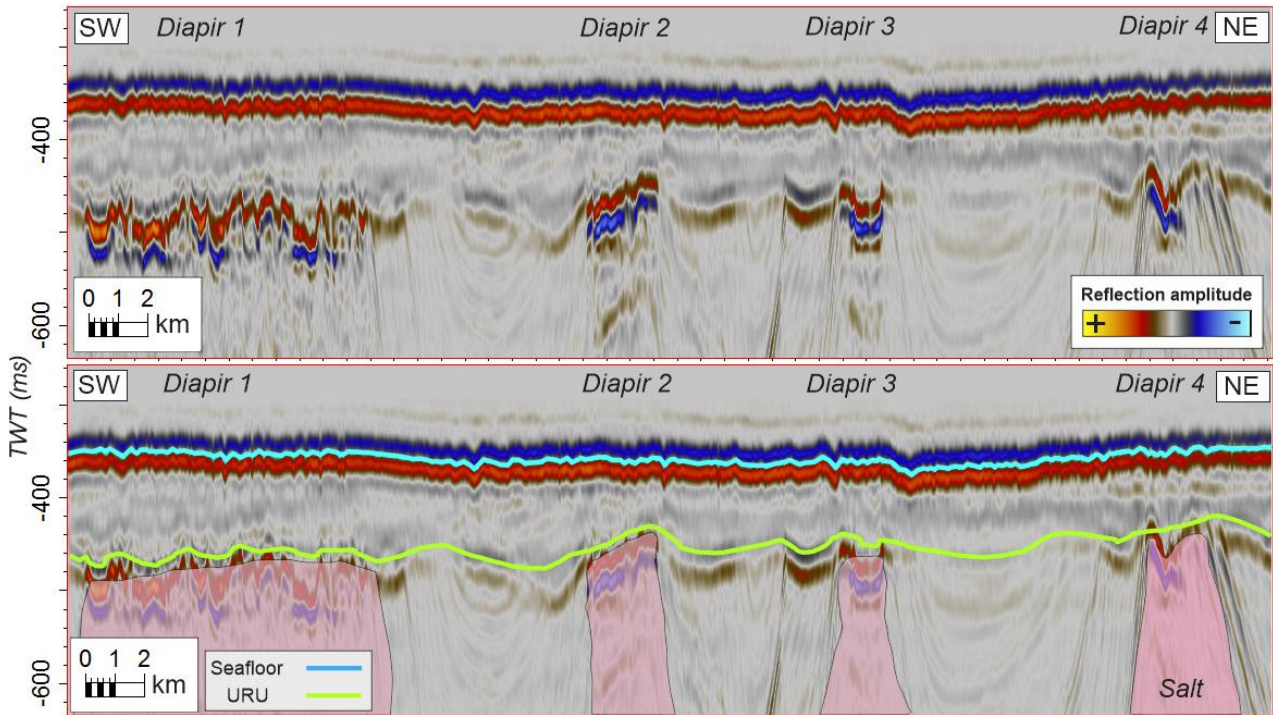


Figure 4.24: Seismic profiles through the top of diapirs 1-4. From 3D data set ST10011.

### Diapir 7-9

The tops of the salt bodies are distinguishable as local high amplitude peak reflections. They are found between 500 and 420 ms (TWT) depth. All the diapirs are truncated by the URU (Figure 4.25 and 4.26). The unconformity reflection is slightly elevated above the diapirs, and shows local depressions adjacent to diapir 7. The center of diapir 8 is partly collapsed, shown by the depression in the top salt reflection (Figure 4.26).

The sediment package above diapir 7 and 9 is uniform in thickness at approximately 100 ms (TWT), while the sediment cover above diapir 8 is thinner, at approximately 70 ms. The sediment package thins across diapir 8, but becomes thicker above the collapsed part of the diapir (Figure 4.26). Intra quaternary horizon B1 above diapir 7 and 9 was interpreted along a continuous medium amplitude peak reflection. The horizon is relatively even across the diapirs and decreases slightly in depth towards the southwest (Figure 4.25).

## 4 Results

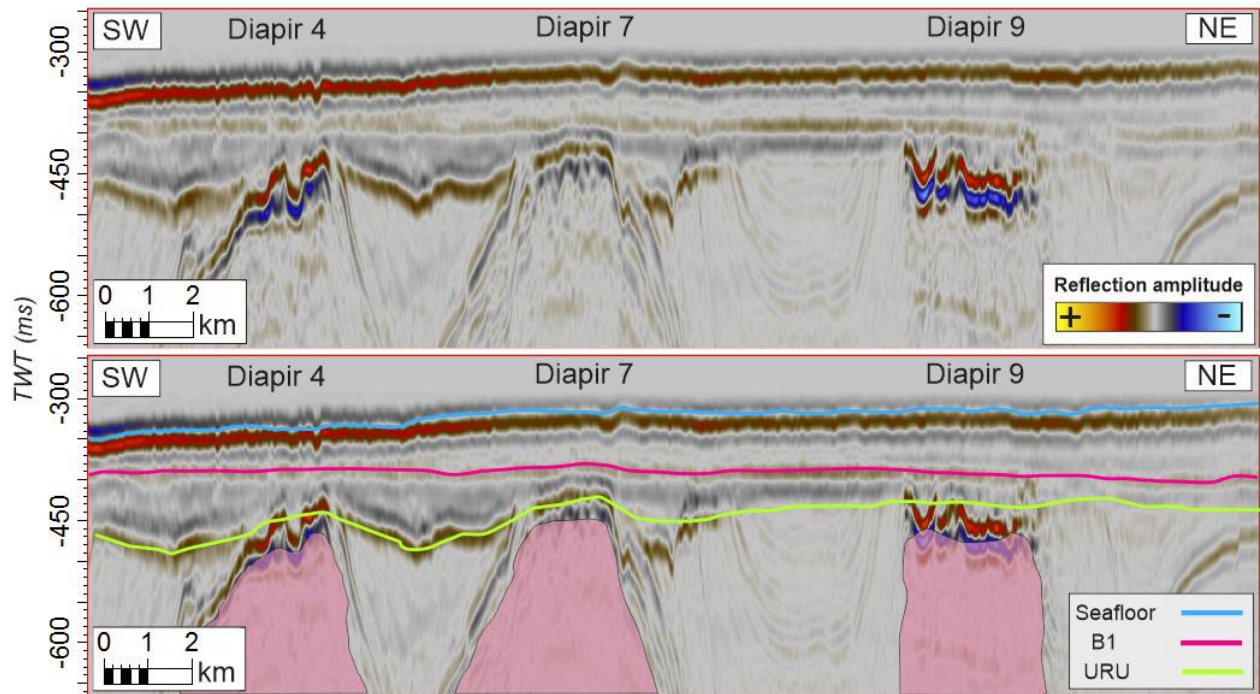


Figure 4.25: Seismic profiles through diapirs 4, 7 and 9. From 3D data set ST10011. Note the positive relief of the unconformity above diapir 4 and 7, and the local depressions adjacent to the diapirs.

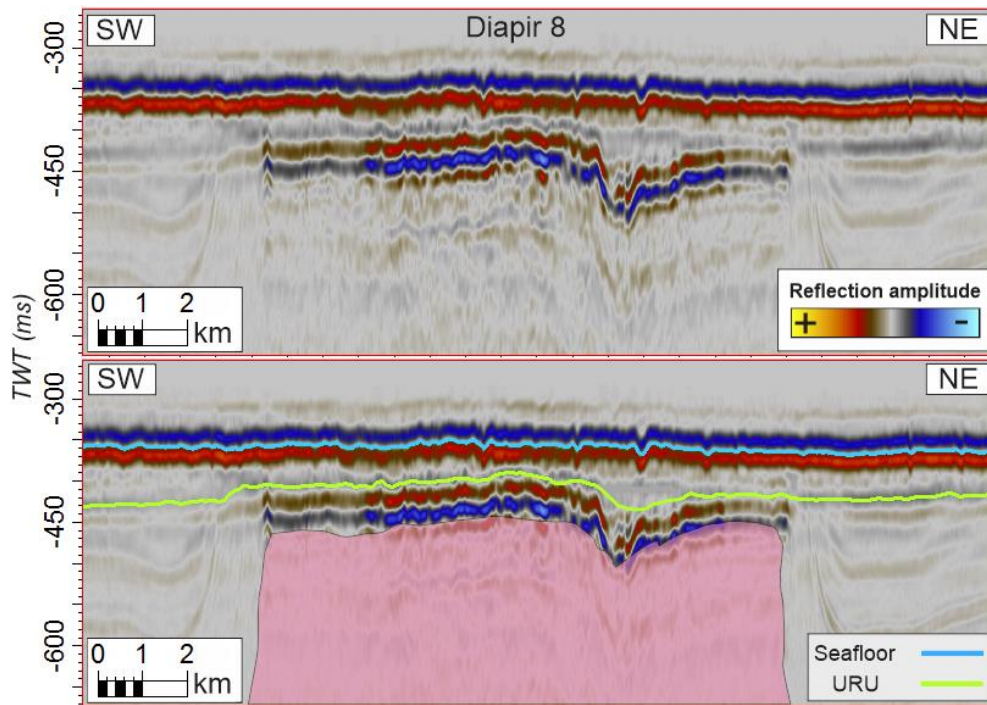


Figure 4.26: Seismic profiles through diapir 8. From 3D data set ST10011. The URU shows a slight depression above central parts of the diapir.

## 4 Results

### Diapir 12-15

The top of the salt bodies in diapirs 13-15 are at an even depth, between 440 and 430 ms (TWT), and are all truncated by the URU (Figure 4.28 and 4.29). The unconformity is slightly elevated above diapir 13 and 14, indicating upwards movement of the salt after the erosion of the ice sheet. The URU cuts the top of diapir 15 as well, but here the surface is not elevated. Compared to the adjacent diapirs, the salt body of diapir 12 is located much deeper. The top salt reflection is uneven and varies in depth, but the top of the salt is located at approximately 500 ms (TWT), supported by an increase in amplitude at this depth (Figure 4.27). The URU truncates the reflections overlying the top salt reflection, but does not cut into the salt body.

Diapir 12 and 13 is located below the arcuate ridge on the Nordkapp Bank. Thus, there is an increase in sediment thickness towards the southwest above the diapirs. The sediment package displays several medium amplitude peak reflections with relatively good continuity, representing intra quaternary interfaces. Two horizons have been interpreted within the ridge. Horizon B1 is relatively even through the ridge, dipping slightly towards northeast. The horizon downlaps the URU in some and subcrops the seafloor in others (Figure 4.28 and 4.29). Horizon B2 is also relatively even and downlaps onto horizon B1 in some locations (Figure 4.29).

### Diapir 17 and 18

The top of the salt bodies of diapir 17 and 18 are located at a slightly shallower depth than in diapir 13-15. The top of the salt is distinguishable as a local high amplitude anomaly at between 400 and 410 ms (TWT) depth for the two diapirs. Both diapirs are truncated by the URU. The unconformity is relatively flat above diapir 17, but has been elevated above diapir 18 (Figure 4.29 and 4.30). In addition, the seafloor is uplifted above diapir 18, indicating late salt activity. The sediment cover above both diapirs is thin, at less than 40 ms (TWT) and there are no distinguishable internal reflections within the sediment package.



## 4 Results

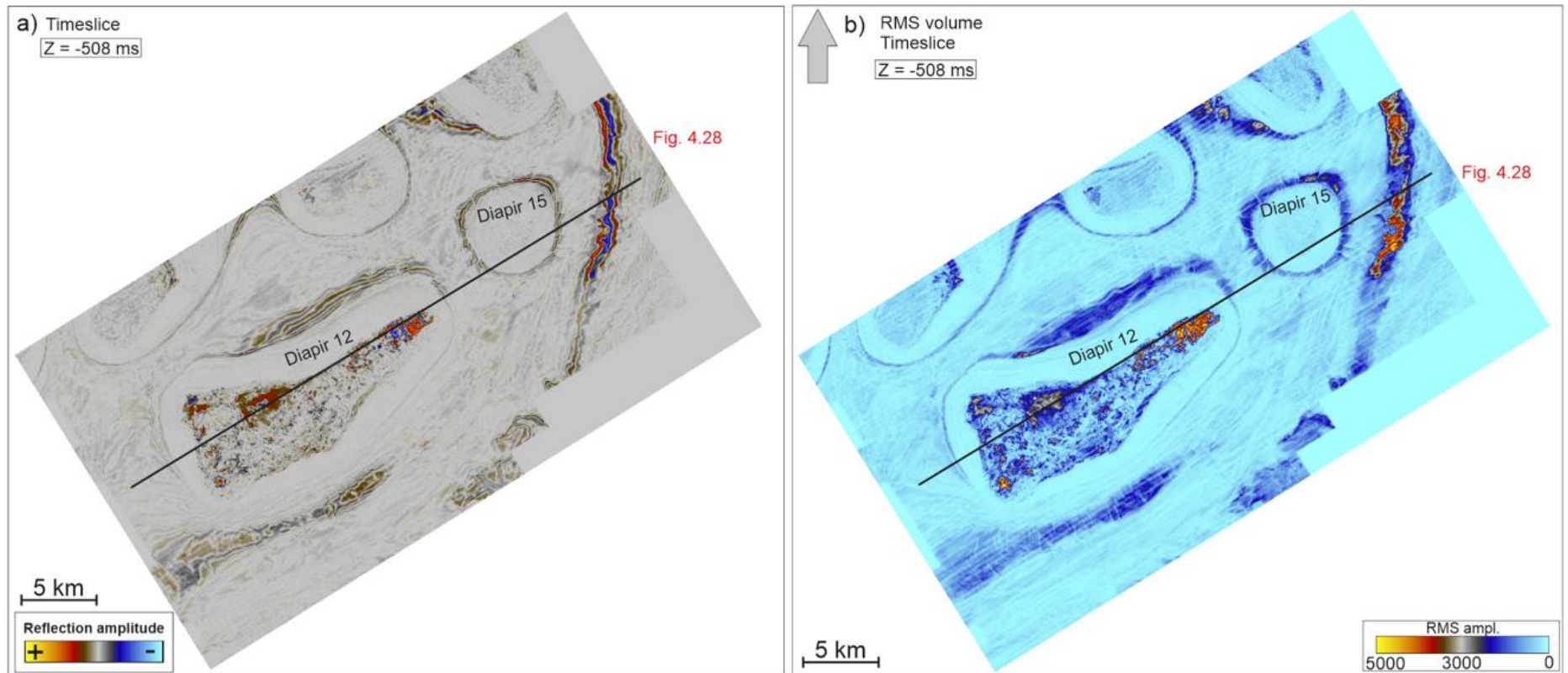


Figure 4.27: a) Time slice and b) RMS amplitude time slice through diapir 12 and 15, showing the difference in amplitude within the diapirs at depth  $z = -508$  ms.

4 Results

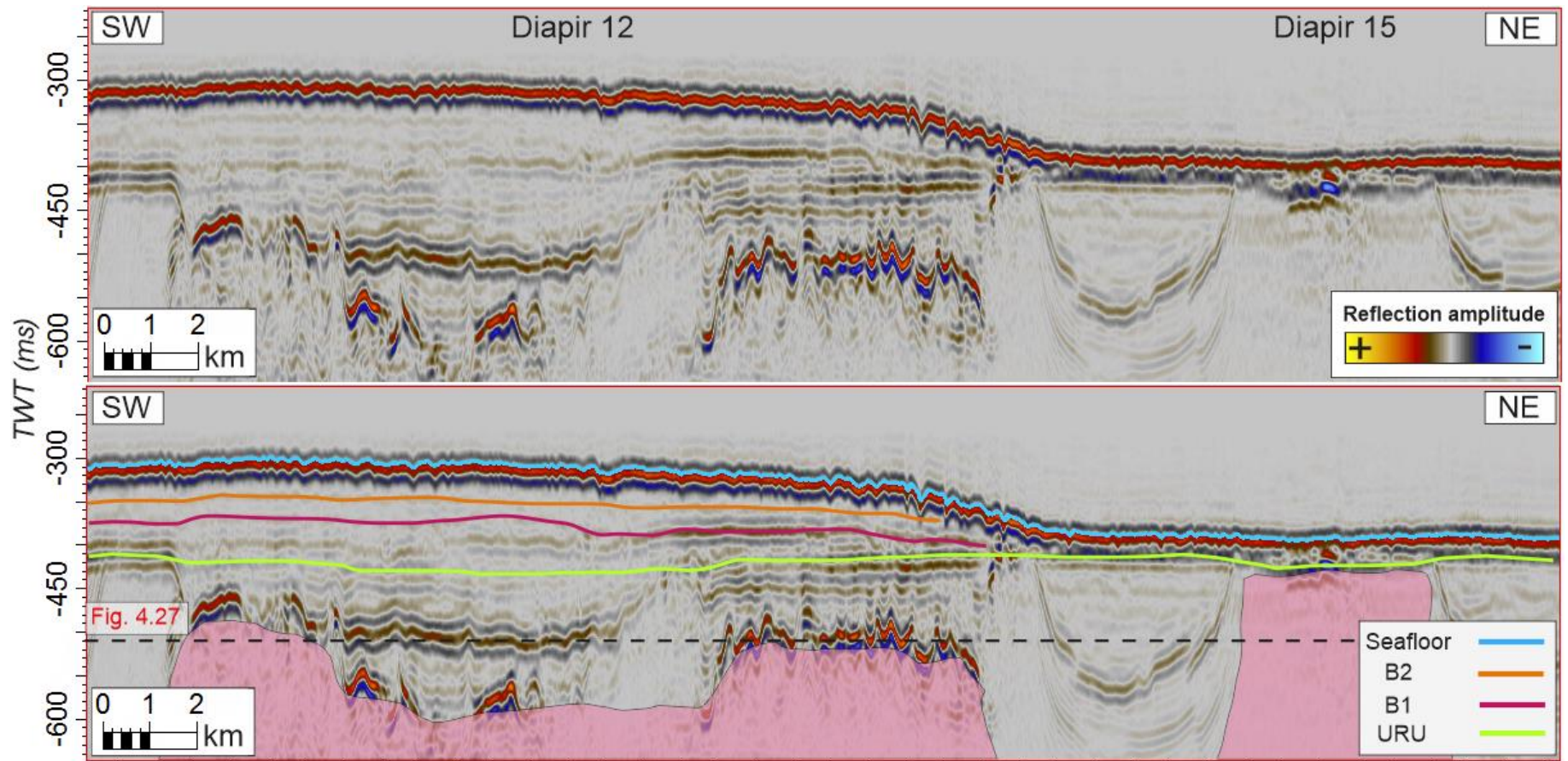


Figure 4.28: Seismic profiles through diapir 12 and 15. From 3D data set ST9403R01. The dashed black line indicates the depth of the time slice in figure 4.27.

4 Results

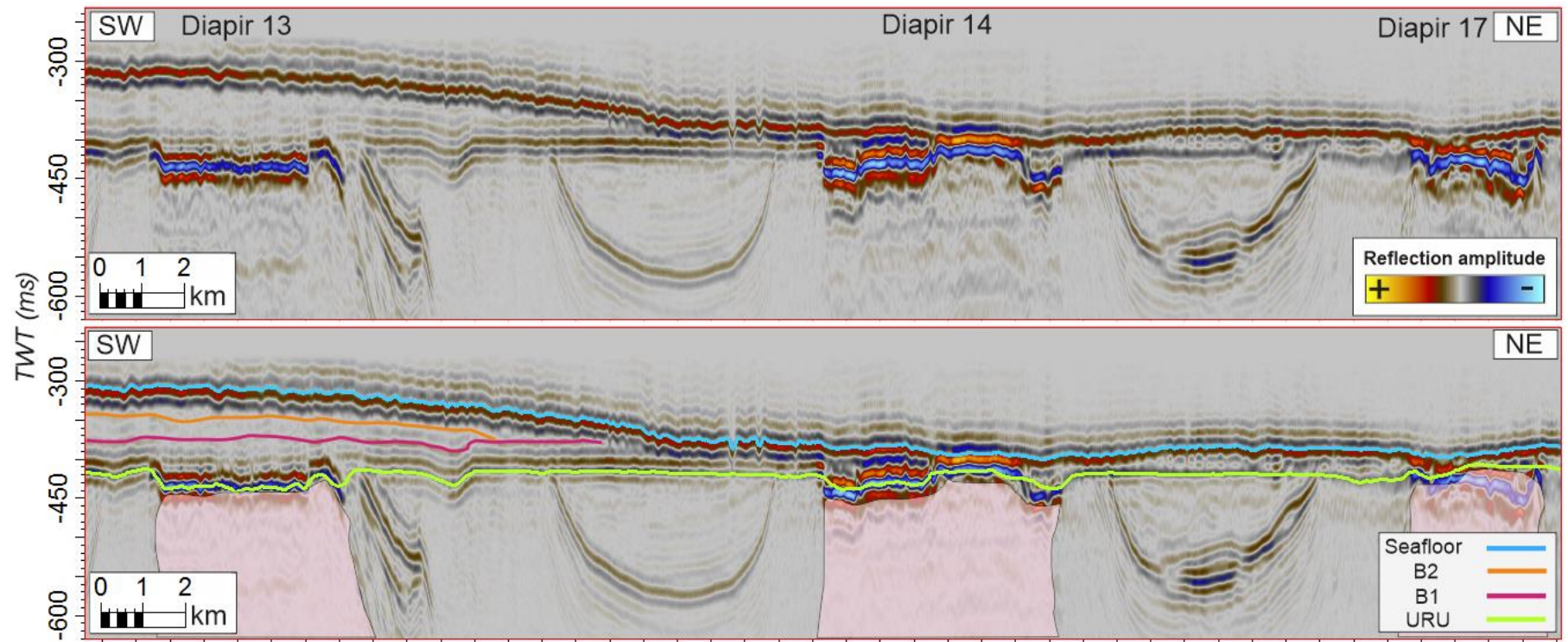


Figure 4.29: Seismic profiles through diapir 13, 14 and 17. From 3D seismic data set ST0309.

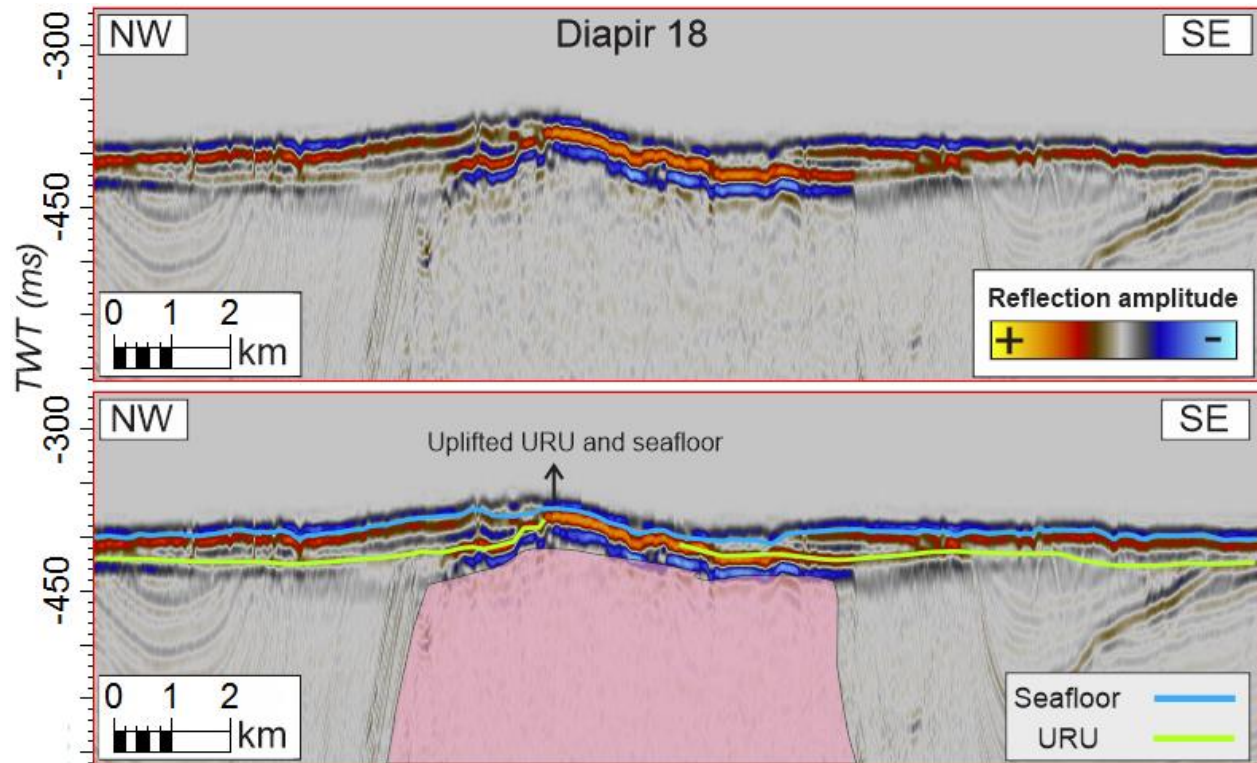


Figure 4.30: Seismic profiles through diapir 18. Arrows indicate uplift of the seafloor and URU above the diapir.

#### Northeastern sub-basin

Several diapirs have been studied in the northeastern sub-basin as well. The positions and orientations of seismic profiles through the diapirs is given in figure 4.31. The relationship between the interpreted horizons and the salt bodies of the diapirs is summarized at the end of this chapter.

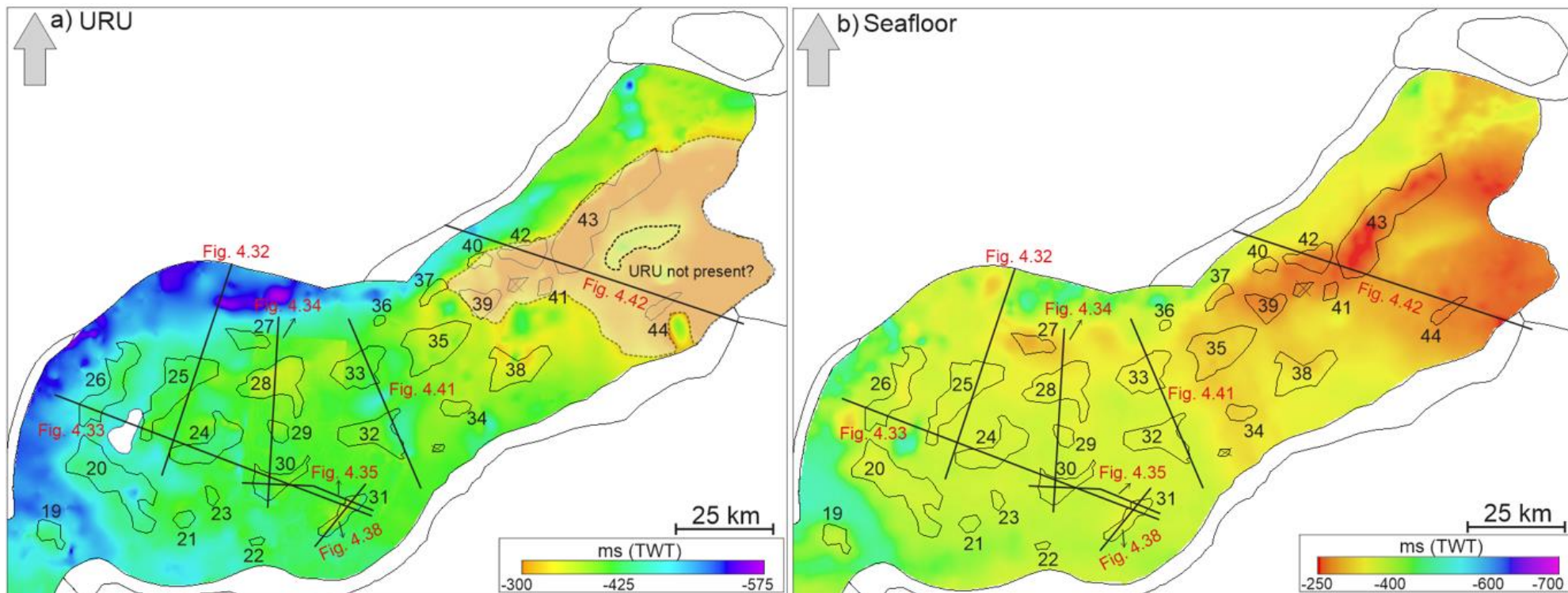


Figure 4.31: a) URU and b) Seafloor in the northeastern Nordkapp sub-basin. The position and orientation of seismic profiles through some of the diapirs is indicating by the black lines. Note the uncertainty of the presence of the URU in the NE, and the depression of the unconformity in the northern central part of the basin, where the seafloor is slightly elevated.

## 4 Results

### Diapir 24-26

The top of the salt bodies of diapirs 24-26 are located at relatively similar depths. The URU truncates all the diapir crests and is represented by a medium amplitude peak reflection on the 2D line (Figure 4.32 and 4.33). The unconformity increases in depth towards the northwest, but is slightly elevated above the diapirs. The seafloor reflection is very undulating and less continuous above diapir 24, where it is slightly uplifted as well. A depression in the seafloor northwest of diapir 25 truncates the URU reflection (Figure 4.33). The unconformity reflection is not distinguishable below the depression.

There is an increase in sediment thickness of the Quaternary northwest of diapir 25, where intra quaternary horizon C2 is distinguishable within the sediment package as a medium amplitude peak reflection. The horizon onlaps diapir 25 to the east and is cut by the depression in the seafloor (Figure 4.33). Horizon C1 has a similar configuration as the overlying C2, and onlaps the elevated URU towards diapir 25, and downlaps the unconformity towards the northeast where the sediment package thins out (Figure 4.32). The sediment package between the URU and C2 thins towards diapir 26 in the northwest (Figure 4.33), where C2 is draped across diapir 26 and laps out towards the seafloor horizons towards the northwest (Figure 4.33).

### Diapir 28 and 29

The salt bodies of diapirs 28 and 29 are both truncated by the URU at 390 and 400 ms (TWT) depth, respectively. The unconformity is represented by a medium to high amplitude reflection with high continuity. The exception is above the diapirs, where the URU reflection is elevated and merges with the seafloor reflection (Figure 4.34). The unconformity truncates the steeply dipping reflections along the flanks of the diapirs. These dipping reflections are also visible on time slices through the structures (Figure 4.36 and 4.37). North of diapir 28, the depth of the URU increases. The quaternary sediment package is thin across the diapirs and increases in thickness to the north of diapir 28 (Figure 4.34). Here, intra Quaternary horizon C2 onlaps diapir 28 towards the south, and laps out towards the seafloor reflection towards the north.

## 4 Results

### Diapir 30 and 31

There is a large difference in depth of the top of the salt bodies of diapirs 30 and 31. The top of the salt in diapir 30 is located relatively deep, at 500 ms (TWT) while the salt in diapir 31 is shallow and near the seafloor, at 400 ms (TWT). The doming strata above diapir 30 is cut and truncated by the flat URU reflection, but the salt is located far below the unconformity (Figure 4.33-4.35). Both the seafloor and the URU remain flat above diapir 30, but are elevated above diapir 31 (Figure 4.33 and 4.35). Here, high amplitudes near the seafloor indicate the top of the salt body being at a shallow depth (Figure 4.35, 4.38 and 4.39). The southern flank of diapir 31 is less elevated (Figure 4.35), and the top of the salt is located lower here compared to the rest of the structure.

The sediment cover above both diapirs is uniform and relatively thin, with an average thickness of 30-40 ms. The uplifted URU horizon intersects with the seafloor above the diapir 31, and is either truncated by the seafloor or not resolvable due to the low sediment thickness. On the seafloor, several plough marks are observed and occur with increasing frequency towards the elevation above the top of the diapir (Figure 4.40).

The difference in depth of the salt bodies of diapir 30 relative to adjacent diapirs such as 28, 29 and 31 is especially visible on timeslices (Figure 4.36 and 4.37). Here, the salt bodies of diapirs 28, 29 and 31 are present at all depths, distinguishable as relatively acoustically transparent features (Figure 4.36). The top of the salt bodies is visible as high amplitude anomalies and are located beneath the seafloor reflection. The salt body of diapir 30 is distinguishable at 600 and 500 ms (TWT) depth, but is not visible near the seafloor at 400 ms (TWT) depth (Figure 4.37).

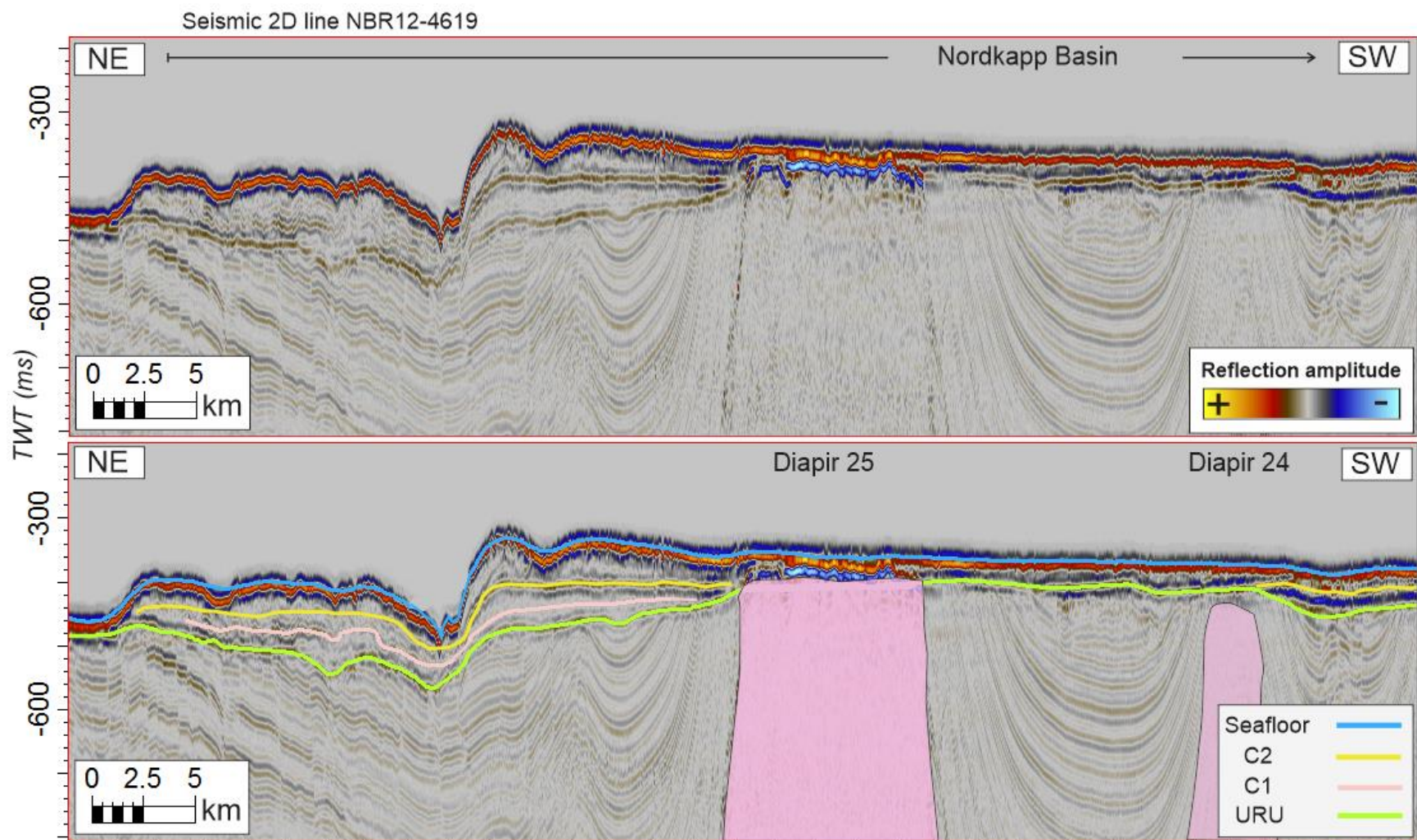


Figure 4.32: An uninterpreted and interpreted seismic profile through diapir 24 and 25 showing the depression of the URU in the northern central Nordkapp Basin. Intra Quaternary horizons C1 and C2 are found within the sediments accumulated in the depression.



## 4 Results

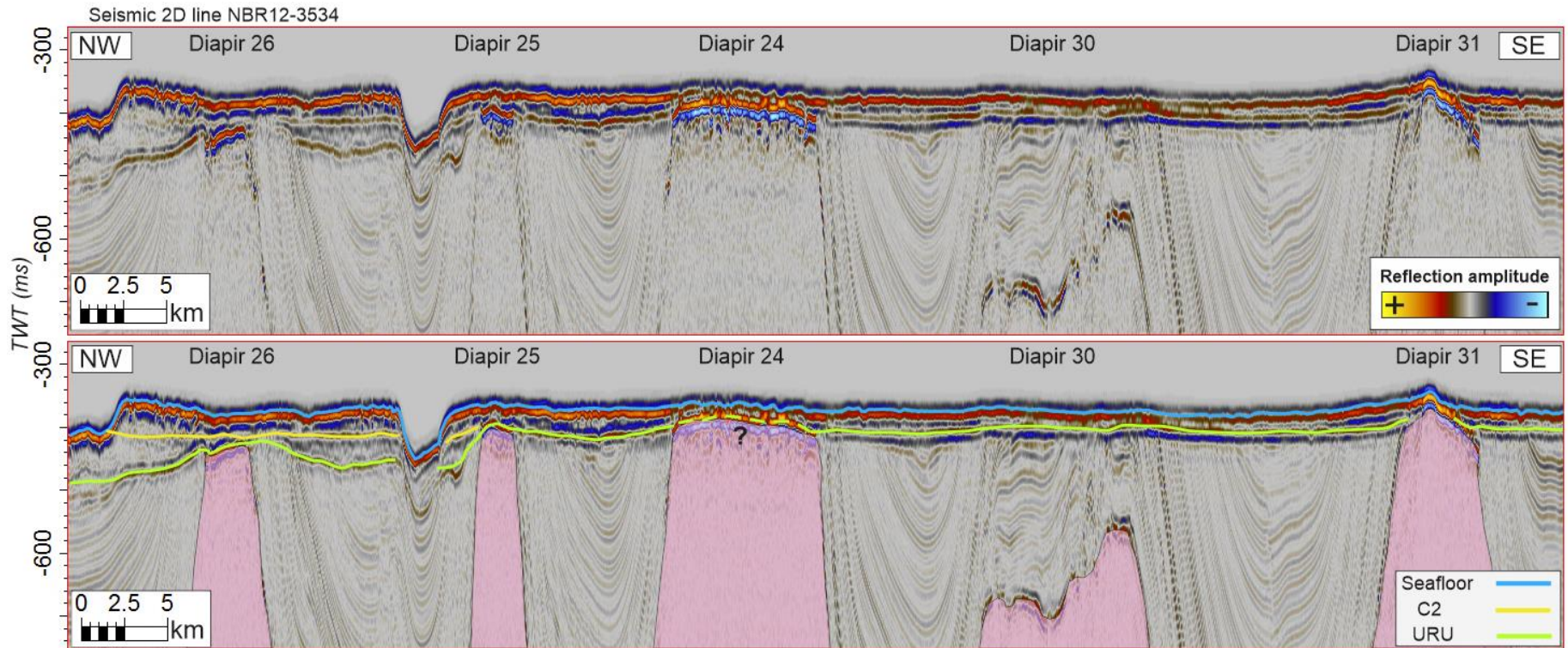
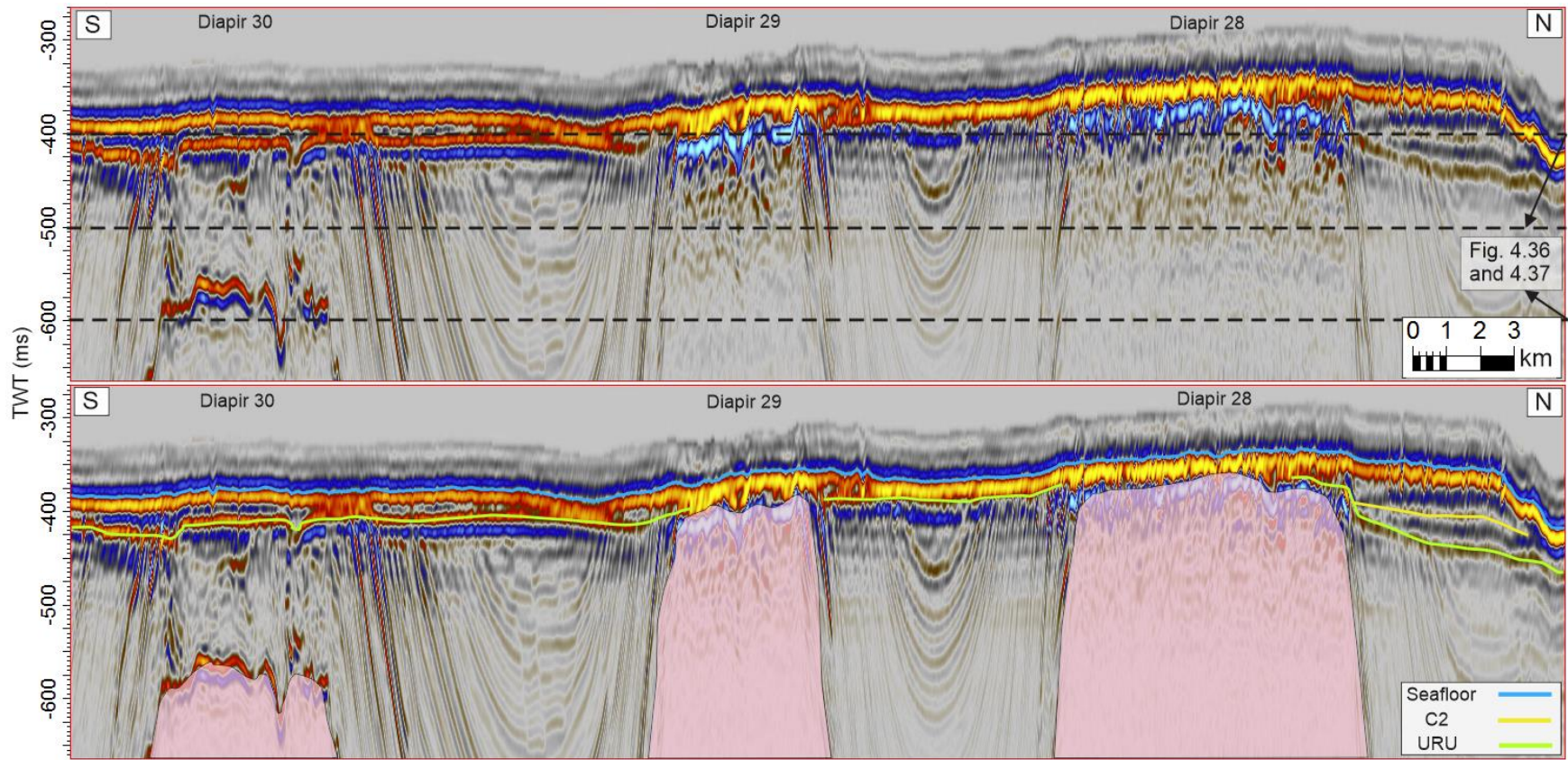


Figure 4.33: An uninterpreted and interpreted seismic profile through diapiers 24-26 and 30-31 showing the local variations in depth of the salt bodies of the diapiers. The URU is present above diapiir 25, 26 and 30, but is truncated by the seafloor above diapiir 24 and 31. Additionally, a seafloor depression between diapiir 25 and 26 truncates the unconformity and cuts into the sediments between the diapiirs. Note that the URU is not distinguishable above diapiir 24.

## 4 Results



## 4 Results

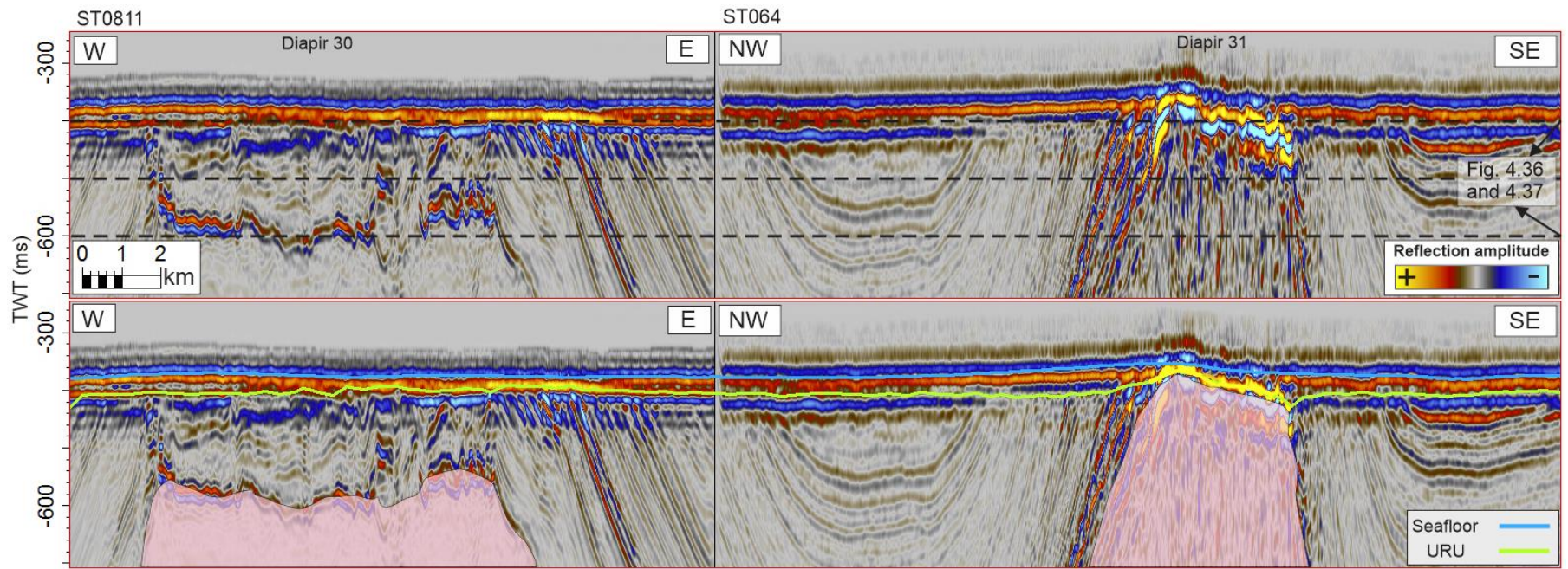


Figure 4.35: Seismic profile through diapirs 30 and 31. The black vertical line marks where the profile changes orientation. The dashed black lines indicate the depth of the time slices shown in figures 4.36 and 4.37.

## 4 Results

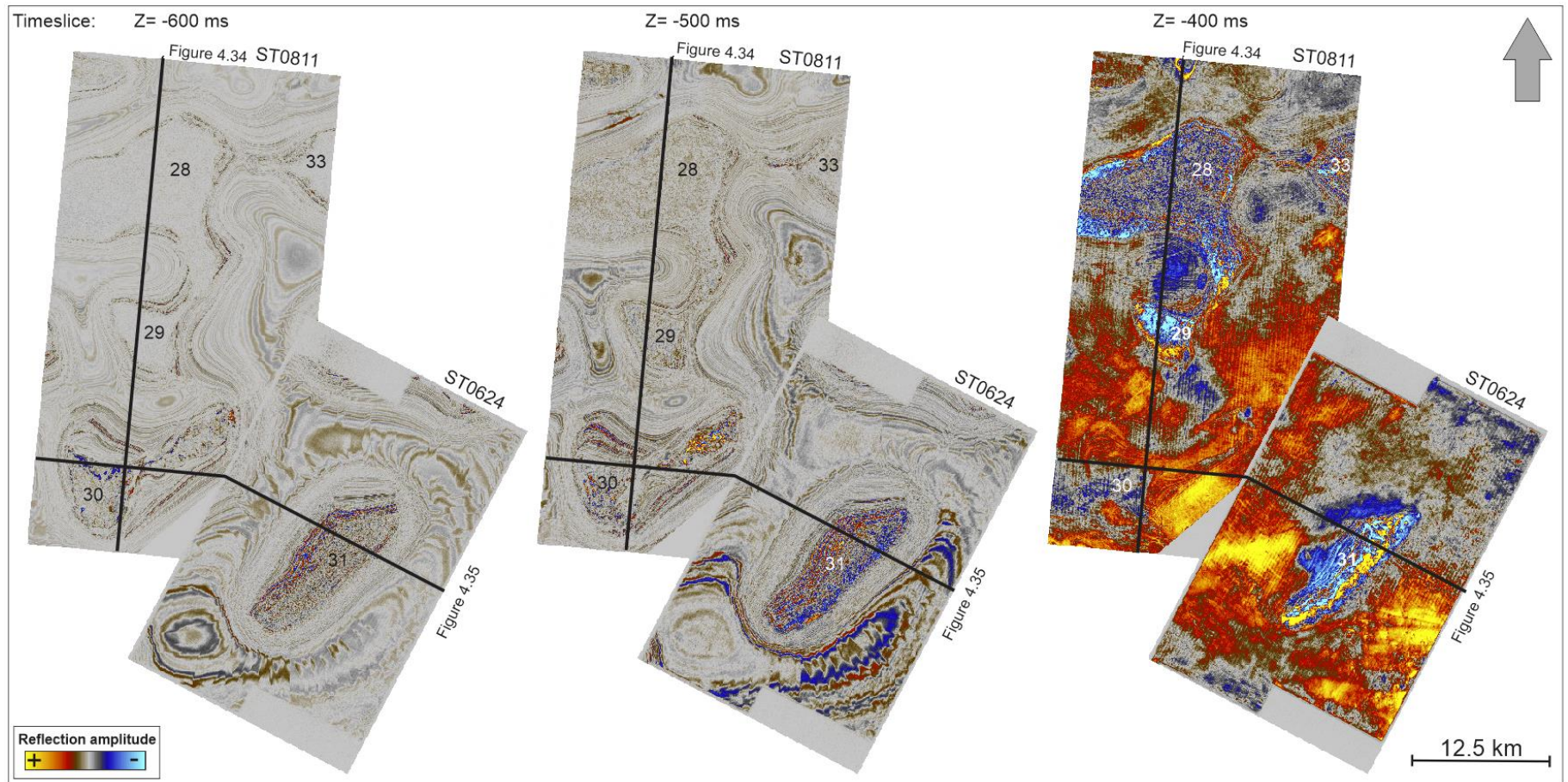


Figure 4.36: Uninterpreted time slices from 3D data sets ST0811 and ST0624 at depths (Z) of 600-, 500- and 400 ms (TWT). Note the high amplitudes of diapir 28, 29, 31 and 33 at 400 ms depth.

## 4 Results

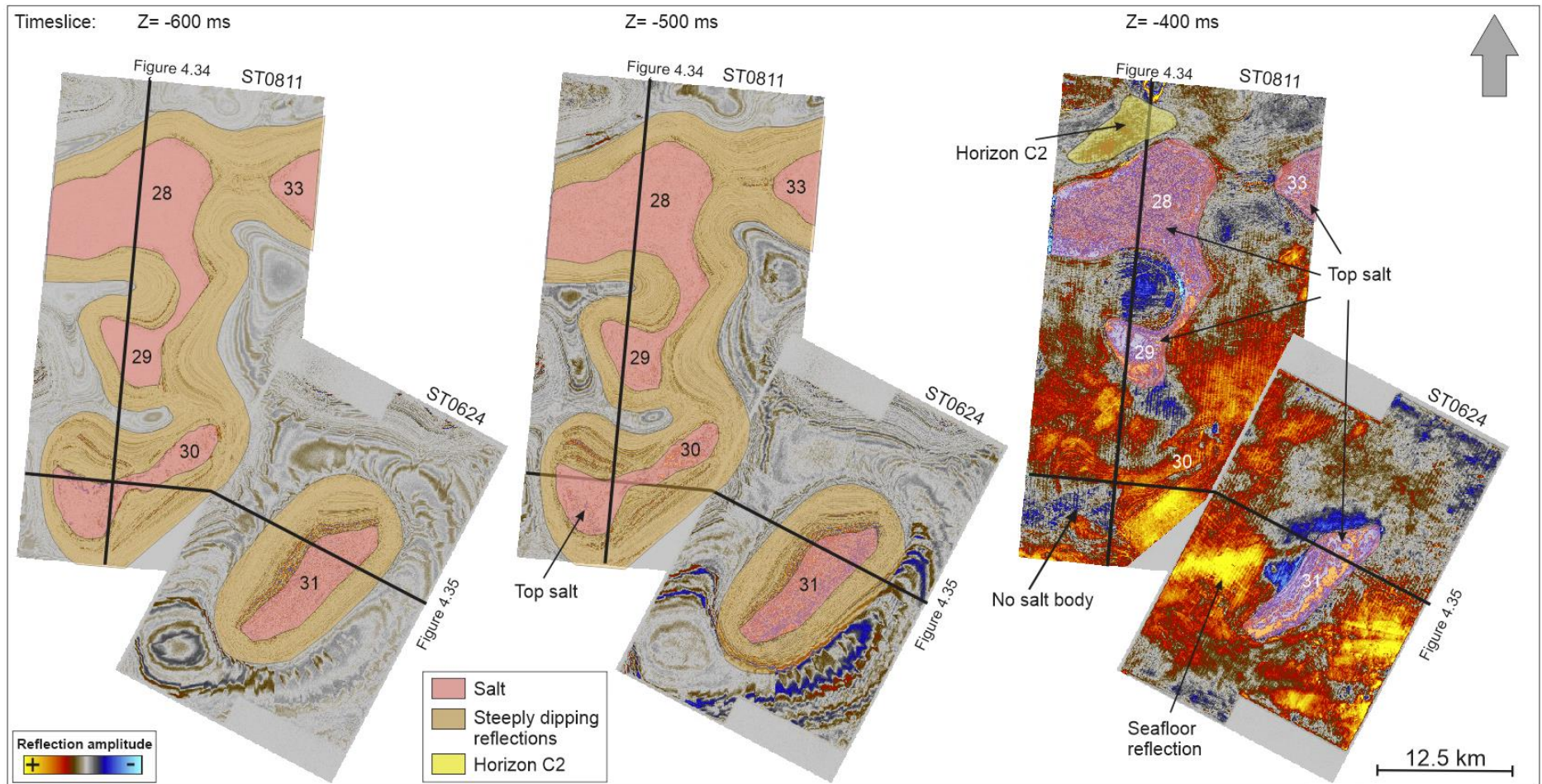


Figure 4.37: Interpreted time slices from 3D data sets ST0811 and ST0624 at depths (Z) of 600-, 500- and 400 ms (TWT). The salt within diapir 30 is assumed to not reach the seafloor, while the bright amplitudes of diapir 28, 29, 31 and 33 are interpreted to represent salt present by the seafloor. Note that intra Quaternary horizon C2 is visible just below the seafloor at 400 ms as an even reflection.

## 4 Results

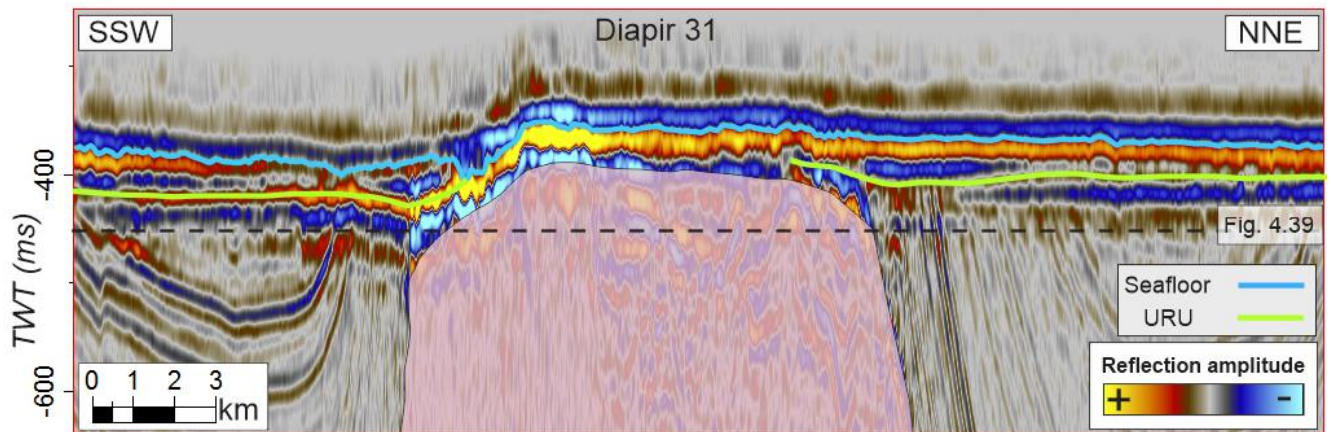


Figure 4.38: Seismic profile through diapir 31. Note the slight depression of the top salt reflection in the southwest and the elevation of the seafloor reflection above the salt. The black dotted line marks the depth of the time slice in fig. 4.39.

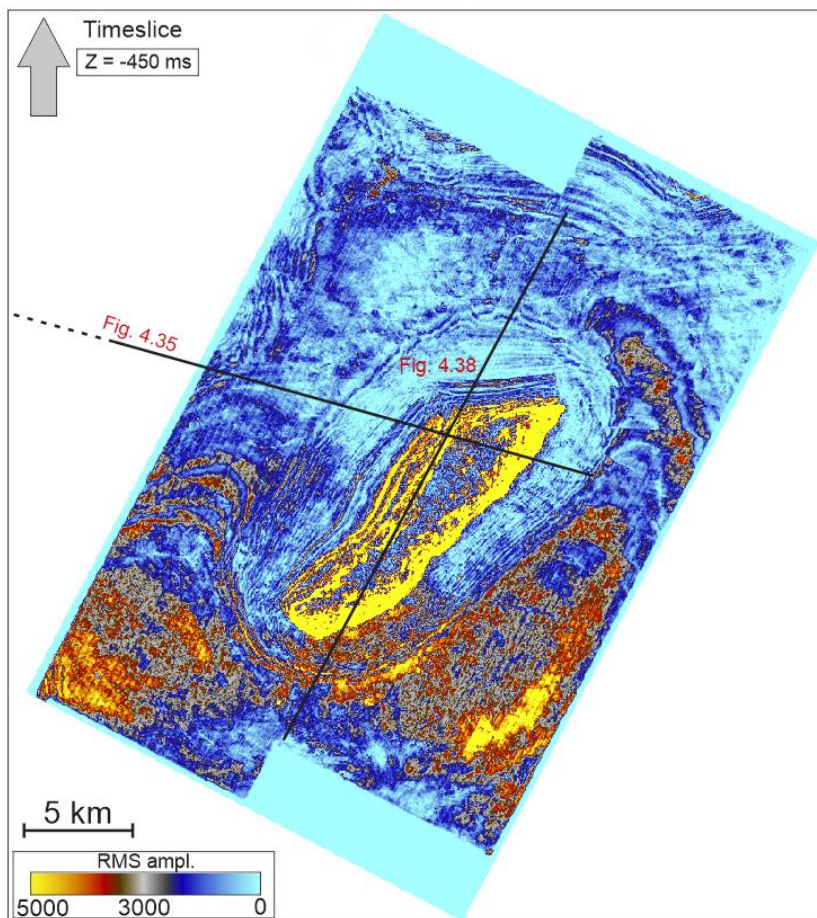


Figure 4.39: RMS amplitude time slice through diapir 31 showing the high amplitude near the seafloor, where the top of the salt is assumed to be very shallow.

## 4 Results

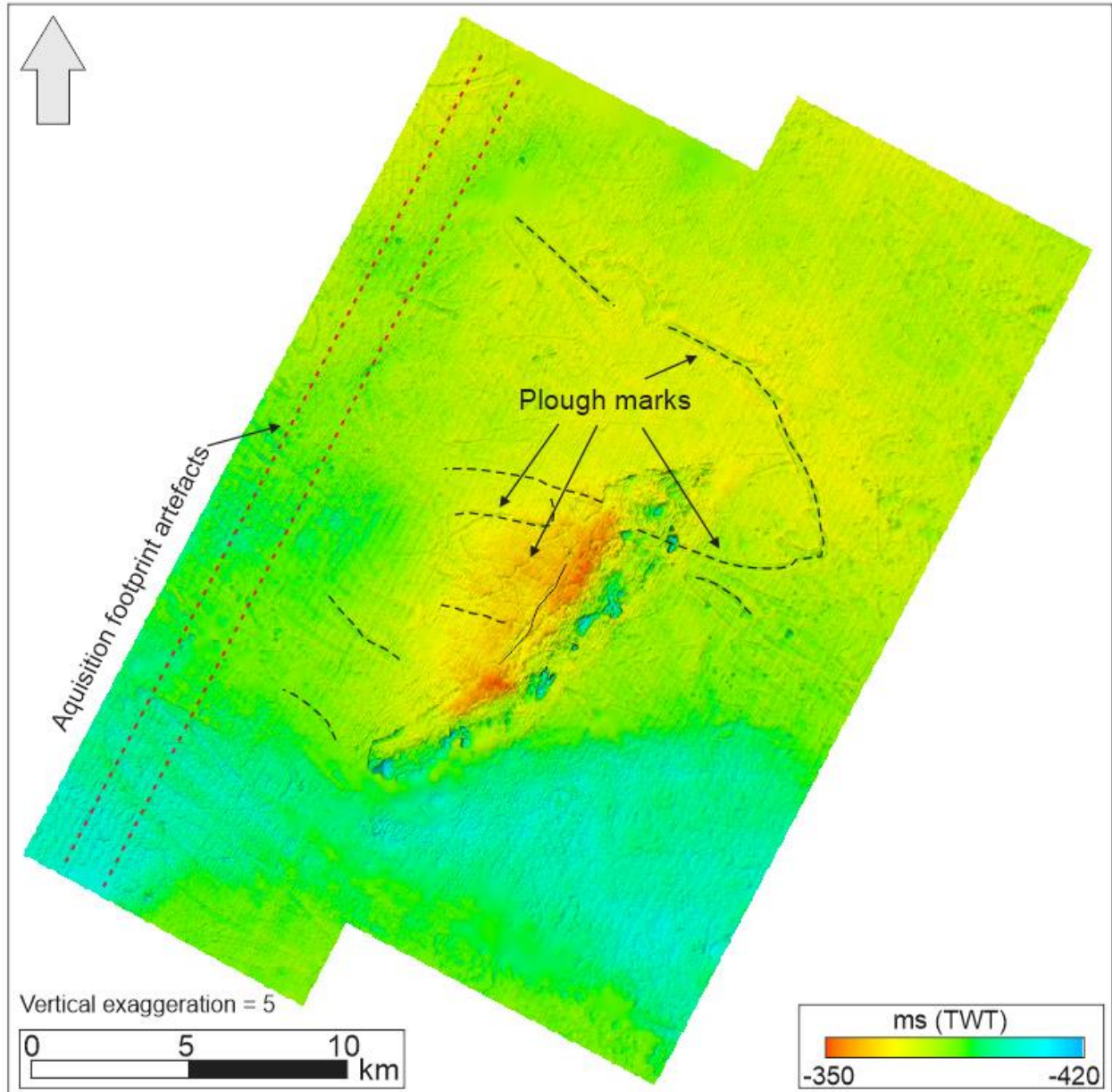


Figure 4.40: Seafloor surface from 3D data set ST0624 above diapir 31, showing an increase in plough mark frequency closer to the elevation above the diapir, from iceberg activity. Note the depression along the southeastern flank of the elevated seafloor.

## 4 Results

### Diapir 32 and 33

Both of the diapir crests are truncated by the URU in central parts, and the top of the salt bodies are located relatively shallow, between 400 and 410 ms (TWT) depth. The URU reflection is represented by a medium amplitude peak reflection. The continuity of the reflection is good west of diapir 33, but decreases towards the east. The unconformity is uplifted above both of the diapirs, but is relatively flat adjacent to the diapirs. Above diapir 33, the unconformity may not be present, as the reflection of the top of the salt body and the seafloor obscures that of the URU (Figure 4.41). Towards the eastern part of diapir 32, the top of the salt body is located deeper (Figure 4.41). Here, the top salt reflection starts at approximately 500 ms (TWT), and the salt body does not reach or uplift the URU reflection.

Intra quaternary horizon C2 is represented by a medium amplitude peak reflection within the overlying sediment package. The reflection is continuous except for above diapir 33, where it onlaps the flank of the diapir on both sides with a gentle angle (Figure 4.41). The sediment cover is relatively even in thickness, averaging at approximately 40 ms (TWT).

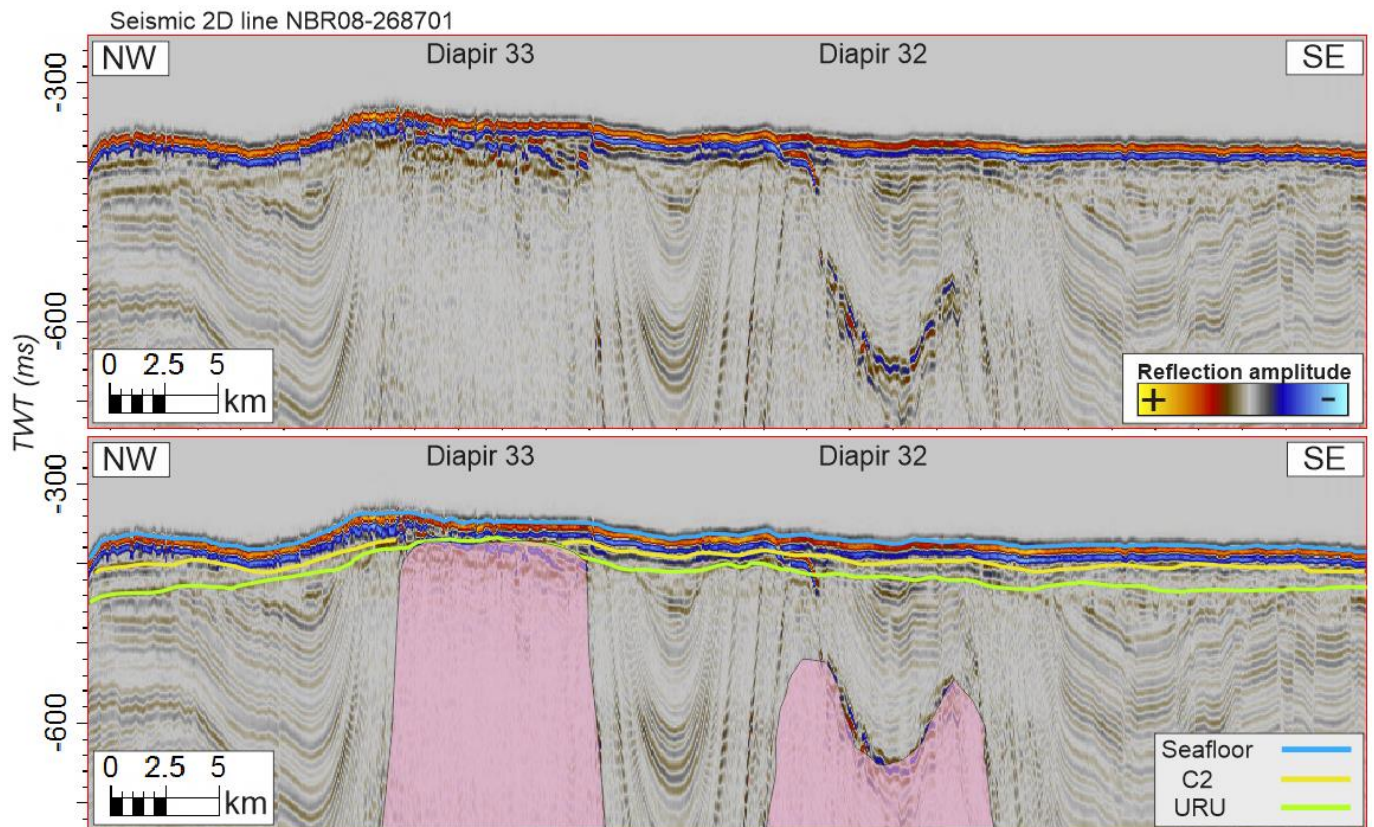


Figure 4.41: Seismic profile through diapirs 32 and 33. Note that the top of the salt in diapir 32 is at -410 ms (TWT) (Table 4.1), but the profile cuts the eastern flank of it, where the salt is lower.



## 4 Results

### Diapir 42-44

The top of the salt bodies of diapirs 42-44 are all located relatively shallow, right beneath the seafloor (Figure 4.42). Diapirs 42 and 43 are part of a larger salt system (see table 4.1) and are visible as a single salt wall on the profile. Northwest of the diapir system, the URU is distinguishable as a high amplitude peak reflection with high continuity. The unconformity horizon forms a depression northwest of diapir 42, and onlaps the diapir towards the southeast. Above the diapir system, the URU is not distinguishable, as the salt body reaches the seafloor. Thus, it is assumed that the unconformity coincides with the seafloor. This is also the case westwards of the diapirs, where the URU is not distinguishable between the seafloor reflection and the dipping reflections of the Cretaceous strata below that appear to subcrop near the seabed (Figure 4.42).

The unconformity is located at a shallow depth and close to the seafloor in general in the northeastern part of the basin (Figure 4.31a). Thus, it raises the question of if the URU is present at all in this area, or if it coincides with the seafloor, that is elevated above this salt system (Figure 4.31b).

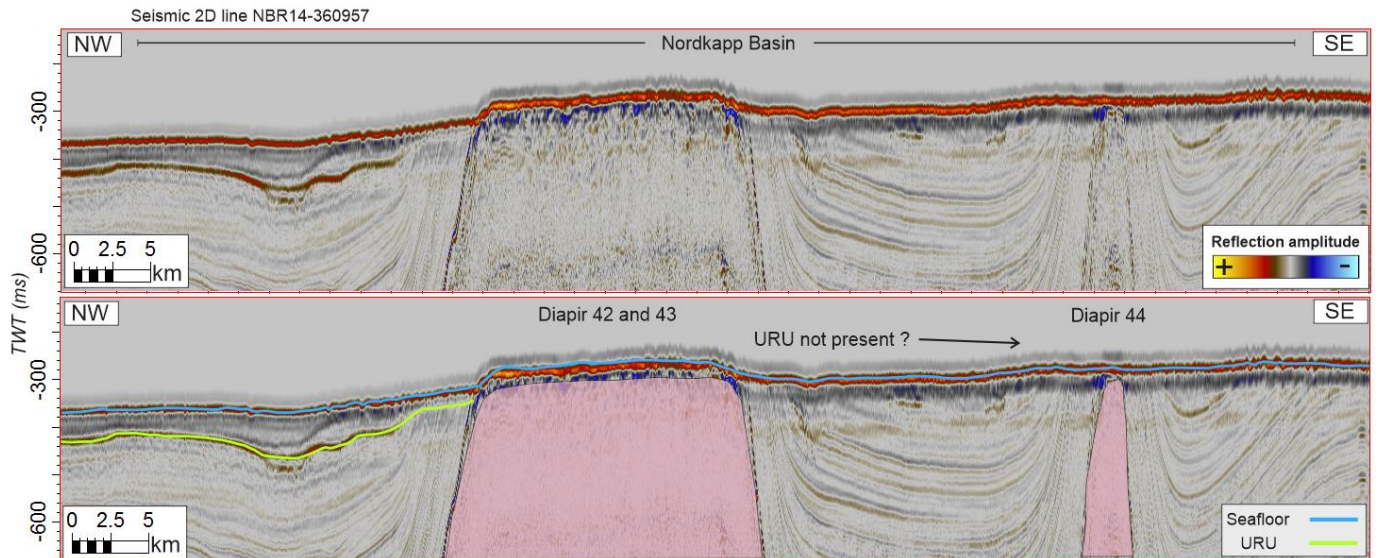


Figure 4.42: Seismic profile through diapirs 42, 43 and 44. Note how the URU is not distinguishable below the seafloor east of diapir 42 and 43.

## 4 Results

From the observations of the diapirs and the relationship between the salt bodies and the overlying URU and seafloor horizons, the salt diapirs and domes in the study area can be systemized. The diapirs are categorized according to if the URU surface remains flat or has been elevated above the salt. The same applies in relation to the seafloor. A summary of the observations and categorization of the diapirs is displayed in table 4.2.

The observations listed may be used as indicators for the relative timing of salt movement of different diapirs. It is however important to note that differences in quality of 2D and 3D data sets, as well as the data coverage of the diapirs vary. Thus, the interpretations of depths of the salt bodies as well as the URU and seafloor may change if data with better resolution is acquired in the future.

*Table 4.2: Overview of the different salt domes and diapirs according to the relationship between salt bodies and the overlying reflections, amplitudes and other seismic stratigraphic characters. Note that “-” indicates the value is the same as the above, and “X” indicates a lack of observation.*

<b>Diapirs</b>	<b>URU elevated</b>	<b>Seafloor elevated</b>	<b>URU visible above diapir</b>	<b>URU configuration above salt</b>	<b>Amplitude along URU</b>
1	Yes	No	Yes	Rugged	Medium
2	-	-	-	Rugged	Medium
3	-	-	-	Rugged	Medium
4	-	-	-	Rugged	Medium
5	-	-	-	Even	Medium
6	No	-	-	Even and concave	Medium
7	Yes	-	-	Uneven	Medium
8	-	-	-	Uneven and discontinuous	Medium to high
9	-	-	-	Relatively even	Medium
10	-	-	-	Rugged	Medium
11	-	-	-	Relatively even	Medium, local highs
12	No	-	-	Uneven, difficult to distinguish	Low to medium
13	Yes	-	-	Undulating	Medium
14	Yes	-	-	Relatively even	Medium
15	No	-	-	Even, but obscure	Low to medium,
16	Yes	-	-	Rugged, close to the seafloor	Medium to high
17	No	-	-	Rugged	Medium to high
18	Yes	Yes	-	Relatively even	Medium
19	-	Yes	No	X	X
20	-	No	Yes	Uneven	Medium
21	-	-	-	Even	Medium

## 4 Results

22	No	-	-	Even	Medium
23	No	-	-	Even	Medium
24	Yes	Yes	Uncertain	X	X
25	-	No	Uncertain	X	X
26	-	-	Yes	Uneven	Medium to high
27	No	-	-	Uneven, possibly concave	Medium
28	Yes	Yes	No	X	X
29	-	Yes	-	X	X
30	No	No	Yes	Even	Medium
31	Yes	Yes	No	X	X
32	-	No	Yes	Even	Medium
33	-	-	Uncertain	X	X
34	-	-	Uncertain	X	X
35	-	-	Yes	Undulating, difficult to distinguish from top salt and seafloor reflection	Low to medium
36	-	-	Yes	Rugged	Medium
37	-	-	Yes	Rugged	Medium
38	-	Yes	No	X	X
39	-	-	-	X	X
40	-	-	-	X	X
41	-	-	-	X	X
42	-	-	-	X	X
43	-	-	-	X	X
44	-	-	-	X	X
<b>Domes</b>					
<i>Svalis Dome</i>	Yes	Yes	No	Onlaps flanks of the dome	Medium
<i>Samson Dome</i>	No	No	Yes	Even	High
<i>Norvarg Dome</i>	No	No	Yes	Undulating/Rugged	Medium, local highs

An overview map of the diapirs with the observations from table 4.2 is given in figure 4.43. The URU remains flat above the Samson and Norvarg domes, and some diapirs within the Nordkapp Basin such as the aforementioned diapirs 12 and 30, where the salt bodies are found relatively deep below the unconformity. The majority of the diapirs in the basin have uplifted the URU. There is a trend of higher elevation of the salt diapirs towards the northeast in the basin, where more and more if the diapirs have uplifted the seafloor. In addition, the seafloor is also uplifted above the Svalis Dome.

## 4 Results

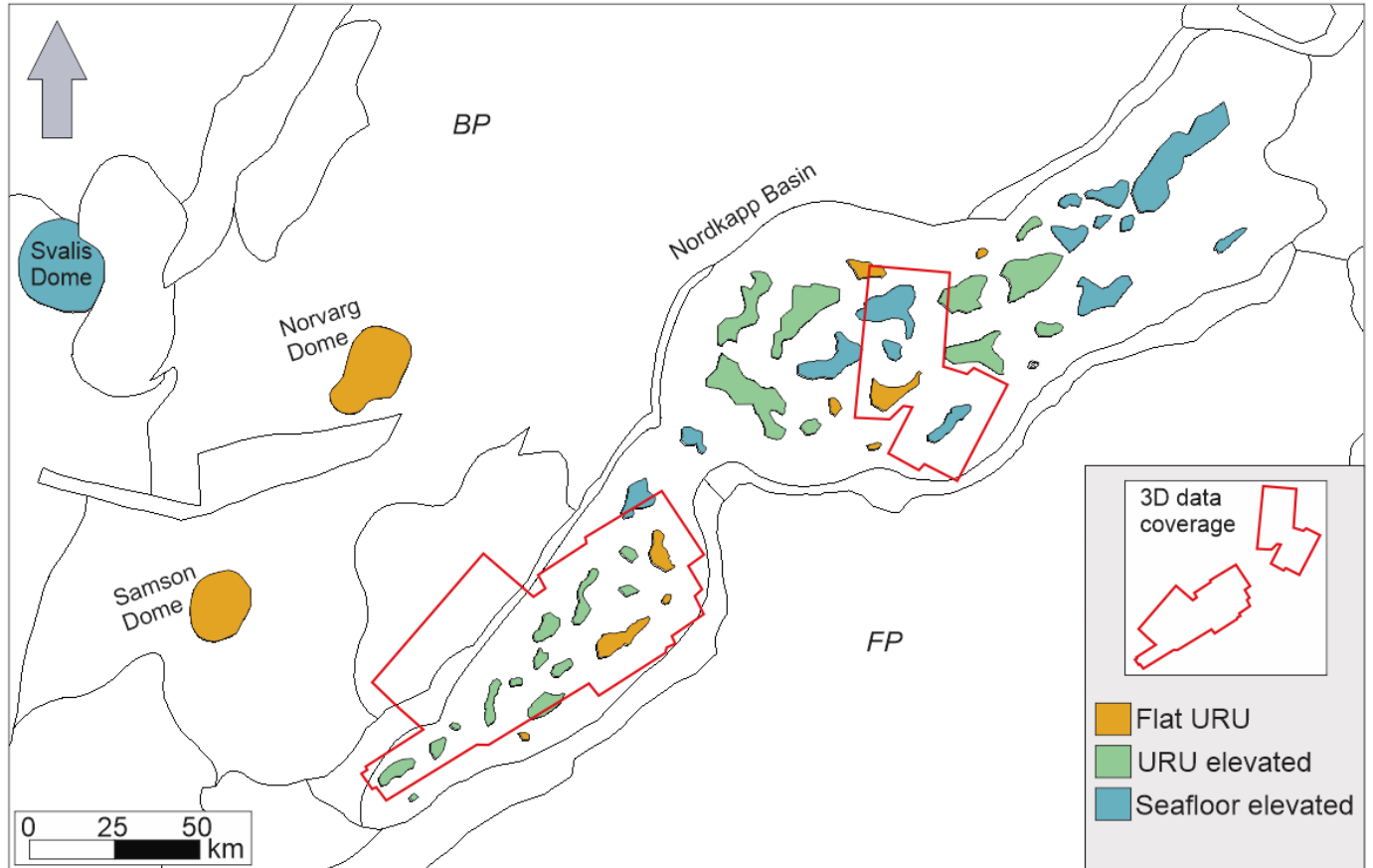


Figure 4.43: Map with an overview of the characteristics of the different salt bodies in the study area and their relationship with overlying surfaces.

## 5 Discussion

In the following chapter a discussion of the Cenozoic development of the study area in the SW Barents Sea will be given, with emphasis on the interplay between salt movement and erosion of the Svalis, Samson and Norvarg domes, as well as selected diapirs in the Nordkapp Basin. It is important to note that all structural elements have experienced one or several phases of Mesozoic salt-related uplift (see chapter 2.4). The focus of this discussion however, is on the Cenozoic development of the study area.

First, the development of the individual structures is discussed with respect to the observations made during the seismic interpretation, with focus on the relative timing of salt movement and glacial erosion. Secondly, factors such as original salt thickness, overburden strength and pre-glacial erosion that may influence salt movement in the study area are discussed. Finally, the interplay between late Cenozoic glacial erosion and deposition and salt movement is discussed.

### 5.1 Salt movement

#### 5.1.1 Svalis Dome

Uplift and truncation of Cretaceous strata in the Maud Basin adjacent to the dome (Figure 4.2, 4.12 and 4.13) indicates salt movement during the late Cretaceous – early Cenozoic, after deposition of the Cretaceous strata and before the onset of glacial erosion. The adjacent Loppa High experienced several phases of early Cenozoic erosion (Figure 2.5) (Lasabuda et al., 2018a). As it is in close proximity to the eroded Loppa High, the Svalis Dome was likely influenced by erosion as well (Figure 5.1a). Evidence of this phase, such as erosional truncations or accumulations of eroded sediments were likely removed during later glacial erosion (Figure 5.1b).

The significant difference in depth of the URU in the SW relative to the NE (Figure 4.5 and 4.12) indicates a deeper glacial erosion on this side of the dome. This may be related to the lithological differences between the Maud Basin in the NE and the Loppa High in the SW, where the unconformity truncates Cretaceous and Early Mesozoic rocks, respectively. The URU is elevated above the dome, indicating late salt movement after the formation of the unconformity. A combination of continuous or stepwise salt movement occurring contemporaneously with repeated glacial erosion and deposition has likely been the main processes affecting the dome in the late Cenozoic (Figure 5.1b-i).

## 5 Discussion

Above the rising salt, elevated strata were more exposed to erosion during glacials, evidenced by the lack of Quaternary sediments directly above the dome. During ice sheet advances, previously deposited glaciogenic sediments and the underlying Paleozoic strata above the rising salt was eroded by the Bear Island Ice Stream (see chapter 2.3.2) (Figure 5.1b, e and h). Intra Quaternary horizons A1 and A2 (Figure 4.14 and 4.15) are interpreted to represent preserved erosional surfaces formed during repeated ice sheet advances. The rise of the salt left the strata above the Svalis Dome more exposed to erosion, while it may have lessened the exposure of the sediments in the adjacent depression. Thus, a thicker sequence of Quaternary sediments was accumulated here (Figure 5.1 e and h), as the depression in the URU provided more accommodation space for the sediments. The sediments may be derived from the eroded strata above the rising dome. They may also have a more distal provenance area and longer transport distance beneath the ice stream.

The elevated seafloor above the dome (Figure 4.12) indicates late salt movement, after the deglaciation (Figure 5.1j). In contrast to what is observed in the Nordkapp Basin, there is no top salt high amplitude reflection observed, indicating that the salt body is located relatively deep. However, the acoustically transparent appearance of the dome on seismic profiles may indicate the presence of salt relatively near the surface. It is speculated that there may be a small diapir present near the seafloor, but the structure is mainly described as cored by Paleozoic rocks (Gabrielsen et al., 1990). The rocks consist of silicified shales and carbonates and are suggested to act as a resistant cap, protecting the salt body from erosion (NPD, 2013), while the adjacent Mesozoic strata consist of softer siliciclastic rocks (Nilsson et al., 1996). This concurs with the assumption that the elevated dome may to some degree have protected the adjacent SW sediment accumulation from erosion. A continuous rise of salt during the late Cenozoic is suggested as a potential reason for the current positive relief of the dome (NPD, 2013), which is supported by the local elevation of the seafloor above the dome.

The development of the Svalis Dome, particularly during the Cenozoic is complex and still relatively poorly understood, mainly due to the extensive erosion of the structure. It experienced active salt rise during the Jurassic and Cretaceous (Gabrielsen et al., 1990), but the main doming period is assumed to be the early Cenozoic, evidenced by the doming Mesozoic strata adjacent to the dome (Mørk and Elvebakk, 1999). Phases of active salt rise are assumed to be closely related to the repeated uplift of the adjacent Loppa High (Gabrielsen et al., 1990) and extension of the Hoop Fault Complex to the north (Bugge and Fanavoll, 1995). During the Cenozoic however, salt movement is likely related to erosion of the shelf.

5 Discussion

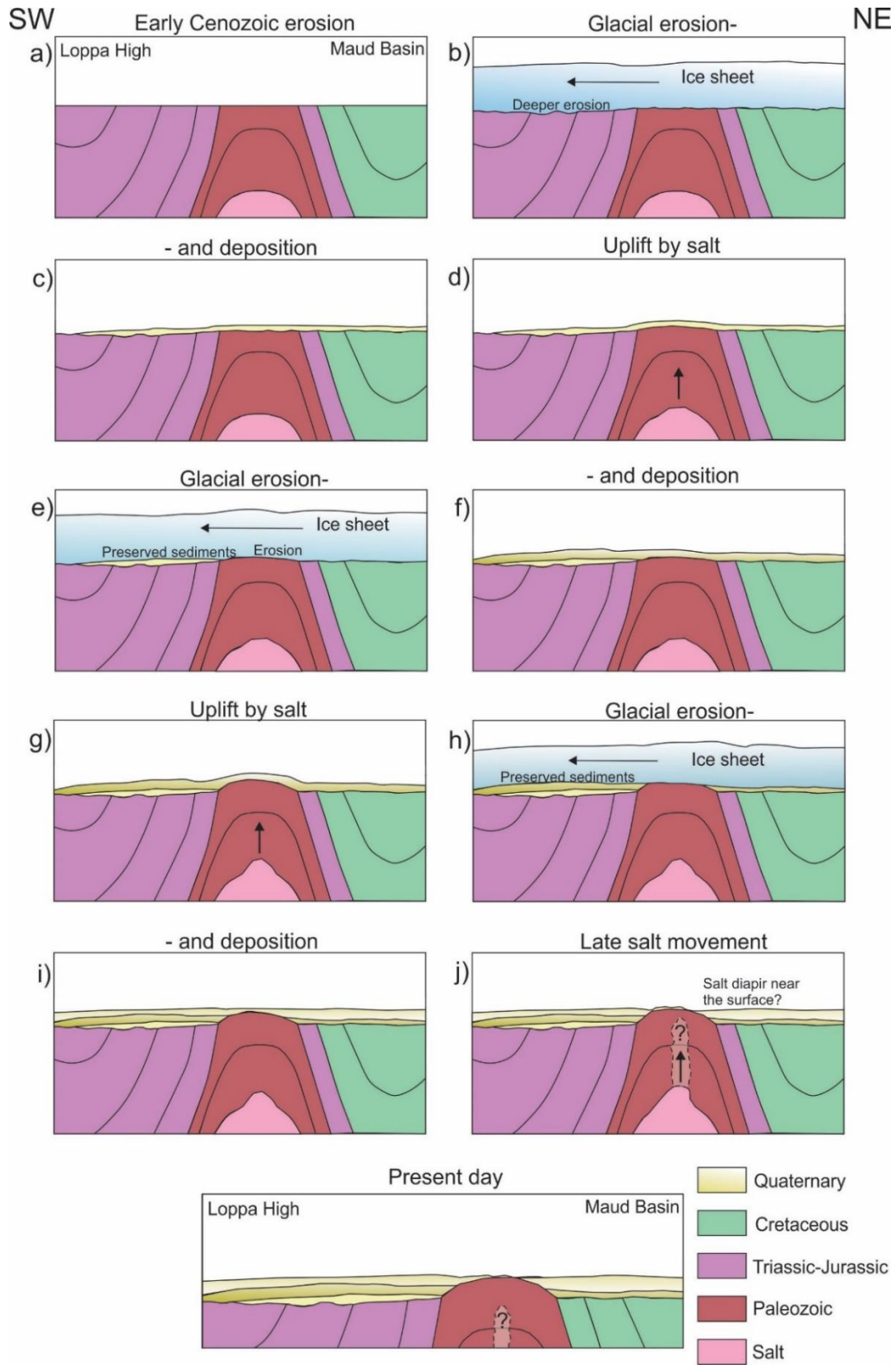


Figure 5.1: Conceptual model showing the Cenozoic development of the Svalis Dome with a) early Cenozoic erosion, b) – i) repeated glacial erosion and deposition interchanging with salt movement of the dome and j) late Cenozoic salt movement after the last deglaciation.

## 5 Discussion

### 5.1.2 Samson Dome

The convex form of the Cretaceous strata above the dome (Figure 4.16) indicates uplift after the deposition of the Mesozoic sequences (Figure 5.2a-c). Additionally, the truncational relationship between the strata and the URU indicates that the uplift occurred prior to the latest phase of the erosion that formed the unconformity. Pre-glacial erosion during the early Cenozoic has also influenced the area, removing large amounts of strata above the dome, but evidence of this was later removed by glacial erosion (Figure 5.2d and e). The dome has likely not experienced local uplift or subsidence, salt-related or otherwise, during the late Cenozoic, inferred from the even surface of the URU above the dome. Thus, repeated glacial erosion and deposition has been the main process affecting the area during this time (Figure 5.2e).

High amplitudes, like the ones observed along the URU and within the Quaternary sediments directly above the dome (Figure 4.17), may indicate the presence of shallow gas. The uplift and subsequent erosion of the dome during the Cenozoic may have enabled hydrocarbons to migrate upflank along the anticline structure and accumulate where the strata subcrop the URU (Figure 5.2f and g).

The main stage of halokinetic activity of the Samson Dome is assumed to be pre-Cretaceous, but a reactivation occurred during the Late Cretaceous-early Cenozoic (Gabrielsen et al., 1990; Mattos et al., 2016), which concurs with the observed doming of the Mesozoic strata, cut by the URU. The Samson Dome and Bjarmeland Platform experienced pre-glacial erosion during the early Cenozoic, though not to the same extent as the Svalis Dome by the elevated Loppa High according to the model by Lasabuda et al. (2018) (Figure 2.5). Thus, large parts of Mesozoic strata were likely removed before the onset of glacial erosion. However, due to the inferred quiescence of the dome during the Cenozoic, both pre-glacial and glacial erosion was likely unaffected by the deeper salt. It did however likely influence fluid flow from the dome during this time, enabling the assumed accumulation of shallow hydrocarbons within the glaciogenic sediments above the dome. According to Martinuk (2017), hydrocarbon leakage from the dome was likely triggered by a reduction of overpressure. This was related to both the removal of overburden through uplift and erosion, and to a loss of pressure during periods of ice sheet retreat during the late Cenozoic.



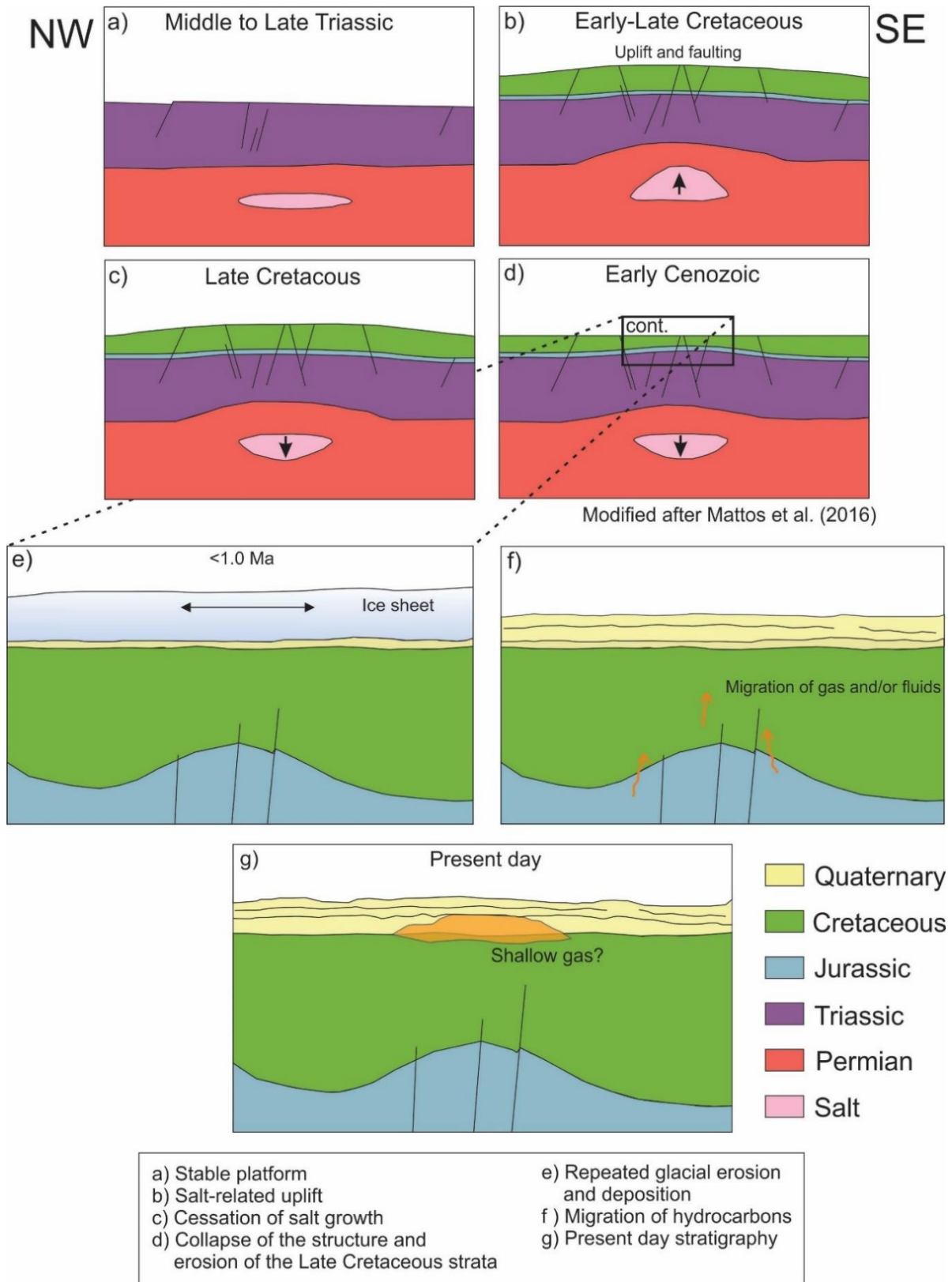


Figure 5.2: Conceptual model showing the development of the Samson Dome. a)-d) modified after Mattos et al. (2016). See text for further discussion.

## 5 Discussion

### 5.1.3 Norvarg Dome

The dome shares some characteristics with the Samson Dome, in terms of the relationship between the strata below the URU and the configuration of the unconformity. The Mesozoic strata is uplifted above the dome, indicating salt movement during the Late Cretaceous and early Cenozoic before the onset of glacial erosion (Figure 5.3a). This is supported by how the uplifted strata subcrops the URU above the dome (Figure 4.18). The termination of faults above the dome against the URU also suggests that both the uplift and subsequent faulting of the strata occurred before the unconformity was formed and that the faults have not been reactivated in the late Cenozoic, most likely indicating that the salt has been stable. The uniform depth of the URU above the dome also supports this, signifying that no local uplift or subsidence, salt-related or otherwise, has occurred after its formation. Pre-glacial erosion during the early Cenozoic likely removed large amounts of sediments before the onset of glacial erosion (Figure 5.3b), as the area did experience early Cenozoic erosion according to the model from Lasabuda et al. (2018a) (Figure 2.5). Evidence of this was likely not preserved as a result of later glacial erosion, as the Quaternary sediments above the URU directly overlie Mesozoic strata above the dome. Thus, repeated glacial erosion is only the latest episode of erosion on the shelf (Figure 5.3c), and the URU represents an extensive and prolonged hiatus in deposition.

The undulating surface of the URU and the local variations in amplitude along this horizon above the dome indicate an uneven interface between the glacial sediments and underlying rocks, as well as lateral variations in acoustic properties (Figure 4.18). This is likely related due to spatial variations in lithology causing changes in erosion of the strata below the Quaternary sediments. Faulting of the uplifted strata below URU and subsequent vertical displacement may have exposed rocks with different properties to erosion. Depressions or channels may form where rocks are more easily eroded or prone to glacial scouring. More resistant rocks may form crags or ridges, giving an uneven and rugged surface (Figure 5.3d), that was later covered by glacial sediments during repeated ice sheet advances and retreats during the Pleistocene, resulting in the present stratigraphy (Figure 5.3e).

The Norvarg Dome is suggested to have a similar geological evolution to the Samson Dome (Gabrielsen et al., 1990), where the main period of doming is estimated to be pre-Cretaceous followed by a reactivation during late Cretaceous – early Cenozoic times. This concurs with the observed relationship between the URU and underlying uplifted Mesozoic strata. The classification of both the Samson and Norvarg domes as salt-related structures is uncertain (Gabrielsen et al., 1990). It is speculated that both structures may be classified simply as doming anticlines above bodies of salt, and that they have mainly been affected by compressional tectonics. Nevertheless, the late Cenozoic development of both domes remains unaffected by uplift, as evidenced by the configuration of the URU.

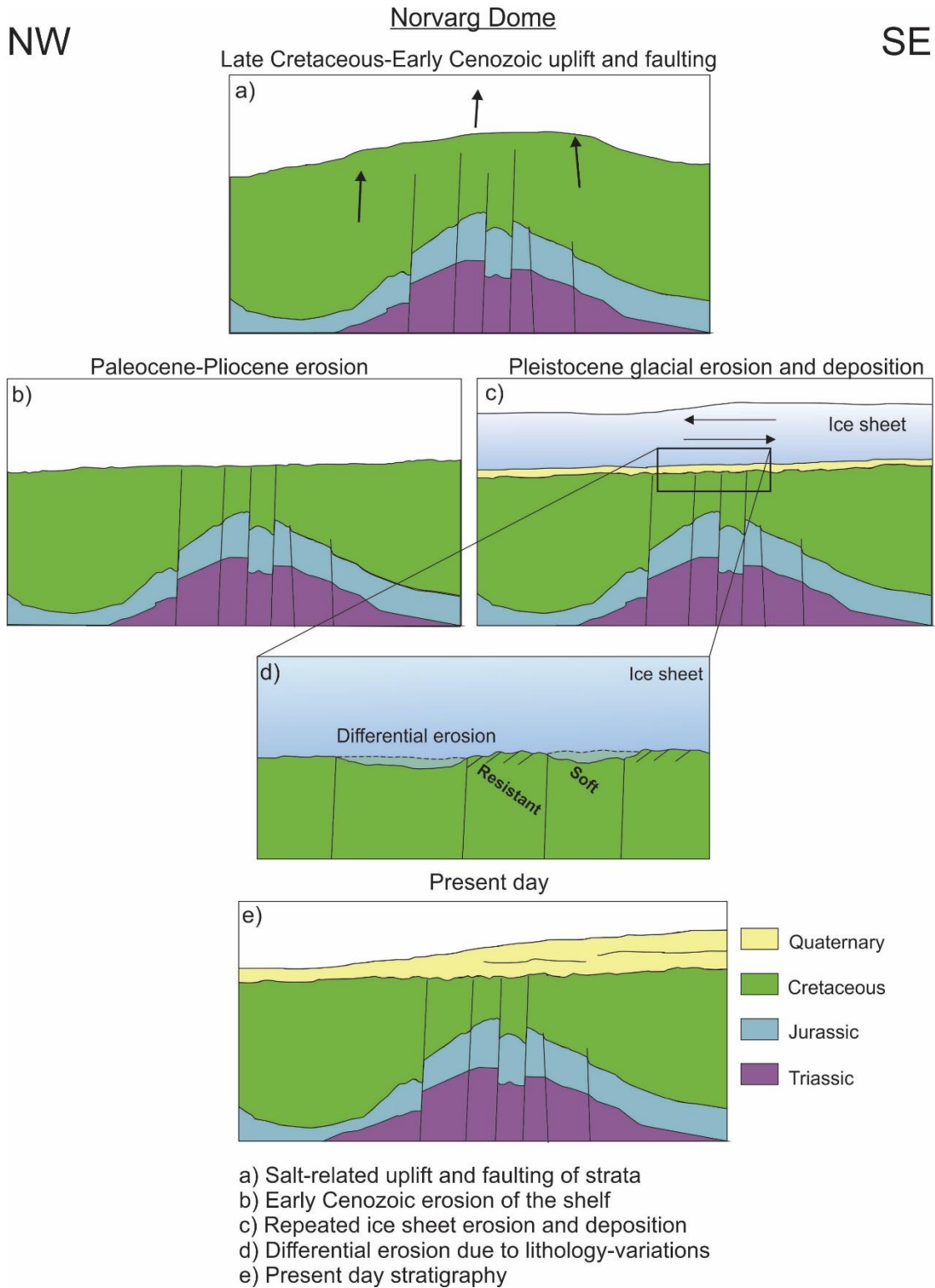


Figure 5.3: Conceptual model of the Cenozoic development of the Norvarg Dome. Note that the Mesozoic development of the dome is assumed as generally similar to that of the Samson Dome (Figure 5.2). See text for further discussion.

## 5.1.4 Nordkapp Basin

The salt diapirs within the Nordkapp Basin display local variations in the relationship between the salt bodies and the adjacent and overlying strata, as evidenced by the observations summarized in Figure 4.42 (see chapter 4.5.2). The differences in depth of the salt bodies as well as the configuration of the URU and seafloor above the diapirs can be attributed to a difference in timing of when the diapirs have experienced active halokinesis. Consequently, the diapirs in the basin can be categorized according to when and if they have been active during the late Cenozoic (Figure 5.4). The different Cenozoic evolutions of the individual diapirs are summarized in the conceptual model in figure 5.9.

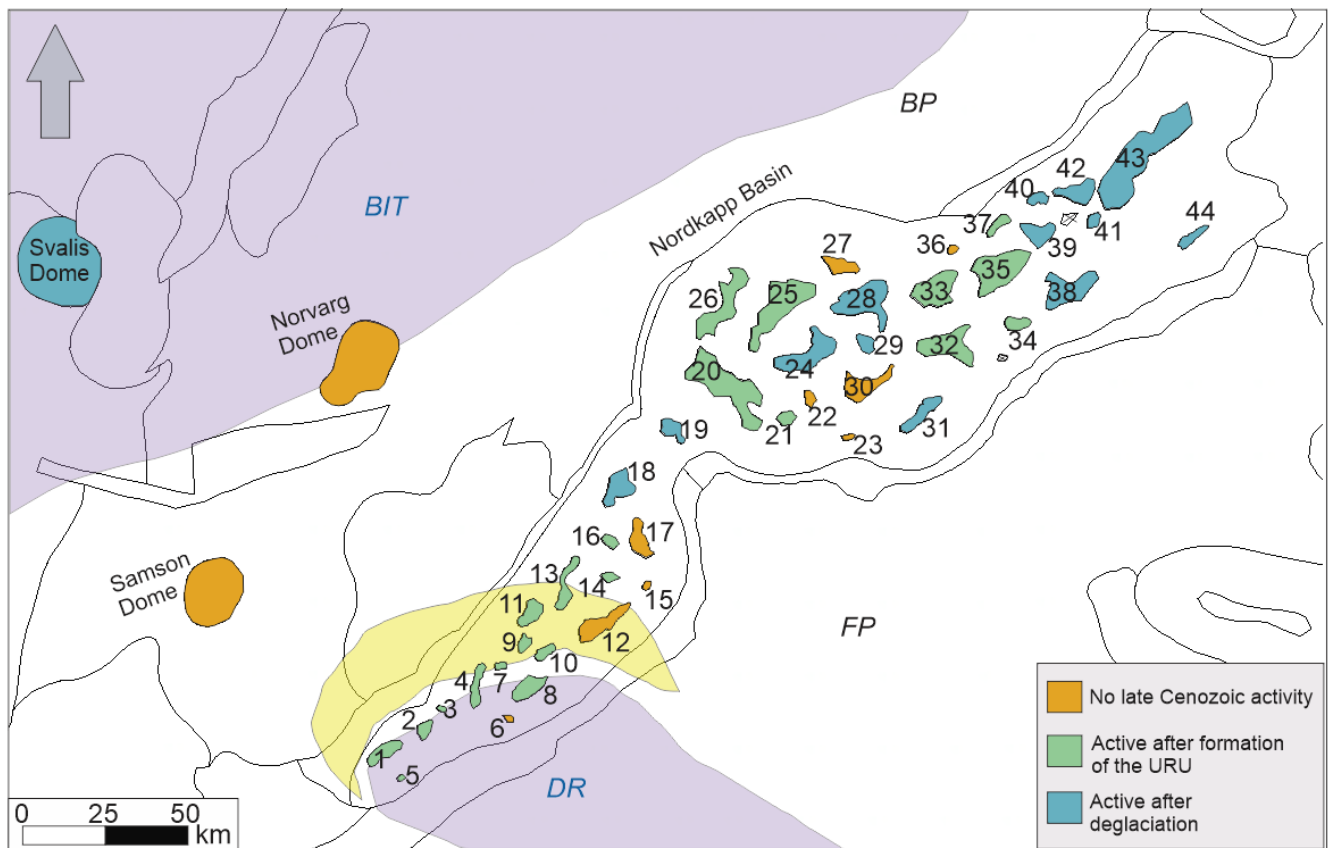


Figure 5.4: Overview of if and when during the Cenozoic the salt structures within the study area experienced activity, based on observations listed in chapter 4.5.2. FP = Finnmark Platform, BP = Bjarmeland Platform, BIT = Bear Island Trough, DR = Djuprenna. The areas of purple shade represent glacially eroded troughs, while areas in yellow represent sediment accumulations.

## 5 Discussion

### *5.1.4.1 Quiescent or collapsed diapirs – no late Cenozoic uplift of overlying strata*

Some of the diapirs within the basin (e.g. diapir 12 and 30) have an even URU surface above (Figure 4.28 and 4.33), indicating that no local uplift or subsidence related to the salt has occurred after glacial erosion formed the unconformity (Figure 5.9i). The top of both salt bodies are located deeper in the stratigraphy relative to adjacent diapirs and the salt bodies are not truncated by the URU, but the uplifted Cretaceous strata adjacent to both diapirs is (Figure 4.28 and 4.33). This indicates Late Cretaceous – Early Cenozoic salt activity that has uplifted previously deposited strata (Figure 5.9a and b), and that the salt bodies were once located higher in the stratigraphy, before subsiding or collapsing (Figure 5.9c). Salt collapse may be related to dissolution near the seafloor, which was described by Grimstad (2016) as a factor influencing the diapirs in the Nordkapp Basin. Percolating seawater or subglacial fluids with low salinity may contribute to the dissolution and subsequent collapse of the salt and overlying strata.

Above diapir 12, there is some uncertainty to where the URU is located (Figure 5.5). A medium amplitude reflection between the here assumed URU and the top of the salt body is found locally above the diapir within the area that has subsided. The reflection may represent an older surface within Cenozoic sediments preserved from glacial erosion within the subsided area. On the other hand, if the lower reflection represents the URU, it would indicate local subsidence of the unconformity above the diapir after it formed. The Quaternary sediments of the arcuate ridge above the diapir are accumulated in a mound and the internal reflections (B1 and B2) in the sequence are relatively horizontal (Figure 5.5), suggesting there has not been subsidence after the deposition of the sediments. Since the unconformity is relatively even across adjacent diapirs, it is more likely that the lowermost reflection represents an intra Cenozoic horizon preserved due to local collapse of the diapir (Figure 5.9c). According to Henriksen et al. (2011a), Paleogene strata is preserved in the Nordkapp Basin, but eroded on adjacent platforms. This is supported by Rojo (2015) and indicates that Cenozoic sediments were preserved above the salt body when it subsided before the onset of glacial erosion, before becoming stable.

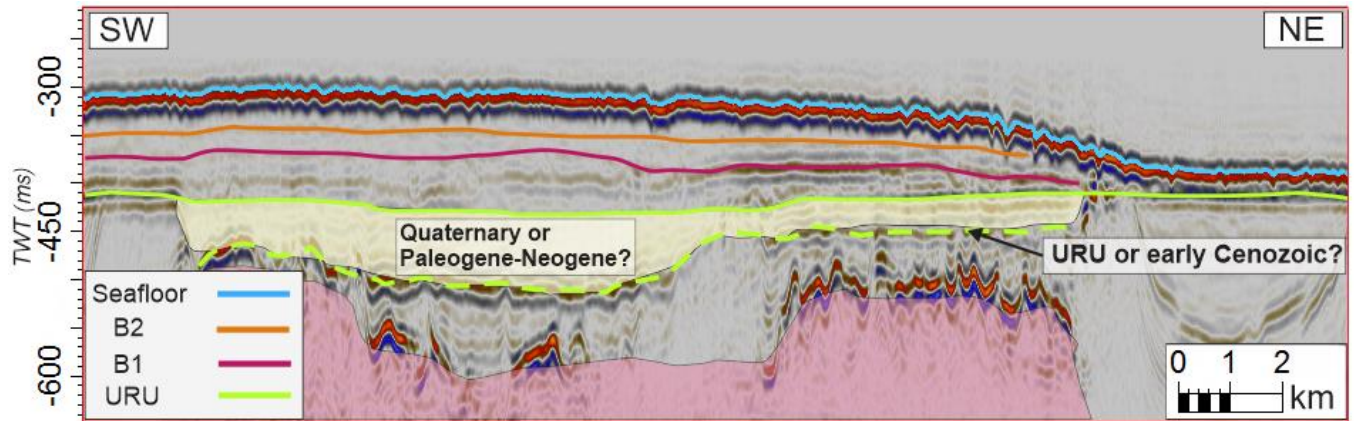


Figure 5.5: Seismic profile through the top of diapir 12, showing the area of uncertainty where the age of the sediments above the salt body are assumed to be of early Cenozoic age. Salt is in pink. Location and orientation is equal to that of figure 4.28

#### 5.1.4.2 Diapirs active after glacial erosion

##### ***Elevated URU – salt activity after onset of glacial erosion***

The majority of the diapirs within the Nordkapp Basin are truncated by the URU. High amplitudes along the URU above the diapirs suggest that the salt bodies are located directly below the unconformity, meaning it either cuts or drapes across the diapirs (Figure 4.26 and 4.32). The unconformity is elevated above many of the diapirs (i.e. diapir 4 and 7 in the SW and diapirs 24-26 further NE) (Figure 4.25 and 4.33), indicating they have been active following the formation of the URU.

Above diapir 4 and 7, the URU forms a depression around the flanks, and has a dome shape above more central parts (Figure 4.25), indicating salt activity after it was formed. The salt body of the diapirs is softer than the surrounding consolidated strata and more easily eroded. Evaporites reach a maximum of 4 on Mohs hardness scale, with dolomite (Table 1.1). Halite, the most common evaporite mineral has a hardness of 2.5 (Jones and Davidson, 2014). Quartz, a common mineral in siliciclastic rocks, has a hardness of 7, making such rocks more resistant to erosion. The URU truncates the top of the salt, or drapes across it. The unconformity might have been deeper, as the glacial erosion was likely more efficient above the diapirs (Figure 5.6a), due to the relative contrast in hardness compared to adjacent rocks. The unconformity surface was likely then elevated due to late salt activity (Figure 5.6b and 5.8ii). Additionally, the flat configuration of horizon B1 above, indicates that the uplift occurred before the formation of this surface. The horizon is found within the arcuate ridge in front of the Djuprenna trough, and is interpreted to represent an erosional surface from an advance of ice (Figure 5.6c), preserved beneath younger glacial sediments (Figure 5.6d) deposited during a later advance of the ice stream.

## 5 Discussion

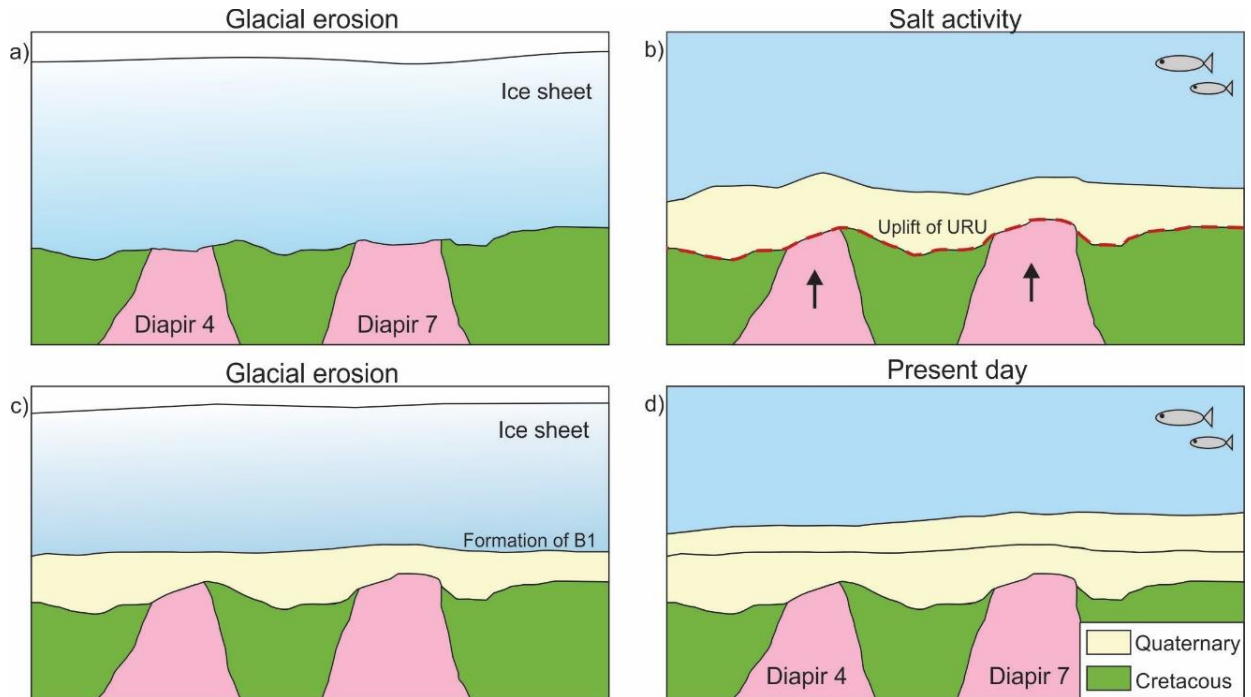


Figure 5.6: Conceptual model of the late Cenozoic development of diapir 4 and 7 in the SW Nordkapp Basin. a) Glacial erosion of the diapirs and adjacent strata, b) Uplift of the URU due to salt activity, c) Later glacial erosion, formation of horizon B1 and d) The present stratigraphy.

Late salt movement is also inferred for diapir 24-26, where the URU is uplifted (Figure 5.9ii). North of the diapirs the unconformity forms a depression (Figure 4.32) while the isochore map shows an increased time-thickness here (Figure 4.21) indicating an accumulation of glacial sediments above. Grimstad (2016) defined two rim syncline sub-basins in the deeper stratigraphy in the northern central Nordkapp Basin. The reflections of the strata below the URU form a synclinal shape that terminates against the diapir (Figure 4.32), likely representing one of the rim synclines formed due to salt withdrawal.

The depression of the URU may thus be linked to activity of this sub-basin in relation to late activity of the adjacent diapirs. Removal of strata or sediments from above the salt during periods of glacial erosion (Figure 5.7a) might trigger salt rise in response, where the rim syncline and overlying URU experienced subsidence (Figure 5.7b). The subsidence of the URU provides increased accommodation space for sediments to accumulate, and during repeated periods of glacial erosion (Figure 5.9d) sediments would be less exposed to erosion than those overlying the rising diapir (Figure 5.7c), resulting in the sediment accumulation preserved today (Figure 5.7d). The depression of the URU may also be linked to a local increase of glacial erosion, or a combination of both. Nevertheless, the area appears to have been a depocenter for glacial sediments.

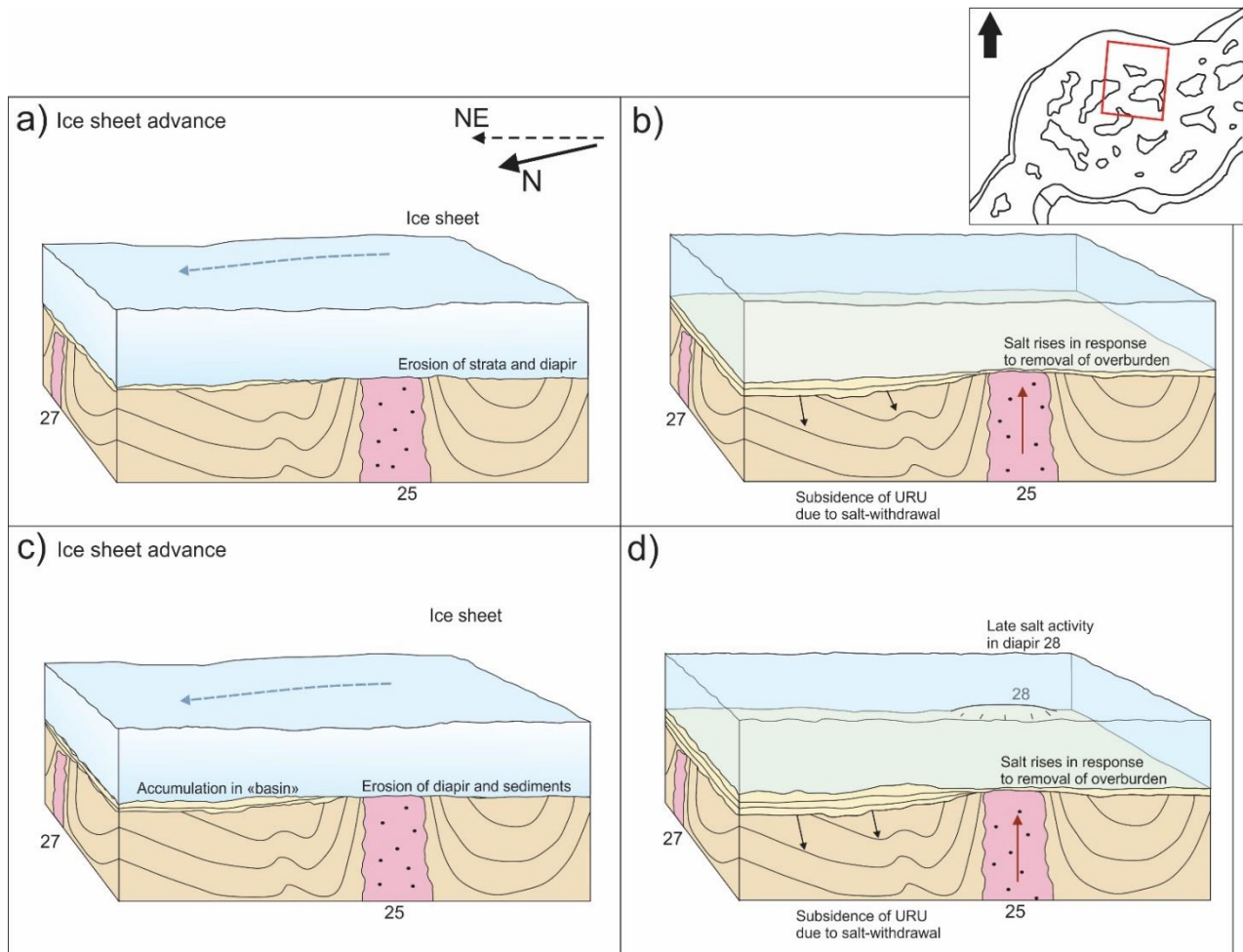


Figure 5.7: Conceptual model showing the evolution of the salt-withdrawal rim syncline north of diapir 25. a) Strata and salt of diapir 25 was eroded by ice during glaciations, b) the removal of strata caused the diapir to rise in response, resulting in subsidence of a pre-Cenozoic rim-syncline and overlying URU. c) This provided more accommodation space for sediments to be preserved after d) more subsidence in response to salt rise due to repeated glacial erosion. The approximate position and orientation of the 3D model is given by the red polygon. Proportions are not to scale.

### ***Elevated Seafloor – salt activity after deglaciation***

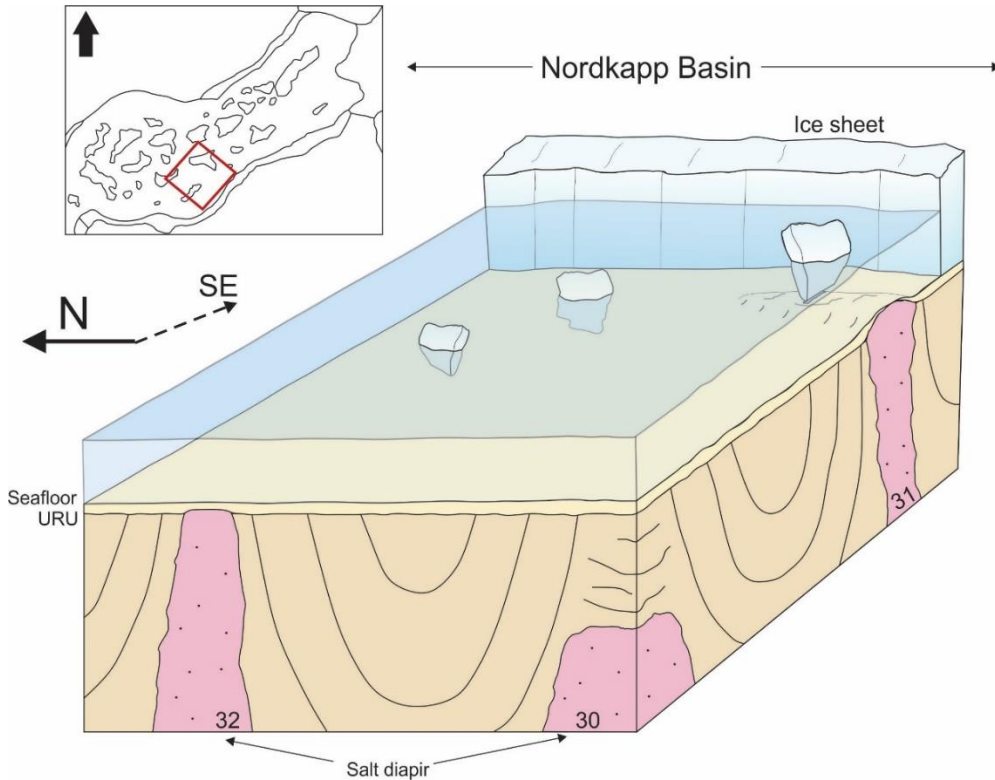
Some diapirs within the basin, especially in the central and northeastern parts (i.e. diapir 31 and 39-44), have uplifted the seafloor, indicating salt activity after deglaciation and formation of the present seafloor (Figure 5.9iv).

Both the URU and seafloor are uplifted above diapir 31 (Figure 4.38), with the unconformity subcropping the seafloor above central parts of the salt body, which is just beneath the seafloor. Opposite to the adjacent diapir 30, this diapir has experienced late salt activity. Along the southwestern margin, the top of the salt is slightly lower in the stratigraphy, as is the seafloor. This may indicate a late subsidence or collapse of the salt (Figure 5.9iii), perhaps related to percolating sea water or low salinity subglacial water (Grimstad, 2016). The increased plough mark frequency on the seafloor near the diapir implies that there was a local



## 5 Discussion

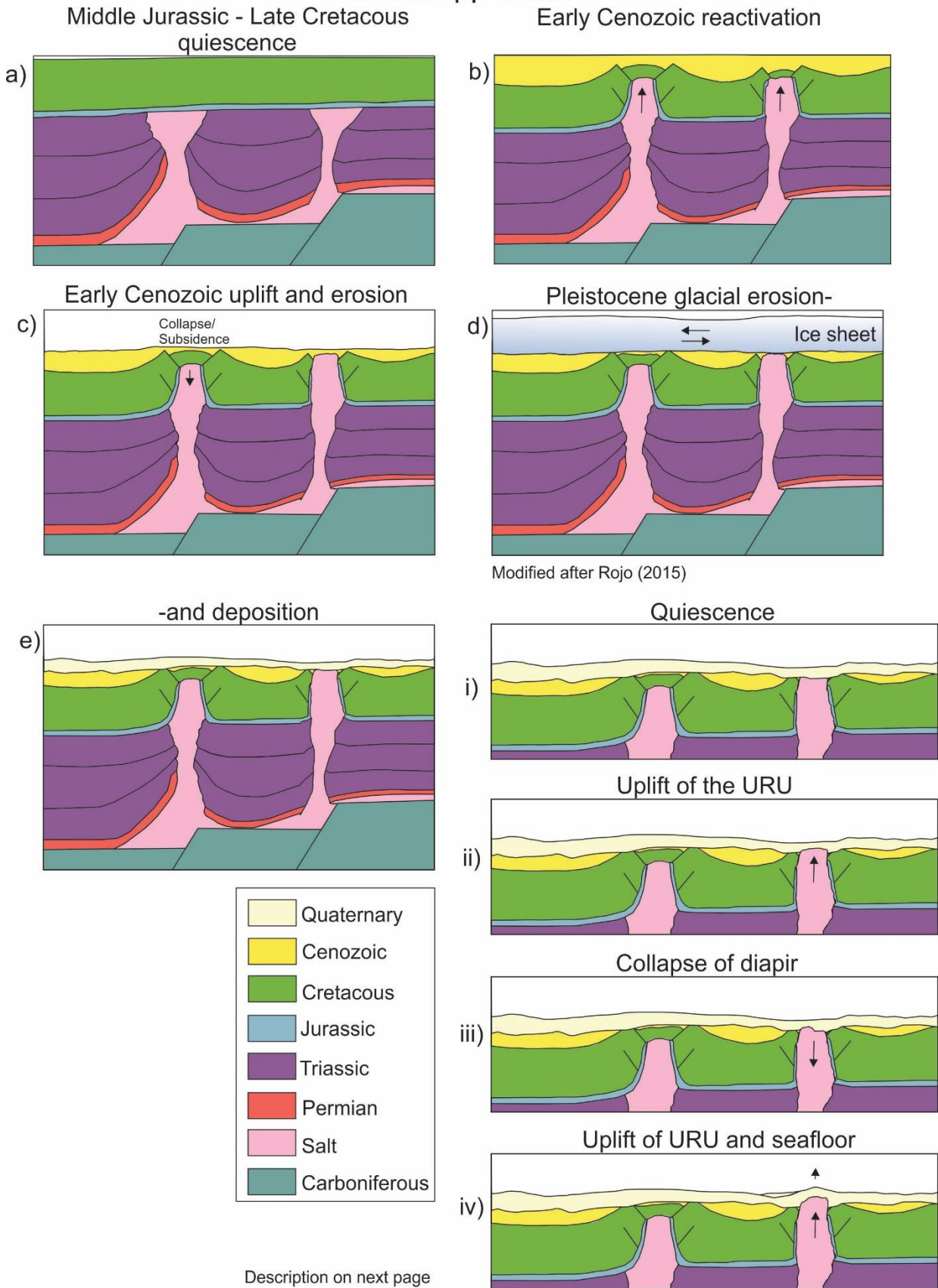
high above the diapir at the time of the last deglaciation. The shallower water depth meant keels of icebergs from the retreating ice sheet could plough the seafloor more easily above diapir 31 (Figure 5.8). The seafloor was more exposed to ice berg ploughing above diapir 31, than the adjacent diapir 30 and 32, where the seafloor has not been elevated by late salt movement (Figure 5.9i and ii).



*Figure 5.8: Conceptual model illustrating the elevation of the URU and/or seafloor above diapir 30-32 during the retreat of the Barents Sea Ice sheet during the last deglaciation. The elevated seafloor above diapir 31 likely caused ice berg to become more easily grounded, resulting in a local increase in plough marks. Proportions are not to scale.*

The presence of the URU is uncertain in the northeastern part of the basin, above the diapir system comprising diapir 39-44 (Figure 4.31.a). The unconformity surface onlaps the northwestern flank of the diapir system and is not visible above it or towards diapir 44 further east (Figure 4.42). This may be due to a thin sediment package above the URU, making it difficult to resolve in seismic data. The vertical resolution of the 2D data sets covering the northeastern part of the Nordkapp Basin (Table 3.3) (Figure 3.2) is estimated to be between 15-20 meters. If the sediment sequence above the URU is thinner than this, the unconformity will be difficult to resolve. The unconformity might also not be present above this part of the basin. This is the shallowest part of the study area (Figure 4.3) and all diapirs have experienced late salt activity that uplifted the seafloor above (Figure 5.9iv). The diapirs may have had a similar evolution to the Svalis Dome, where the URU is also not present above the most uplifted part of the structure.

## Nordkapp Basin



Modified after Rojo (2015)

## 5 Discussion

*Figure 5.9: Conceptual model of the different developments of the salt diapirs in the Nordkapp Basin. The generic development is a) late Mesozoic quiescence and deposition, b) early Cenozoic reactivation and active diapirism, c) uplift and erosion, d) and e) repeated erosion and deposition during ice sheet advance and retreat. The individual diapirs have had different developments during these processes: i) Quiescent salt, ii) Salt activity causing uplift of the URU, iii) Collapse or subsidence of the diapir or iv) Salt activity causing uplift of both the URU and seafloor. Note that the developments of the individual diapirs summarized in i)-iv) had spatial and temporal variations. Step a) – d) modified after Rojo (2015).*

### 5.2 Pre-Cenozoic factors influencing salt movement and erosion

Before discussing the interplay between Cenozoic salt movement and erosion, it is important to note there are other pre-existing factors influencing the late development of the salt structures during glaciations. Some main components affecting the Cenozoic evolution of the study area are discussed below.

#### 5.2.1 Original salt thickness

There is an observed difference in timing and extent of salt movement when comparing the Norvarg and Samson domes to the Svalis Dome and Nordkapp Basin. The Norvarg and Samson domes have not experienced late Cenozoic salt movement, and the strata above the salt bodies have not experienced uplift and erosion to the same extent as that above the Svalis Dome and Nordkapp Basin. Additionally, there is a trend of more late salt activity towards the northeast in the Nordkapp Basin, evidenced by the increase in uplift of the seafloor (Figure 5.4). One factor causing this could be the difference in thickness of the Late Carboniferous and Permian evaporite sequence deposited in the areas.

A study of a salt-complex in Germany by Trusheim (1960) suggests that original thickness of salt deposits largely influences the size and shape of salt structures. Thus, the difference in activity may partly be a result of a relatively smaller evaporite accumulation below the Norvarg and Samson domes compared to the Nordkapp and Maud basins (Gernigon et al., 2018). The larger the thickness, the more salt is available to mobilize and move upwards. The original thickness of evaporites is estimated to be 2-2.5 km in the southwestern Nordkapp Basin (Bergendhal, 1989; Jensen and Sørensen, 1992), increasing towards 4-5 km in the northeast. Below the Norvarg and Samson domes, evaporite sequences up to 2-2.7 km thick have been found (Breivik et al., 1995; Mattos et al., 2016).

#### 5.2.2 Overburden weight and strength

The study by Trusheim (1960) also concluded that weight and properties of the overburden above the salt is a significant influence on later development of salt structures. This is likely a significant reason for the lack of late salt movement of the Samson and Norvarg domes, along with the aforementioned difference in salt thickness. The domes both experienced less tectonic activity during the Mesozoic compared to the adjacent Maud and Nordkapp basins (Breivik et al., 1995; Gernigon et al., 2018). The more stable platform environment likely resulted in a thicker and more compacted overburden, restricting salt movement and

## 5 Discussion

haltering diapir-evolution (Breivik et al., 1995). Additionally, faulting or fracturing of the overburden due to tectonic activity will weaken mechanical strength, benefitting salt movement (Vendeville and Jackson, 1992). Thus, the lack of tectonic activity and thick overburden is likely a main reason for why the Norvarg and Samson domes have not experienced any late Cenozoic salt activity.

### 5.2.3 Early Cenozoic erosion

The pre-glacial erosion (see chapter 2.3.1) of the shelf during the early Cenozoic is also a component that likely influenced the circumstances of salt movement during and after glacial erosion occurred, and was estimated to be between 858-1362 meters (Lasabuda et al., 2018a). From the paleo-environmental reconstruction of Lasabuda et al. (2018a), the Bjarmeland Platform and Loppa High where the Norvarg, Samson and Svalis domes are located or adjacent, are among the structures in the study area exposed to more significant erosion during the Paleogene-Neogene. The Nordkapp Basin received sediments from the adjacent highs through the Paleocene and Eocene (Figure 2.5a and b). The northeastern basin was later uplifted and more exposed to erosion, while the southwestern part remained a minor zone of sediment accumulation (Figure 2.5c and d).

From observations made from seismic interpretation, the URU truncates Mesozoic strata around or above the Norvarg, Samson and Svalis domes, implying a large hiatus in deposition in these locations. In the southwestern Nordkapp Basin however, above i.e. diapir 12, Cenozoic sediments are assumed to have been preserved below the unconformity (Figure 5.5), indicating that this area likely received the sediments eroded from adjacent highs and platforms. Sediments were locally preserved from erosion above the diapir due to subsidence of the salt body, providing accommodation space for sediments.

## 5.3 Interplay between salt movement and late Cenozoic erosion

### 5.3.1 Ice sheet dynamics above the salt structures

The structural elements within the study area experienced different subglacial conditions and ice sheet dynamics during the glaciations of the Barents Sea shelf. The Svalis Dome, in the northwestern study area, was beneath the Bear Island Ice Stream. During the latest phase of glaciations, the last 0.7 Ma, glacial erosion was concentrated below the fast flowing ice in cross shelf troughs (Laberg et al., 2012) (See chapter 2.3.2) (Figure 2.9d). Thus, the Svalis Domes likely experienced the most severe glacial erosion out of the structural elements during this time. The area was also exposed to significant glaciofluvial erosion prior to this, from 2.7-1.5 Ma (Laberg et al., 2012).

The Norvarg and Samson domes, located on the southwestern Bjarmeland Platform, were less subjected to glacial erosion during the last 0.7 Ma when the erosion was concentrated below ice streams (Laberg et al.,

## 5 Discussion

2012). The platform did however experience erosion during 1.5-0.7 Ma when glacial erosion was not topographically restricted to the same degree. The Norvarg and Samson domes were therefore not exposed to glacial erosion to the same extent that the Svalis Dome was. However, glacial erosion was still the main process on the shelf during this time and resulted in removal of large amounts of strata from above the domes.

The Nordkapp Basin, located below the bathymetric Nordkapp Bank, also experienced limited erosion during the last 0.7 Ma, when ice flow was more constricted within cross shelf troughs. Like the Norvarg- and Samson domes erosion here was likely more significant during 1.5-0.7 ma, when ice flow was less restricted (Laberg et al., 2012). In the southwestern basin, fast flowing ice drained through the Djuprenna trough during the last glacial (Winsborrow et al., 2010), eroding the subsurface and later depositing the arcuate ridge observed above some diapirs.

### 5.3.2 Response of salt structures to erosion

Generally, the removal of strata above a salt body will affect the potential for more salt activity. The loss of overburden directly above the salt would likely promote upwards movement. In contrast, sediment loading has been identified as a factor likely to trigger halokinesis, so the loss of strata adjacent to the salt may also reduce the potential for later activity.

The Samson and Norvarg domes did not experience late Cenozoic salt movement, and were thus not activated in response to the removal of overburden. This may be linked to factors such as salt thickness and overburden strength, which gave the two domes different preconditions for late Cenozoic salt movement compared to the Svalis Dome. Here, the removal of significant amounts of strata was likely a trigger that caused the salt to move upwards in response.

Within the Nordkapp Basin, the timing of salt activity varies laterally between the diapirs, making it difficult to determine what triggered the movement of the individual diapirs. This area did not experience glacial erosion to the same degree as the Svalis Dome, but large amounts of overburden was still removed and likely triggered the late salt activity of some of the diapirs. The additional removal of strata in Djuprenna and later loss of pressure due to glacial retreat may have been a triggering factor for the late salt activity that uplifted the URU above some of the diapirs in the SW basin.

## 5 Discussion

### 5.3.3 Influence of salt movement on erosion and sediment dispersal

The relationship between salt movement and erosion is mutually influential. Elevation of strata due to salt movement will promote erosion, which in turn might trigger further uplift. Local highs above the diapirs within the Nordkapp Basin controlled sediment pathways during Cretaceous deposition (Brennhaugen, 2018). While salt-related highs act as areas of sediment bypass (Matthews et al., 2007), they have likely influenced the spatial variation in glaciofluvial erosion and deposition when these processes dominated the shelf during 2.7-1.5 Ma (Laberg et al., 2012).

While elevated strata above diapirs is more exposed to erosion, the local highs may also give protection from erosion to some degree to adjacent sediment accumulations (i.e. the mini basin SW of the Svalis Dome (Figure 4.11-4.13)). Sediment depocenters are known to develop in salt-withdrawal related rim synclines (Matthews et al., 2007). The sediment accumulation north of the central Nordkapp Basin likely represents a depocenter like this, where the late salt-withdrawal caused the URU surface to subside and create accommodation space for glacial sediments. The loading of sediments above the rim syncline may also have contributed to further salt movement.

## 6 Conclusions

The late Cenozoic evolution of the southwestern Barents Sea has been studied with emphasis on the relationship between uplift, erosion, glaciations and salt movement. The study has been conducted in order to understand how these processes have affected the development of the Svalis, Samson and Norvarg domes and the Nordkapp Basin. The interplay between salt diapirism and developments during glacial activity is found to be complex, with many influential factors. The salt structures within the study area have had different pre-Cenozoic evolutions and experienced varying degrees of Cenozoic erosion, which have influenced if and how later salt movement occurred. This is evidenced by the differences between the Svalis, Samson and Norvarg domes and the relatively significant local variations between the salt diapirs in the Nordkapp Basin. The main findings of the study are listed below:

- The salt domes within the study area have experienced activity at different times: the Svalis Dome was active during the late Cenozoic, the Samson and Norvarg domes were inactive, and the Nordkapp Basin had both active and inactive areas.
- Different preconditions before the onset of Cenozoic uplift and erosion, such as a Mesozoic stable platform environment and a relatively small original salt thickness, are assumed to be the main reason for the lack of salt movement of the Norvarg- and Samson domes.
- The Svalis Dome is likely still experiencing active salt growth. Extensive glacial erosion in the Bear Island Trough is an important influence on the salt movement, as the late activity of the dome was likely a response to the removal of strata above it. A mini-basin filled with Quaternary glacial sediments formed SW of the Svalis Dome, due to a combination of deeper glacial erosion of less resistant Mesozoic rocks on the Loppa High, and the rising dome protecting the sediment accumulation from further erosion to some extent.
- Removal of overburden due to uplift and erosion, and a loss of overpressure related to ice sheet retreat has likely triggered fluid migration from deeper within the Samson Dome, resulting in accumulation of shallow gas along the URU or within the glacial sediments above.
- The salt diapirs within the Nordkapp Basin have been active at different times during the Cenozoic. These can be categorized as follows according to the relationship between the salt bodies, URU and seafloor: i) early Cenozoic reactivation, ii) active after the formation of the URU, iii) collapsing or subsiding after early Cenozoic movement or after the onset of glacial erosion, iv) active after the last deglaciation.
- There is a trend of NE increase in late salt movement of the diapirs within the Nordkapp Basin, likely closely related to the original thickness of the evaporite sequence deposited in the basin.

## 6 Conclusions

- Late salt movement of some diapirs in the Nordkapp Basin caused iceberg grounding and plough mark formation during the last deglaciation of the Barents Sea.
- Salt dissolution near the seafloor has likely contributed to the collapse of some of the salt diapirs within the Nordkapp Basin.
- An accumulation of glacial sediments north of the central Nordkapp Basin is likely a result of a salt-withdrawal mini-basin forming adjacent to some of the diapirs rising in response to the removal of sediments during Quaternary glaciations.



## 7 Further work

This study reveals that the interplay and feedback between salt diapirism and uplift and erosion in the Barents Sea is complex, with many factors influencing one another. This is a regional study which gives a general overview, so in order to further investigate how these processes have influenced the evolution of individual structural elements more detailed work is required. Below are recommendations for further work that will improve our understanding of the evolution of the structures within the study area during the late Cenozoic.

- The majority of the categorization of the diapirs within the Nordkapp Basin is based on 2D seismic data. While the line spacing is quite dense in some areas, a more detailed study of the shallow stratigraphy around the diapirs using 3D seismic data with better spatial resolution could give a more accurate classification. It could also change the estimation of timing of salt movement in some of the diapirs made in this study, as the seismic stratigraphic relationship between the salt and overlying horizons may appear different.
- 3D seismic data would also be beneficial to further understand the late Cenozoic development of the Svalis Dome. Further seismic stratigraphic analysis of the assumed glacial sediments in the mini-basin adjacent to the dome could provide more information about the timing and nature of the erosion that is assumed to be the reason for their accumulation.
- Some of the observed salt bodies in the Nordkapp Basin are estimated to be very close to the seabed, close to outcropping at the seafloor. Collecting cores above these could prove the presence of shallow salt bodies. This would also be beneficial to determine if there is a diapir present near the top of the Svalis Dome, as suggested by some studies.
- A more detailed study of the URU above the Norvarg- and Samson domes using 3D seismic data and a correlation with the faults in the strata below could help in understanding how pre-Cenozoic doming and faulting of the strata affected later erosion.



## 8 References

- Alsop, G. I., Archer, S. G., Hartley, A. J., Grant, N. T. and Hodgkinson, R. 2012. Salt tectonics, sediments and prospectivity. Geological Society Special Publications, 363.
- Andreassen, K., Ødegaard, C.M., and Rafaelsen, B. 2007. Imprints of former ice streams, imaged and interpreted using industry 3D seismic data from the south-western Barents Sea, in Davies, R.J., Posamentier, H.W., Wood, L.J., and Cartwright, J.A., eds., *Seismic Geomorphology: Applications to Hydrocarbon Exploration and Production*, Volume 277, Geological Society of London Special Publication, p. 151-169.
- Badley, M. E. 1985. *Practical seismic interpretation*. Boston: International Human Resources Development Corporation.
- Bergendhal, E., 1989, Halokinetisk utvikling av Nordkappbassengets sørvestre segment.
- Breivik, A. J., Gudlaugsson, S. T. and Faleide, J. I. 1995. Ottar Basin, SW Barents Sea: A major Upper Palaeozoic rift basin containing large volumes of deeply buried salt. *Basin Res*, 7, 239-312.
- Brennhaugen, A. A. 2018. A combined 3D seismic and sedimentological study of the Lower Cretaceous succession in the northeastern part of the Nordkapp Basin.
- Brown, A. R. 1999. *Interpretation of three-dimensional seismic data*. American Association of Petroleum Geologists, 5<sup>th</sup> edition, vol. 42.
- Bugge, T., Elvebakk, G., Fanavoll, S., Mangerud, G., Smelror, M., Weiss, H.M., Gjelberg, J., Kristensen, S.E. and Nilsen, K. 2002. Shallow stratigraphic drilling applied in hydrocarbon exploration of the Nordkapp Basin, Barents Sea: *Marine and Petroleum Geology*, v. 19, p. 13–37
- Bugge, T. & Fanavoll, S. 1995. The Svalis Dome, Barents Sea - a geological playground for shallow stratigraphic drilling. *First Break* 13(6), 237-251.
- Butt, F. A., Drange, H., Elverhøi, A., Otterå, O. H. and Solheim, A. 2002. Modelling Late Cenozoic isostatic elevation changes in the Barents Sea and their implications for oceanic and climatic regimes: preliminary results. *Quaternary Science Reviews*, v. 21 p. 1643-1660.
- Catuneanu, O. (2006). *Principles of Sequence Stratigraphy*: Elsevier Science.
- Corfu, F., Polteau, S., Planke, S., Faleide, J. I., Svensen, H., Zayoncheck, A. and Stolbov, N. 2013. U–Pb geochronology of Cretaceous magmatism on Svalbard and Franz Josef Land, Barents Sea Large Igneous Province. *Geological Magazine*, vol. 150(6), p. 1127-1135.
- Dengo, C. A., and K. G. Røssland, 1992, Extensional tectonic history of the western Barents Sea, in R. M. Larsen et al., eds., *Structural and tectonic modelling and its application to petroleum geology*: Norwegian Petroleum Society Special Publication, p. 91–107.
- Doré, A.G. 1995. Barents Sea Geology, Petroleum Resources and Commercial Potential: *ARCTIC*, v. 48, p. 207–221.
- Dowdeswell, J. A. and Cofaigh, C. Ò. 2002. Glacier-influenced sedimentation on high-latitude continental margins: introduction and overview. Geological Society, London, Special Publications, vol. 203(1), p. 1-9.

## 8 References

- Engen, Ø., Faleide, J.I. and Dyreng, T.K. 2008. Opening of the Fram Strait gateway: a review of plate tectonic constraints. *Tectonophysics* 450, 51–69.
- Faleide, J.I., Bjørlykke, K., and Gabrielsen, R.H., 2015. *Geology of the Norwegian Continental Shelf*, in *Petroleum Geoscience*, Berlin, Heidelberg, Springer Berlin Heidelberg, p. 603–637.
- Faleide, J. I., Solheim, A., Fiedler, A., Hjelstuen, B. O., Andersen, E. S. and Vanneste, K. 1996. Late Cenozoic evolution of the western Barents Sea-Svalbard continental margin. *Marine and Petroleum Geology*, Vol. 8, 317-340.
- Faleide, J.I., Tsikalas, F., Breivik, A.J., Mjelde, R., Ritzmann, O., Engen, O., Wilson, J. and Eldholm, O. 2008. Structure and evolution of the continental margin off Norway and the Barents Sea. *Episodes* 31, 82–91.
- Faleide, J.I., Vågnes, E., and Gudlaugsson, S.T.. 1993. Late Mesozoic-Cenozoic evolution of the south western Barents Sea in a regional rift-shear tectonic setting: *Marine and Petroleum Geology*, v. 10, p. 186–214.
- Fiedler, A., Faleide, J.I. 1996. Cenozoic sedimentation along the southwestern Barents Sea margin in relation to uplift and erosion of the shelf. *Global Planet. Change* 12, 75–93
- Fossen, H.. 2010. *Structural Geology*, in *Structural Geology*, Cambridge, Cambridge University Press, p. 371–393.
- Gabrielsen, R.H., Færseth, R.B., Jensen, L.N., Kalheim, J.E., and Riis, F. 1990 NPD Bulletin No 6 *Structural Elements of the Norwegian continental shelf: Norwegian Petroleum Directorate Bulletin*, v. 6, p. 1–47.
- Gabrielsen, R. H., Rasmussen, K. A., and Stølan, T. 1992. Interaction between halokinesis and faulting: structuring of the margins of the Nordkapp Basin, Barents Sea region In B. T. Larsen & E. Talleraas (Eds.), (Vol. Norwegian Petroleum Society (NPF) 1992, pp. 121-131).
- Gernigon, L., Brönnner, M., Dumais, M-A., Gradmann, S., Grønlie, A., Nasuti, A. and Roberts, D. 2018. Basement inheritance and salt structures in the SE Barents Sea: Insights from new potential field data. *Journal of Geodynamics*, v. 119, p. 82-106.
- Giles, K.A., and Rowan, M.G. 2012. *Concepts in halokinetic-sequence deformation and stratigraphy: Geological Society, London, Special Publications*, v. 363, p. 7–31.
- Gjelberg, J. and Steel, R. J. 1995. Helvetiafjellet formation (Barremian-Aptian), Spitsbergen: characteristics of a transgressive succession. *Norwegian Petroleum Society Special Publications*, vol. 5, p. 571-593.
- Glørstad-Clark, E., Faleide, J.I., Lundschiene, B.A., and Nystuen, J.P. 2010. Triassic seismic sequence stratigraphy and paleogeography of the western Barents Sea area: *Marine and Petroleum Geology*, v. 27, p. 1448–1475.
- Grimstad, S. 2016. Salt tectonic in the central and northeastern Nordkapp Basin, Barents Sea.
- Henriksen, E., Bjørnseth, H. M., Hals, T. K., Heide, T., Kiryukhina, T., Kløvjan, O. S., Larseen, G. B., Ryseth, A. E., Rønning, K., Sollid, K. and Stoupakova, A. V. 2011b. Uplift and erosion of the greater Barents Sea: impact on prospectivity and petroleum systems. *Geological Society, London, Memoirs* 2011, 35, 271-281.

## 8 References

- Henriksen, E., Ryseth, A. E., Larssen, G. B., Heide, T., Rønning, K., Sollid, K. and Stoupakova, A. V. 2011a. Tectonostratigraphy of the greater Barents Sea: implications for petroleum systems. Geological Society, London, Memoirs 2011, 35, 163-195.
- Hjelstuen, B.O., Elverhøi, A., Faleide, J.I. 1996. Cenozoic erosion and sediment yield in the drainage area of the Storfjorden Fan. *Global Planet. Change* 12, 95–117.
- Jackson, M.P.A., and Hudec, M.R. 2017. *Salt Tectonics*: Cambridge, Cambridge University Press, 498 p.,
- Jakobsson, M., Mayer, L., Coakley, B., Dowdeswell, J. A., Forbes, S., Fridman, B., Hodnesdal, H., Noormets, R., Pedersen, R., Rebesco, M., Schenke, H. W., Zarayskaya, Y., Accettella, D., Armstrong, A., Anderson, R. M., Bienhoff, P., Camerlenghi, A., Church, I., Edwards, M., Gardner, J. V., Hall, J. K., Hell, B., Hestvik, O., Kristoffersen, Y., Marcussen, C., Mohammad, R., Mosher, D., Nghiem, S. V., Pedrosa, M. T., Travaglini, P. G. and Weatherall, P. 2012. The International Bathymetric Chart of the Arctic Ocean (IBCAO) Version 3.0. *Geophysical Research Letters*, vol. 39.
- James, N. P. & Dalrymple, R. W. 2010. *Facies Models 4*, Geological Association of Canada.
- Jensen, L. N., and Sørensen, K. 1992, The tectonic framework and halokinesis of the Nordkapp Basin, Norwegian Barents Sea, in R. M. Larsen et al., eds., *Structural and tectonic modelling and its application to petroleum geology: Norwegian*
- Jenyon, M. K. 1986. *Salt Tectonics*, Springer.
- Jones, I.F., and Davison, I. 2014. *Seismic imaging in and around salt bodies: Interpretation*, v. 2, p. SL1 SL20, doi: 10.1190/INT-2014-0033.1.
- Kearey, P., Brooks, M., & Hill, I. 2002. *An Introduction to Geophysical Exploration (Third Edition ed.)*: Blackwell Science Ltd.
- Klausen, T. G., Müller, R., Slama, J. and Helland-Hansen, W. 2017. Evidence for Late Triassic provenance areas and Early Jurassic sediment supply turnover in the Barents Sea Basin of northern Pangea. *Lithosphere*, vol. 9, p. 14-28.
- Knies, J., Matthiessen, J., Vogt, C., Laberg, J.S., Hjelstuen, B.O., Smelror, M., Larsen, E., Andreassen, K., Eidvin, T., Vorren, T.O. 2009. The Plio-Pleistocene glaciation of the Barents Sea–Svalbard region: a new model based on revised chronostratigraphy. *Quaternary Science Review*, vol. 28, p. 812–829.
- Koson, S., Chenrai, P. and Choowong, M. 2014. Seismic attributes and their applications in seismic geomorphology. *Bulletin of Earth Sciences of Thailand*, vol. 6, p. 1-9.
- Koyi, H., C. J. Talbot, and B. O. Tørudbakken. 1995. Salt tectonics in the northeastern Nordkapp Basin, southwestern Barents Sea, in M. P. A. Jackson, D. G. Roberts, and S. Snelson, eds., *Salt tectonics: a global perspective: AAPG Memoir 65*, p. 437-447.
- Kristoffersen, Y., 1990. On the Tectonic Evolution and Paleooceanographic Significance of the Fram Strait Gateway, *Geological History of the Polar Oceans: Arctic versus Antarctic*. Springer, pp. 63–76.
- Kristoffersen, Y., Talwani, M. 1977. Extinct triple junction south of Greenland and the Tertiary motion of Greenland relative to North America. *Geol. Soc. Am. Bull.* 88, 1037–1049.

## 8 References

- Ktenas, D., Henriksen, E., Meisingset, I., Nielsen, J. K. and Andreassen, K. 2017. Quantification of the magnitude of net erosion in the southwest Barents Sea using sonic velocities and compaction trends in shales and sandstones. *Marine and Petroleum Geology*, vol. 88, p. 826-844.
- Laberg, J.S., Andreassen, K., Knies, J., Vorren, T.O., Winsborrow, M. 2010. Late Pliocene–Pleistocene development of the Barents Sea ice sheet. *Geology* 38, 107–110.
- Laberg, J.S., Andreassen, K., Vorren, T.O. 2012. Late Cenozoic erosion of the high-latitude southwestern Barents Sea shelf revisited. *Geol. Soc. Am. Bull.* 124, 77–88.
- Laberg, J.S., and Vorren, T.O. 1995, Late Weichselian submarine debris flow deposits on the Bear Island Trough Mouth Fan: *Marine Geology*, v. 127, p. 45-72.
- Laberg, J. S., and Vorren, T. O. 1996. The Middle and Late Pleistocene evolution and the Bear Island Trough Mouth Fan. *Marine Geology*, 127(1), p. 45-72.
- Landvik, J.Y., Bondevik, S., Elverhøi, A., Fjeldskaar, W., Mangerud, J., Salvigsen, O., Siegert, M.J., Svendsen, J.I., and Vorren, T.O. 1998, The Last Glacial Maximum of the Svalbard and the Barents Sea area: Ice sheet extent and configuration: *Quaternary Science Reviews*, v. 17, p. 43-75.
- Larsen, E., Kjaer, K.H., Demidov, I.N., Funder, S., Grosfjeld, K., Houmark, N.M., Jensen, M., Linge, H., and Lysa, A. 2006, Late Pleistocene glacial and lake history of northwestern Russia: *Boreas*, v. 35, p. 394-424.
- Lasabuda, A., Laberg, J. S., Knutsen, S.-M. and Høgseth, G. 2018a. Early to middle Cenozoic paleoenvironment and erosion estimates of the southwestern Barents Sea: Insights from a regional mass-balance approach. *Marine and petroleum Geology* 96, 501-521.
- Lasabuda, A., Laberg, J. S., Knutsen, S.-M. and Safronova, P. 2018b. Cenozoic tectonostratigraphy and pre-glacial erosion: A mass-balance study of the northwestern Barents Sea margin, Norwegian Arctic. *Journal of Geodynamics* 119, 149-166.
- Lebesbye, E. and Vorren, T. O. 2000. Morphology and morphogenesis of the southwestern Barents Sea shelf; an evaluation of the regional late Cenozoic erosion surface based on high-resolution seismics.
- Mangerud, J., Dokken, T., Hebbeln, D., Heggen, B., Ingólfsson, Ó., Landvik, J.Y., Mejdahl, V., Svendsen, J.I., & Vorren, T.O. 1998, Fluctuations of the Svalbard-Barents sea ice sheet during the last 150 000 years: *Quaternary Science Reviews*, v. 17, p. 11-42.
- Martinuk, D. 2017. 3-D seismic interpretation of the Samson Dome in the framework of the tectonostratigraphic and fluid migration development of the Western Barents Sea.
- Matthews, W. J., Hampson, G. J., Trudgill, B. D. and Underhill, J. R. 2007. Controls on fluviolacustrine reservoir distribution and architecture in passive salt-diapir provinces: Insights from outcrop analogs. *AAPG Bulletin*, vol. 91, p. 1367-1403.
- Mattos, N. H., Alves, t. M., Omosanya, K. O. 2016. Crestal fault geometries reveal late halokinesis and collapse of the Samson Dome, Northern Norway: Implications for petroleum systems in the Barents Sea. *Tectonophysics* vol. 690, p. 76-96.

## 8 References

- Mitchum, R. M., Vail, P. R., & Sangree, J. B. (1977). Seismic Stratigraphy and Global Changes of Sea Level: Part 6. Stratigraphic Interpretation of Seismic Reflection Patterns in Depositional Sequences: Section 2. Application of Seismic Reflection Configuration to Stratigraphic Interpretation. In *Seismic Stratigraphy--Applications to Hydrocarbon Exploration* (pp. 1171-133).
- Mørk, A. and Elvebakk, G. 1999. Lithological description of subcropping Lower and Middle Triassic rocks from the Svalis Dome, Barents Sea. *Polar research*, vol. 18, p. 83-104.
- Nansen, F. 1904. *Farthest North: Being the Record of a Voyage of Exploration of the Ship "Fram" 1893-96 and of a Fifteen Months' Sleigh Journey by Dr. Nansen and Lieut. Johansen*. Library of Alexandria, vol. 1.
- Nejbert, K., Krajewski, K. P., Dubinska, E. and Pecskay, Z. 2011. The dolerites from Svalbard, NW Barents Sea Shelf: age, geochemistry and significance for geotectonic interpretation of the High Arctic large igneous province. *Polar Research*, vol. 30.
- Nichols, G. 2009. *Sedimentology and Stratigraphy*. Wiley – Blackwell, 2<sup>nd</sup> edition.
- Nilsen, K. T., Vendeville, B. C., Johansen, J.-T. 1995. Influence of regional tectonics on halokinesis in the Nordkapp Basin, Barents Sea, in M.P.A. Jackson, D.G. Roberts, and S. Snelson, eds., *Salt tectonics: a global perspective: AAPG Memoir 65*, p.413–436.
- Nilsson, I., Mangerud, G. & Mork, A. 1996. Permian stratigraphy of the Svalis Dome, southwestern Barents Sea. *Nor.sk Geologisk Tidsskrift* 76. 127-146.
- NPD. 2013. Barents Sea South-East. Retrieved from <http://www.npd.no/en/Publications/ResourceReports/2013/Chapter-6/>
- NPD. 2014. Compiled CO2 atlas for the Norwegian Continental Shelf.
- NPD. 2019. Fact map NPD. Retrieved from <https://www.npd.no/en/facts/factpages/>
- Nøttvedt, A., Berglund, L., Rasmussen, E., Steel, R. 1988. Some aspects of Tertiary tectonics and sedimentation along the western Barents Shelf. *Geological Society*, vol. 39, p. 421–425, London, Spec. Publ.
- Ottesen, D., Stokes, C.R., Rise, L., and Olsen, L. 2008. Ice-sheet dynamics and ice streaming along the coastal parts of northern Norway: *Quaternary Science Reviews*, in press, 19 pp.
- Polteau, S., Hendriks, B. W. H., Planke, S., Ganerød, M., Corfu, F., Faleide, J. I., Midtkandal, I., Svensen, H. S. and Myklebust, R. 2016. *Palaeogeography, Palaeoclimatology, Palaeoecology*, vol. 441, p. 83-95.
- Rasmussen, E. and Fjeldskaar, W. 1996. Quantification of the Pliocene-Pleistocene erosion of the Barents Sea from present-day bathymetry. *Global and Planetary Change*, v. 12 p. 119-133.
- Reynolds, J. M. 2011. *An Introduction to Applied and Environmental Geophysics*. John Wiley & Sons.
- Richardson, G., Vorren, T.O., Tørudbakken, B.O. 1993. Post-Early Cretaceous uplift and erosion in the southern Barents Sea: a discussion based on analysis of seismic interval velocities. *Nor. Geol. Tidsskr.* 73, 3–20.

## 8 References

- Riis, F., Lundschieen, B. A., Høy, T. Mørk, A., Mørk, M-B. E., Evolution of the Triassic shelf in the northern Barents Sea region. *Polar Research*, vol. 27 (3), p. 318-338.
- Rojo, L. A. 2015. Interpretation, modeling and halokinetic evolution of salt diapirs in the Nordkapp Basin.
- Rojo, L. A. and Escalona, A. 2018. Controls on minibasin infill in the Nordkapp Basin: Evidence of complex Triassic syndepositional deposition influenced by salt tectonics. *AAPG Bulletin*, V. 102, No 7, pp 1239-1272.
- Rowan, M. G. and Lindsø, S. 2017. Permo-Triassic Salt Provinces of Europe, North Africa and the Atlantic margins. Elsevier Inc. *Tectonics and Hydrocarbon potential*, p. 265-286.  
<http://dx.doi.org/10.1016/B978-0-12-809417-4.00013-6>
- Ryseth, A., Augustson, J.H., Charnock, M., Haugerud, O., Knutsen, S.-M., Midbøe, P.S., Opsal, J.G., Sundsbø, G., 2003. Cenozoic stratigraphy and evolution of the Sørvestsnaget Basin, southwestern Barents Sea. *Norw. J. Geol.* 83, 107–130.
- Ryseth, A. 2014. Sedimentation at the Jurassic-Triassic boundary, south-west Barents Sea: Indication of climate change. Special Publication Number 46 of the International Association of Sedimentologists.
- Sheriff, R. E. 1977. *Seismic Stratigraphy – Applications to Hydrocarbon Exploration*. Association of American Petroleum Geologists Memoir, vol. 26, p. 3-14.
- Sheriff, R. E. 1985. *Seismic Stratigraphy: An Integrated Approach to Hydrocarbon Exploration*.
- Sheriff, R. E. 2002. *Encyclopedic Dictionary of Applied Geophysics*. Society of Exploration Geophysics, 4<sup>th</sup> edition, series 13.
- Siegert, M. J. and Dowdeswell, J. A. 2002. Late Weichselian iceberg, surface-melt and sediment production from the Eurasian Ice Sheet: results from numerical ice-sheet modelling. *Marine Geology*, vol. 188, p. 109-127.
- Smelror, M., Petrov, O., Larsen, G.B., and Werner, S. 2009. *Atlas: Geological History of the Barents Sea*. Trondheim, Geological Survey of Norway.
- Stemmerik, L., and Worsley, D. 1989. Late Paleozoic sequence correlations, North Greenland, Svalbard and the Barents shelf, in J. D. Collinson, ed., *Correlation in hydrocarbon exploration: Graham and Trotman*, Norwegian Petroleum Society, p. 303–331.
- Svendsen, J.I., Alexanderson, H., Astakhov, V.I., Demidov, I., Dowdeswell, J.A., Funder, S., Gataullin, V., Henriksen, M., Hjort, C., Houmark-Nielsen, M., Hubberten, W., Ingolfsson, O., Jakobsson, M., Kjør, K.H., Larsen, E., Lokrantz, H., Lunkka, J.P., Lyså, A., J., M., Matiouchkov, A., Murray, A., Møller, P., Niessen, F., Nikolskaya, O., Polyak, L., Saarnisto, M., Siegert, C., Siegert, M.J., Spielhagen, R.F., and Stein, R. 2004a. Late Quaternary ice sheet history of northern Eurasia: *Quaternary Science Reviews*, v. 23, p. 1229-1271.
- Svendsen, J.I., Gataullin, V., Mangerud, J., and Polyak, L., 2004b, *The glacial History of the Barents and Kara Sea Region*, in Ehlers, J., and Gibbard, P., eds., *Quaternary Glaciations - Extent and Chronology*: Amsterdam, Elsevier.
- Sømme, T. O., Dorè, A. G., Lundin, E. G. and Torudbakken, B. O. 2018. Triassic-Paleogene paleogeography of the Arctic: Implications for sediment routing and basin fill. *AAPG Bulletin*.



## 8 References

- Talwani, M., Eldholm, O., 1977. Evolution of the Norwegian-Greenland Sea. *Geological Society America Bulletin*. 88, 969–999.
- Trusheim, F., 1960, Mechanism of Salt Migration in Northern Germany: *AAPG Bulletin*, v. 44
- Vail, P. R. 1987. Seismic stratigraphy interpretation using sequence stratigraphy. In A. W. Bally (Ed.), *Atlas of Seismic Stratigraphy: AAPG Studies in Geology*, vol. 1, p. 1-10.
- Veeken, P. C. H. 2007. *Seismic stratigraphy, basin analysis and reservoir characterization*. Elsevier, vol. 37.
- Vendeville, B. C. and Jackson, M. P. A. 1992. The rise of diapirs during thin-skinned extension. *Marine and Petroleum Geology*, vol. 9.
- Vorren, T. O., Kristoffersen, Y. 1986. Late Quaternary glaciations in the south-western Barents Sea. *Boreas* vol. 15, p. 51-59.
- Vorren, T. O. and Laberg, J. S., 1997. Trough mouth fans – palaeoclimate and ice-sheet monitors. *Quaternary Science Reviews*, vol. 16(8), p. 865-881.
- Vorren, T. O., Lebesbye, E., Andreassen, K. and Larsen K. B., 1989. Glacigenic sediments on a passive continental margin as exemplified by the Barents Sea. *Marine Geology*, vol. 85(2), p. 251-272.
- Vorren, T.O., Richardsen, G., Knutsen, S.-M. and Henriksen, E., 1991. Cenozoic erosion and sedimentation in the western Barents Sea. *Marine Petroleum Geology* vol. 8, p. 317–340.
- Winsborrow, C. M., Andreassen, K., Corner, G. D., Laberg, J. S., 2010. Deglaciation of marine based ice sheet: Late Weichelian paleo-ice dynamics & retreat in the southern Barents Sea reconstructed from onshore & offshore glacial geomorphology. *Quaternary Science Review*.
- Wood, R. J., Eldrich, S. P. and Hutchinson, I. 1989. Influence of North Atlantic tectonics on the large scale uplift of the Stappen High and Loppa High, Western Barents Shelf. *American Association of Petroleum Geologists*, vol. 46, p. 559-566.
- Worsley, D. 2008. The post-Caledonian development of Svalbard and the western Barents Sea: *Polar Research*, v. 27, p. 298–317.